CRANFIELD UNIVERSITY

XIONG PENG

AIRCRAFT ENVIRONMENTAL CONTROL SYSTEMS MODELING FOR CONFIGURATION SELECTION

SCHOOL OF ENGINEERING
MSc by Research

MSc Thesis
Academic Year: 2012 - 2013

Supervisor: Dr Craig Lawson
November 2013

CRANFIELD UNIVERSITY

SCHOOL OF ENGINEERING
MSc by Research

MSc Thesis

Academic Year 2012 - 2013

XIONG PENG

AIRCRAFT ENVIRONMENTAL CONTROL SYSTEMS MODELING FOR CONFIGURATION SELECTION

Supervisor: Dr Craig Lawson
November 2013

This thesis is submitted in partial fulfilment of the requirements for the degree of Master of Science

ABSTRACT

According to the statistics about civil transportation aircraft Environmental Control system (ECS), the three-wheel high pressure water separation system (HPWS) and low pressure water separation system (LPWS) are the most common choices for the 150-seat airliners. Although the former has become the mainstream configuration for air conditioning pack, the latter is still used on Boeing 737-600/700. In order to compare the two configurations and choose the better one for a specific aircraft, simulation and analysis are done.

The cabin heat load is calculated at first in order to calculate required engine bleed air mass flow. Then a specific aircraft is defined so that required structural dimensions and cabin comfort indexes can be obtained based on Airbus 320. Thirdly, the component models are built by Matlab/Simulink according to the fundamental knowledge of heat transfer and aerodynamics, the working principles and mechanical dimensions of the components, the ambient environmental parameters and some data from Airbus 320. Consequently, the complete system model can be assembled. After confirming the validity of the model by checking the required ram air mass flow and temperature deviation of the state points referred to Airbus 320, the simulation model is used to do analyze the specific aircraft. Finally, through comparing the different values of ram air mass flow and turbine expansion ratio, as well as the system mass, economic cost and reliability, the better configuration is selected.

It can be summarized that the three-wheel LPWS requires less ram air mass flow (0.012kg/s) and a little lower expansion ratio (0.02) than the HPWS, and it also has lower weight (63% of HPWS), lower (83% of HPWS) cost and higher reliability (140% of HPWS), thus it is the suitable configuration for the specific aircraft.

Keywords:

Three-wheel high pressure water separation system, Three-wheel low pressure water separation system, Airbus 320, Simulation, Temperature, Pressure.

ACKNOWLEDGEMENTS

First of all I would say sincere thanks to my supervisor Dr. Craig Lawson for providing me with so much support and guidance during the IRP.

Then I want to say thanks to the staff members in the university, especially for whom once gave me help and instruction, like Dr. A Zare Shahneh and Bing Xia.

I also have to say great thanks to my sponsor, Commercial Aircraft Corporation of China, Ltd, for giving me such a chance studying in Cranfield University.

Finally, I would like to say immense thanks to my parents for raising me up and giving me love and encouragement all the time.

TABLE OF CONTENTS

LIST OF FIGURES

LIST OF TABLES

LIST OF EQUATIONS

LIST OF ABBREVIATIONS

ACCS	Air Cycle Cooling System
ACS	Air-conditioning System
ACM	Air Cycle Machine
AIS	Anti-icing System
APU	Auxiliary Power Unit
BACS	Bootstrap Air Cycle System
BAS	Bleed Air System
CBV	Cross Bleed Valve
COMAC	Commercial Aircraft Corporation of China, Ltd
CPCS	Cabin Pressure Control System
CPCV	Cabin Pressure Control Valve
ECS	Environmental Control System
EE Bay	Electronic-Electrical Bay
EPS	Electrical Power System
FCV	Flow Control Valve
HPWS	High Pressure Water Separation System
ID	Ice Detector
IDS	Ice Detection System
IPCV	Intermediate Pressure Check Valve
LPWS	Low Pressure Water Separation System
IRP	Individual Research Project
ISA	International Standard Atmosphere
MHE	Main Heat Exchanger
MTBF	Mean Time Between Failures
PHE	Primary Heat Exchanger
PRSOV	Pressure Regulating and Shut-Off Valve
REH	Reheater
CON	Condenser
RFAN	Recirculation Fan
TAV	Trim Air Valve
TBC	To Be Confirmed
WAIS	Wing Anti-icing System

WAIV	Wing Anti-icing Valve
WE	Water Extractor

1 INTRODUCTION

1.1 Background and Motivation

Currently, almost all the Environmental Control System (ECS) on civil transportation aircrafts need to bleed air from the engines. This contributes greatly towards providing a life support environment to the passengers and crew members. But it is acknowledged that bleeding air from engines affects the engine thrust performance and results in higher fuel consumption. It has been stated that 3%~5% power produced by the engines is consumed by the system [1]. On the other hand, different ECS configurations bring different system weights, costs and reliabilities. Therefore, it is quite important to make the relationship harmoniously among cabin comfort requirement, bleed air requirement and system cost. Based on related research, the current challenges encountered in the aviation industry mainly include three aspects, ‘reduction of power consumption, better overall reliability with free of scheduled maintenance and improved passenger comfort [2].

According to the information comes from COMAC Market Forecast, there will be around 35,000 aircrafts operating in the world till 2029, while 78% of them are the single-aisle trunk-liners and regional airliners. Based on the statistics which will be shown later, most of the single-aisle trunk-liners and regional airliners have been using a three-wheel bootstrap air cycle system. And the three-wheel bootstrap air cycle system consists of two subsystems, which are the low pressure water separation system and the high pressure water separation system. Although both of them are used on the civil transportation aircrafts, which configuration would be better when it is aiming at a specific aircraft can be judged only after analysis and comparison.

At the same time, due to the development of simulation, it is possible to simulate a complete system and find out corresponding variation trend by using simulation software like Matlab/Simulink. This is very helpful to choose, evaluate and improve system efficiency, and even to deal with the problems

that occur after the aircraft is delivered. The simulation models can also be used as both teaching and practical industrial design.

1.2 Aims and Objectives

The aim of this Individual Research Project (IRP) is to analyze and compare the different ram air mass flow and turbine expansion ratio of the three-wheel low and high pressure water separation system by Matlab/Simulink under the same mix manifold inlet temperature based on a specific aircraft. Finally a conclusion is made regarding the better configuration for the aircraft during cruise. The data about system weight, economic cost and reliability from related research are also attached in order to help making decision.

In order to finish such a goal, the objectives mainly consist of three aspects. The first task is to calculate the cabin heat load which is caused by the fuselage wall, the solar radiation, the aircraft occupants and the electronic-electrical equipments. Then, a specific aircraft is defined, which is mainly about the thickness and material of different layers of the fuselage wall, the area of aircraft transparent area, the number of occupants and the flight profile. The third but the most important task is to build simulation model for each of the component based on the fundamental knowledge of heat transfer and aerodynamics, the working principles and mechanical dimensions of the components, the ambient environmental parameters and some data from Airbus 320. Finally, the assembled model can be used to do demanded analysis and comparison after the validity is confirmed.

1.3 Structure of the Thesis

Chapter 2 explores the background to the research topic. In noting the aircrafts launched dates and the adopted type of Bootstrap Air Cycle System, the system development trend can be discovered. Then the key points are summarized and the research topic is identified.

Chapter 3 introduces the research method based on the background, objectives, and related methodologies. A flow chart is depicted to describe required inputs and the research process.

Chapter 4 illustrates the heat sources of cabin heat load. The common calculation method is adopted and related statistics is used to verify the calculation result. The flight phase chosen as the research object is also discussed.

Chapter 5 defines a specific aircraft which uses the three-wheel bootstrap air cycle system. The parameters are about the fuselage wall, aircraft transparent area, cabin layout and comfort requirements, which are mainly cited from Airbus 320. Meanwhile, a flight profile is defined for the specific aircraft since it will be used to calculate the temperature of fuselage skin.

Chapter 6 analyzes the ECS components according to the parameters provided by the supplier, the state point data from Airbus 320 and some estimation based on related research and engineering experience. It is the basis for building models by Matlab/Simulink.

Chapter 7 uses Matlab/Simulink to build corresponding models for both of the low and high pressure water separation system in terms of the analysis shown in Chapter 6. Then, under the precondition that both of the two configurations need to satisfy the same mix manifold inlet temperature, the required ram air mass flow should meet related research result and temperature of the key state points should have small deviation compared with that on Airbus 320.

Chapter 8 shows the required engine bleed air mass flow for both of the two configurations at first. Then, two conditions that the turbine expansion ratio is the same and the ram air mass flow is the same are discussed respectively, which are used to find out the different requirements about the ram air mass flow and turbine expansion ratio. Finally the results and discussion are drawn.

Chapter 9 draws a conclusion about which configuration is better for the specific aircraft, what are the limits, and describes further research which can be done in the future work.

2 LITERATURE REVIEW

2.1 Necessity of ECS

In order to achieve a lower specific fuel consumption and improve the comfort during flight, almost all the modern commercial transportation airliners have a cruise altitude of no less than 32,800ft (10,000m). For example, the typical cruise altitude of Boeing 737-800 is 35,000ft and the economical cruise altitude of Airbus 320 is 37,000ft. But people can not survive in such an atmosphere of that altitude if exposed to the environment. It is stated that the atmospheric pressure is about 19.4kpa at an altitude of 12km, where half of the passengers would die in 5 minutes [3]. Figure 2-1 shows the environmental parameters at different altitudes. Therefore, it is obviously that the aircrafts flying over 10,000ft must be equipped with an ECS, so as to protect the passengers and crew members from the ambient environment of low temperature, low pressure and nearly an absolute humidity of zero.

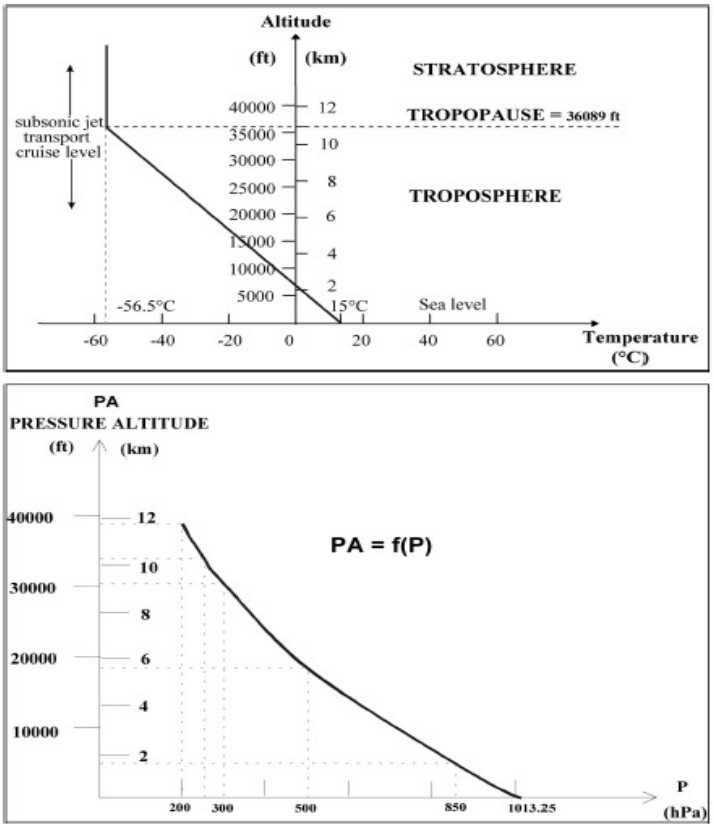

Figure 2- 1 International standard atmosphere [4]

2.2 Importance of the Classic ECS

Nowadays, almost all the civil transportation aircrafts need to bleed air from the engines or APU as the source of ECS. Although the Boeing 787 Dreamliner has changed to adopt the no-bleed air configuration, other new generation aircrafts, such as the Airbus 320neo, Airbus 350XWB, Boeing 737max and Bombardier CSeries are still using the conventional pneumatic system that bleeds air from the engines. The concept that more-electric and all-electric aircraft is an inevitable development trend can be shared because they indeed have many advantages, like consuming less fuel, producing less air pollution and having higher efficiency than the conventional configuration. But it is obviously that there would be a long way for achieving such a goal, especially for the large commercial aircrafts. Huge power requirement and complicated system configuration are difficult to deal with. For instance, Boeing 787 has been forced to stop flight for three months because of the problem caused by big power lithium battery. Moreover, the research cost and development is also an important factor which can not be ignored. Therefore, to analyze and optimize the classic ECS is still meaningful.

Firstly of all, the classic ECS has been used for more than 50 years and it has been regarded as a mature technology. For the no-bleed air configuration which is used on Boeing 787, although Boeing stated that the configuration has evident advantages on weight and fuel consumption, the engine suppliers RR and GE stated that no-bleed is similar with bleed based on the engine cycle impact, and the system reliability and the maintenance costs are TBC [5]. This means the no-bleed air configuration still needs test through a long term operation and the advantages still need verification.

Secondly, even if the bleed air system of classic ECS will be replaced by the no-bleed air system in the future, to analyze and optimize the classic ECS is still significant, all the civil transportation aircrafts running now in the world are using such a configuration except Boeing 787. These aircrafts can not be replaced in a short term and the number is still continually increasing.

Taking the Airbus as an example, according to the data published in January 2013, there were 588 aircrafts be delivered in 2012 and at least 4682 aircrafts will be delivered in the next ten years as shown in Table 2-1. The ECS of all these aircrafts are based on the conventional engine bleed air system. Since the lifespan of an aircraft is about 30 years, it is absolutely that the conventional engine bleed air system is still important in the aircraft systems and it will keep a long-term importance in the future.

Table 2- 1 Airbus Summary Results (2003-2012) update on Jan 2013 [6]

Year	2003	2004	2005	2006	2007	2008	2009	2010	2011	2012
Aircraft orders (gross)	284	370	1111	824	1458	900	310	644	1608	914
Cumulative orders (net)	4886	5252	6307	7097	8438	9215	9486	10060	11479	12312
Aircraft deliveries	305	320	378	434	453	483	498	510	534	588
Cumulative deliveries	3432	3752	4130	4564	5017	5500	5998	6508	7042	7630
Order backlog	1454	1500	2177	2533	3421	3715	3488	3552	4437	4682

2.3 Introduction of the Classic ECS

On one hand, in order to create a comfortable environment in the aircraft cabin, ECS needs to regulate the temperature, pressure, humidity and airspeed of the airflow and makes sure air in cabin is in good quality. On the other hand, ECS is also responsible for preventing some parts of the aircraft from icing or melting the formed ice in time. Thus the classic ECS can be regarded as consists of four subsystems, which are the Bleed Air System (BAS), the Air Conditioning System (ACS), the Cabin Pressure Control System (CPCS) and the Anti-icing System (AIS). These four subsystems are not independent. For example, the Bleed Air System is the source of the other three systems thus the temperature

of the bleed air must meet the requirements from both the Anti-icing System and Air Conditioning System. The typical configuration of a classic ECS is shown in Figure 2-2.

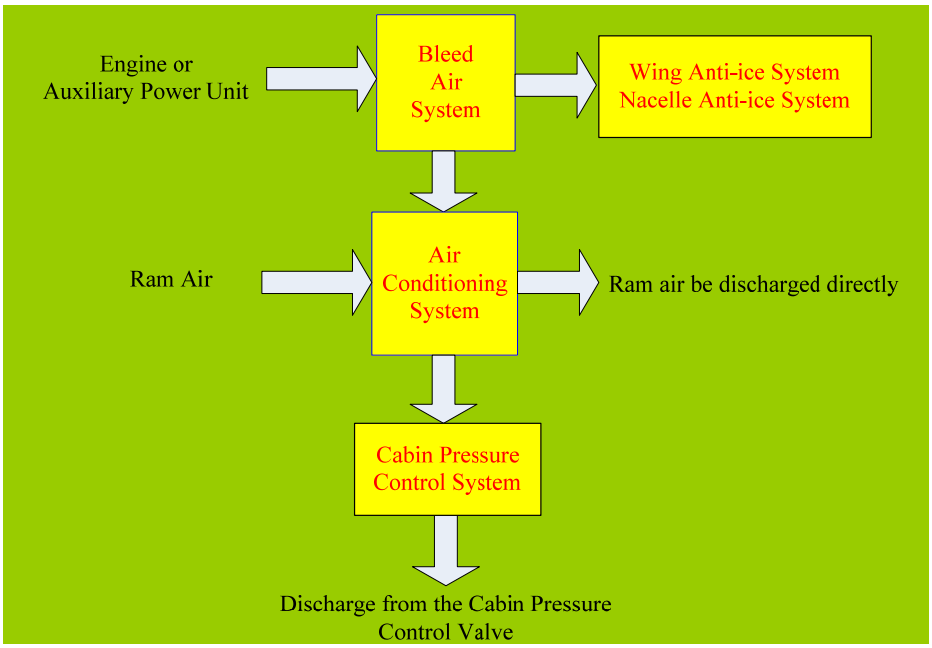

Figure 2- 2 Configuration of a typical ECS

2.3.1 Bleed Air System

The Bleed Air System provides compressed air to the downstream air utilization systems from the engines or Auxiliary Power Unit (APU). The configuration of a conventional engine bleed air system of a turbofan aircraft is shown in Figure 2-3, while the actual configuration may be modified based on practical requirements.

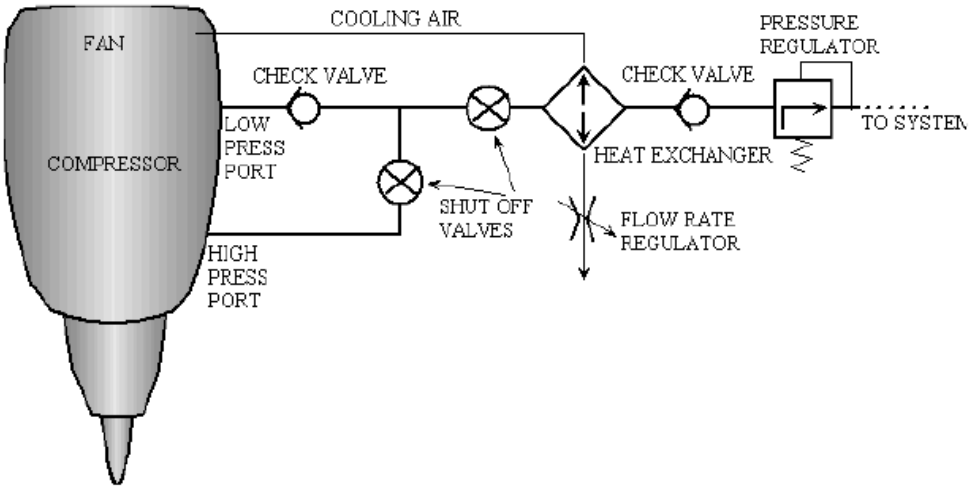

Figure 2- 3 Bleed air system of classic ECS [7]

It can be seen that aircraft can bleed air from two different ports of the engine compressor. One is the low pressure port at the intermediate stage of the engine. The other one is the high pressure port at the final stage of the engine. During most of the time in flight, bleeding air from the low pressure port is adequate for the ACS and CPCS. When the bleeding air is not sufficient because the engine is operating in the low engine power or considerable airflow quantity is required, such as when the Wing Anti-icing System (WAIS) or the nacelle anti-icing system is operating, the system would switch to the high pressure port automatically.

The heat exchanger and the cold air from the fan work together to regulate the temperature of the airflow comes from the engine by discharging excess energy into the atmosphere. It makes sure that the regulated air can be used to the wing anti-icing system directly and would not damage the ducts that are used in the system. At the same time, it also ensures the high temperature airflow is as acceptable to the downstream air conditioning pack. Therefore, normally the outlet temperature of the engine bleed air system should be higher than 180℃ but less than 250℃.

The Check Valve located at the low pressure duct now is always named as Intermediate Pressure Check Valve (IPCV). Its function is to prevent the airflow flowing from the high pressure port to the low pressure port.

The shut off valve locates at the high pressure duct is to control the high pressure bleed air function. It opens automatically when the low pressure port bleed air can not satisfy the requirements from downstream systems. The shut off valve and pressure regulator which are located at the main duct now always be integrated and named the Pressure Regulating and Shut-off Valve (PRSOV). It regulates the airflow from the engine to the downstream systems according to pressure and temperature signals. The valve can be shut off automatically or manually once some extreme conditions appear, such as the bleed air is over-pressure or over-temperature, or the engine is catching fire.

There is another important equipment in the bleed air system named as Cross Bleed Valve (CBV). It is located between the left and right bleed air system. Normally the valve is on the closed position. It isolates the left and right bleed air system to avoid the whole system failing if there is leakage in one side of the bleed air system. At the same time, when one side bleed air is failed or the ground pneumatic cart is supplying high pressure air to the aircraft, opening the CBV can balance the airflow requirements for the downstream air utilization systems.

2.3.2 Anti-icing System

According to the certification guidance defined in FAR Part 25, it can be predicted that some parts of the aircraft probably get icing during some flight phases, mainly during ground, take off, climb, descent and landing, which is related with the cloud liquid water content, the mean effective diameter of the cloud droplets and the ambient air temperature of the atmospheric environment [8].

Figure 2-4 depicts the limiting icing envelope in terms of altitude and temperature which is defined in Appendix C of FAR Part 25. It can be seen that when the flight altitude is less than 6,700m (22,000ft) and the ambient temperature is less than 0℃, the aircraft has the risk of getting ice.

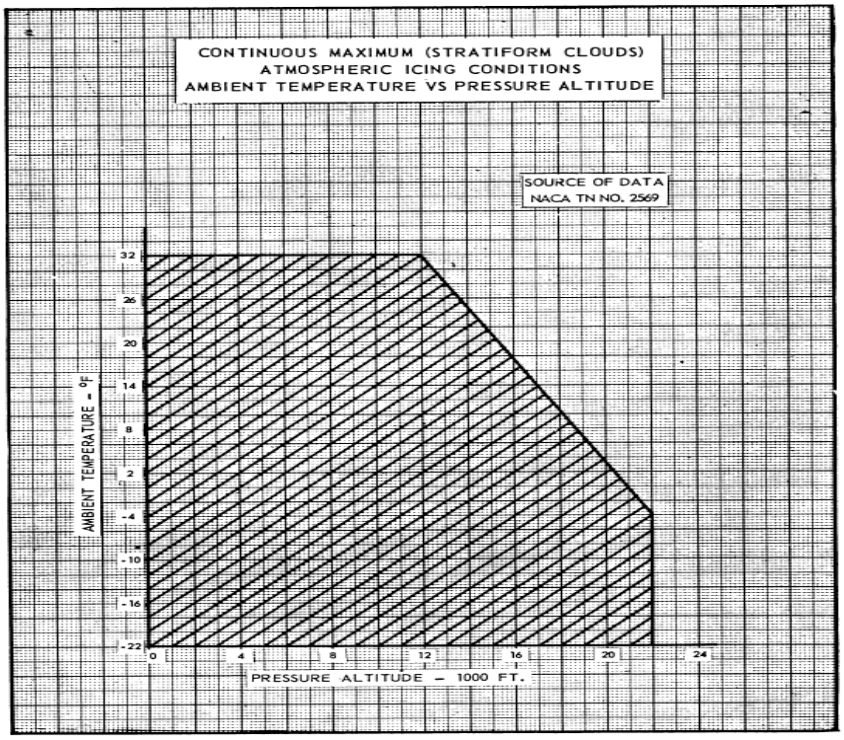

Figure 2- 4 The limiting icing envelope in terms of altitude and temperature [8]

Icing is a quite adverse condition that may cause a disaster, like the American Eagle ATR-72 in 1994 and the EMB-120 in 1997. Normally, the Ice Detection System (IDS) sends signals to the aircraft to indicate the icing environment so that the anti-icing system can start to operate automatically. When the pilots want to activate the system manually, they can switch the control button on the cockpit control panel. The pilots also can shut off the system manually if there is any leakage, over-pressure or over-temperature.

The anti-icing system of classic ECS mainly consists of three parts, the wing anti-icing system, the nacelle anti-icing system and the windshield anti-icing system. Because the nacelle anti-icing system is integrated in the engine and it has an independent pathway compared with the wing anti-icing system, and the windshield anti-icing system uses resistance heating instead of consuming the engine bleed air, thus the wing anti-icing system is the only one introduced here.

The wing anti-icing system is used to prevent some of the wing leading edge slats from icing and ensure the formed ice can be removed instantly. The typical system configuration is shown in Figure 2-5.

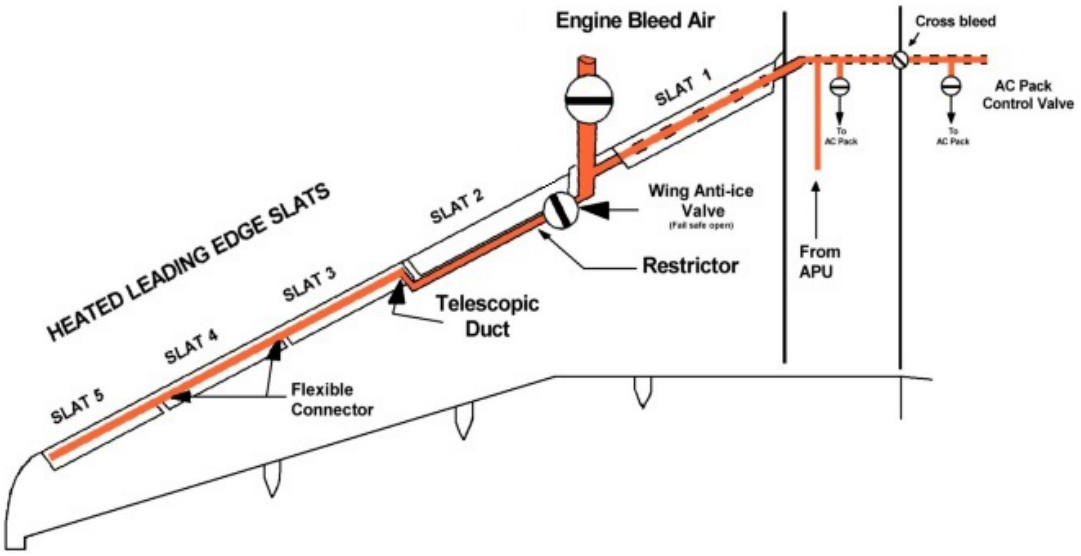

Figure 2- 5 Configuration of a typical Wing Anti-icing System [9]

The engine bleed air is regulated by the engine cooling air when it goes through the heat exchanger as shown in Figure 2-3. Then the WAIS can use the hot air directly to prevent icing or remove ice. First of all, the hot air goes through a component named Wing Anti-Icing Valve (WAIV). The WAIV is a regulating valve and also has the function of shutting off the system. It regulates the inlet air mass flow and provides protection to the system from over-pressure or over-temperature damage. It can be controlled either automatically or manually. The Ice Detector (ID) sends signals to trigger the system if it is on the automatic control mode. When the pilots decide to start the system based on observation, they also can activate it manually.

After passing through the WAIV, the hot air enters the venturi, which is used to limit the air mass flow and speed it up. There are also some temperature, pressure and flow sensors in the system. They feedback the signals to the system controller and help it to control the opening angle of the WAIV.

Finally, the regulated air with suitable pressure and temperature is diffused in the slats to prevent icing or melt the ice. If the system failed, the aircraft should descend and find the nearest airport for landing as soon as possible because ice on the leading edge may probably stall the aircraft.

2.3.3 Air Conditioning System

As Section 2.1 introduced, half of the passengers can not survive for even 5 minutes if exposed to the ambient environment when the aircraft is flying at a high altitude, thus the ECS must provide a life support environment to the aircraft occupants. The Air Conditioning System (ACS) is one important part of the ECS and it is focusing on such requirement.

The ACS can be divided into three parts based on different subsystem functions, which are the air conditioning packs, the recirculation system and the air distribution system. The typical configuration of an ACS is shown in Figure 2-6.

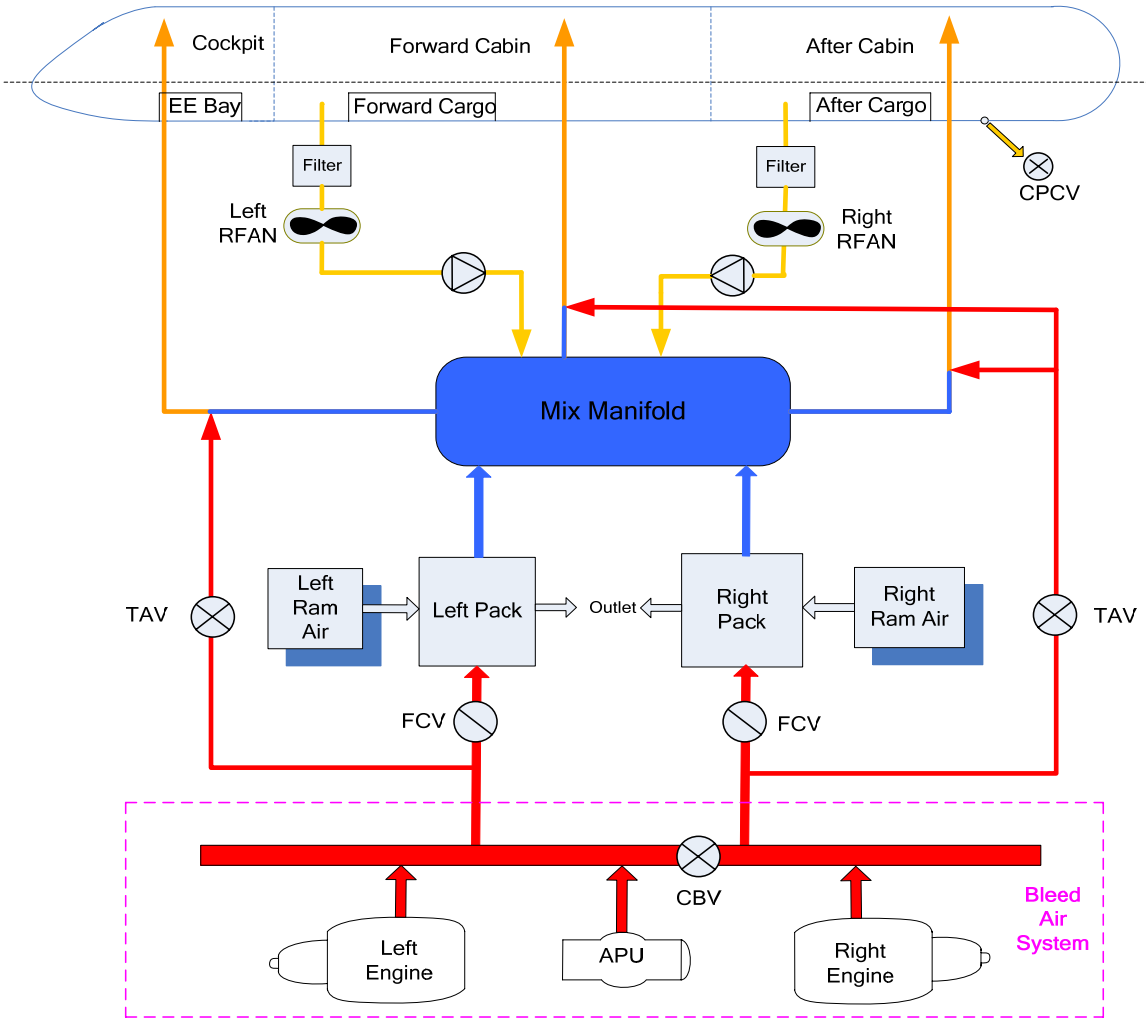

Figure 2- 6 Configuration of a typical Air Conditioning System

Table 2- 2 Explanation of Figure 2-6

Item No.	Symbol or Abbreviation	Explanation
1		Hot Air
2		Warm Air
3		Cold Air
4	EE Bay	Electronic-Electrical Bay
5	RFAN	Recirculation Fan
6	CPCV	Cabin Pressure Control Valve
7	TAV	Trim Air Valve
8	FCV	Flow Control Valve
9	CBV	Cross Bleed Valve

Note: The schematic neglects some mechanical components which do not need analysis in this research, such as the check valves and safety valves.

2.3.3.1 Air Conditioning Packs

The bleeding air from engines or APU firstly passes through the Flow Control Valve (FCV). FCV regulates the inlet air mass flow and supplies stable airflow to corresponding air conditioning pack. It also has the function of shutting off the air supply when required. Trim Air Valve (TAV) is used to control the flow rate of inlet hot air from engine or APU to the air supply duct.

The air conditioning packs are the core components of the ACS. It regulates the air comes from the engines or APU to a regular temperature and pressure that can be delivered to the cabin after mixing with the recirculated air. Normally each pack would provide 50% of the required airflow to the cabin. When one pack failed, another pack can operate at 180% nominal flow rate to meet the

requirement [2]. If both of the two packs are failed, the aircraft should descend to the safety altitude and use ram air to regulate the cabin temperature directly. The structure of a typical air conditioning pack which uses a Bootstrap Air Cycle System is shown in Figure 2-7. The configuration is the most common choice adopted by the civil transportation aircrafts.

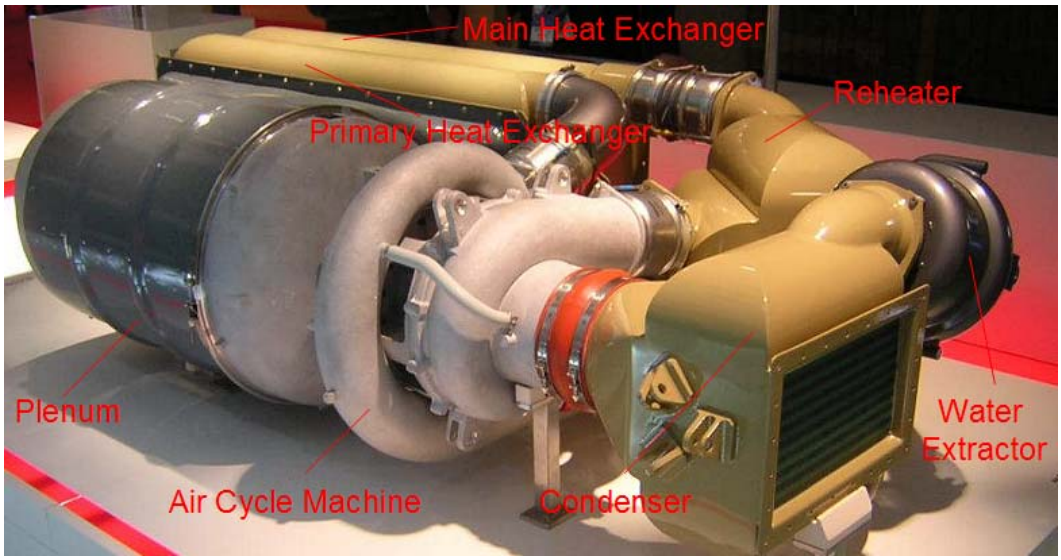

Figure 2- 7 Configuration of a typical air conditioning pack [10]

The system sketch for such a configuration is shown as follows.

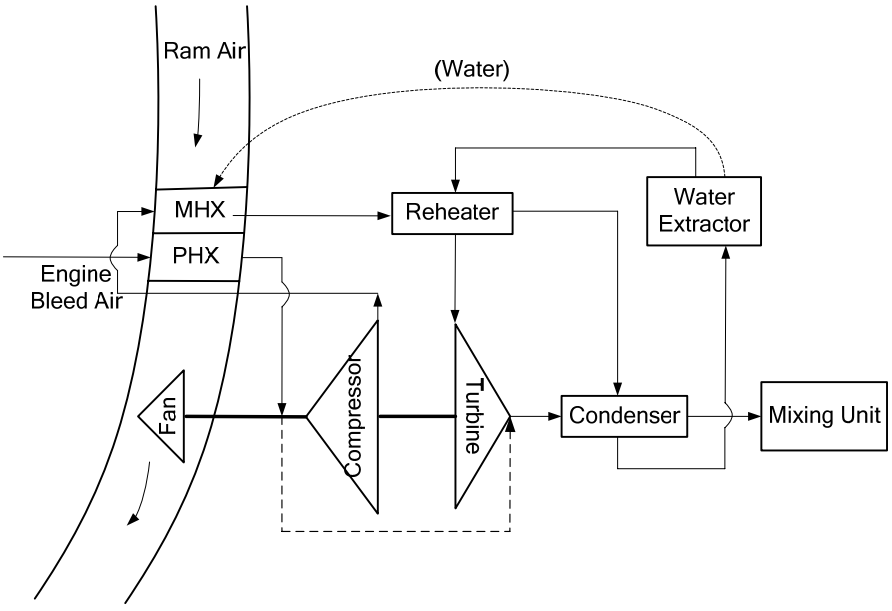

Figure 2- 8 System sketch of a typical air conditioning pack

Combing the information shown in Figure 2-7 and 2-8, the main components list and their functions in an air conditioning pack are described in Table 2-3.

Table 2- 3 Functions of the main components in an air conditioning pack

Component Name	**Function**
Primary Heat Exchanger (PHE)	Cool the airflow before it enters corresponding Air Cycle Machine (ACM) compressor
Main Heat Exchanger (MHE)	Cool the discharged airflow comes from the ACM compressor
Air Cycle Machine (ACM)	Compressor: compress the hot air to a higher pressure that a required expansion ration can achieve in the turbine Turbine: cool the airflow and produce power to drive the coaxial compressor and fan Fan: generate or increase ram air mass flow for the heat exchangers when the aircraft is landing on the ground or at low altitude flight
Reheater	Reduce the temperature difference between the main heat exchanger outlet and the turbine inlet, reduces the free water content before it enters the turbine, and increase the efficiency of the turbine
Condenser	Use turbine outlet air to cool the airflow to a enough level that moisture can be condensed for subsequent removal by the water extractor
Water Extractor	Collect water droplets and sprays it to ram air inlet to increase the efficiency of the MHE

Component Name	Function
Plenum	Conduct the airflow discharged from the PHE and prevents reverse airflow.

Although the principle of each Air Cycle Cooling System (ACCS) is almost the same, the configurations of the exact air conditioning packs are different for they have to meet different performance requirements of different aircrafts. However, it can be counted that there are only five types of ACCS have been used on the civil transportation aircrafts till now as shown in Table 2-4. In order to find out the trend of development, not only the aircraft types and system configurations are stated, but also the launched years are attached.

Table 2- 4 Introduction of the types of civil aircraft ACCS

Aircraft Type	Launched Year	Low pressure water separation system		High pressure water separation system		
		Two-wheel bootstrap cycle	Three-wheel bootstrap cycle	Two-wheel bootstrap cycle	Three-wheel bootstrap cycle	Four-wheel bootstrap cycle
B727	1965	▲				
DC-10	1966		▲			
A300	1969		▲			
MD-80	1977	▲				
A310	1978		▲			
B767	1978				▲	

Aircraft Type	Launched Year	Low pressure water separation system		High pressure water separation system		
		Two-wheel bootstrap cycle	Three-wheel bootstrap cycle	Two-wheel bootstrap cycle	Three-wheel bootstrap cycle	Four-wheel bootstrap cycle
B757	1979				▲	
B737-300	1981	▲				
AIRBUS 320	1984				▲	
B747-400	1985		▲			
MD-11	1985	▲				
B737-400	1986			▲		
B737-500	1987	▲				
A330	1987				▲	
A340	1987				▲	
MD-90	1989	▲				
B777	1990					▲
MD-95	1991		▲			
B737-700	1993		▲			

Aircraft Type	Launched Year	Low pressure water separation system		High pressure water separation system		
		Two-wheel bootstrap cycle	Three-wheel bootstrap cycle	Two-wheel bootstrap cycle	Three-wheel bootstrap cycle	Four-wheel bootstrap cycle
A380	1994					▲
B737-800	1994				▲	
B737-600	1995		▲			
B737-900	2000				▲	
B747-800	2005				▲	
C919	2008				▲	
Total		6	7	1	9	2

Based on the statistics shown in Table 2-4, four key points about the Bootstrap Air Cycle System are summarised related to this research.

Δ Most of the civil transportation aircrafts utilized low pressure water separation system before 1980.

Δ The number of aircrafts using high pressure water separation system increased continually between 1981 and 1989.

Δ The high pressure water separation system began to predominate from 1990 but the low pressure water separation system has not disappeared.

Δ The super large aircrafts are more likely to use four-wheel high pressure water separation system, such as the Boeing 777 and Airbus 380.

At the same time, it can be stated that Airbus never uses low pressure water separation system since Airbus 310, while Boeing still chose the low pressure water separation system on Boeing 737-700 in 1993. Although the high pressure water separation system has many advantages, such as high efficient water separation function, high efficient cooling function and less system congestion, the low pressure water separation system also has many advantages like fewer accessories, less mass and lower cost, so that some manufacturers are still willing to use it [11].

But in general, it can be stated that the three-wheel water separation system has been playing an important role in Bootstrap Air Cycle System since 1978. For the next new generation aircrafts, such as Boeing 737MAX and Airbus 320neo, it can be speculated that they will probably use this type of configuration.

The configuration of a typical three-wheel low pressure water separation system is shown in Figure 2-9.

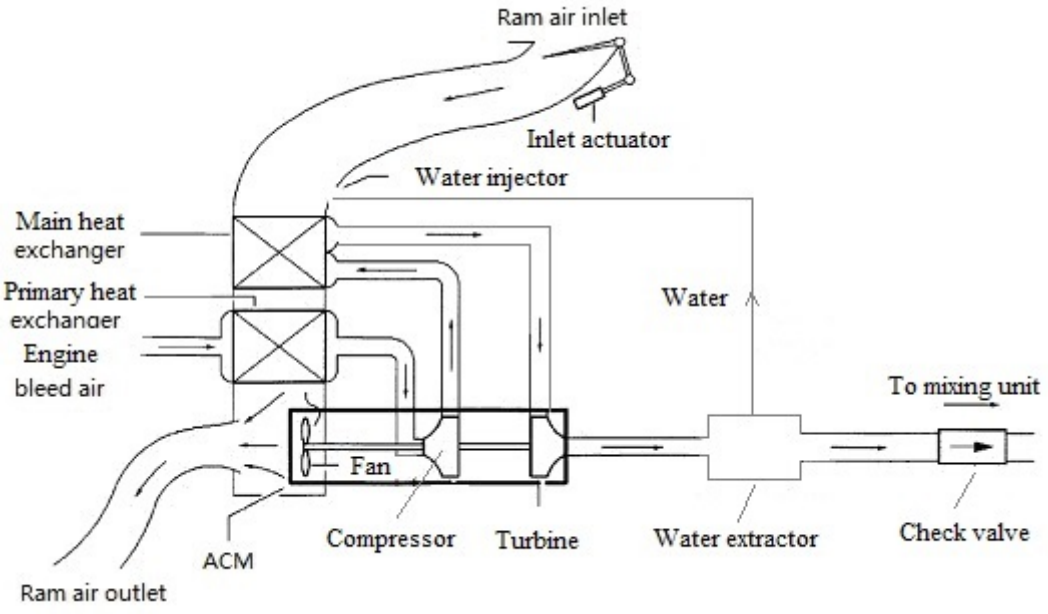

Figure 2- 9 Configuration of a typical three-wheel low pressure water separation system [12]

In such a configuration, the engine or APU bleed air firstly flows to the ACM compressor after being cooled by the PHE. Then the high pressure and temperature compressed air is delivered to the MHE to be cooled to appropriate temperature. After that the ACM turbine expands the air to decrease the temperature and pressure, and drives the coaxial compressor with 85% expansion power and fan with 15% expansion power [13]. Then, the water extractor separates the water from the ACM discharged airflow where the vapour has been cooled under the dew point, and sends it to the ram air inlet to increase the MHE efficiency. Finally, cold dry air with suitable temperature and pressure flows into the mixing unit to mix with the recirculated air and then be delivered to the cabin and cockpit.

The configuration of a typical three-wheel high pressure water separation system is shown in Figure 2-10.

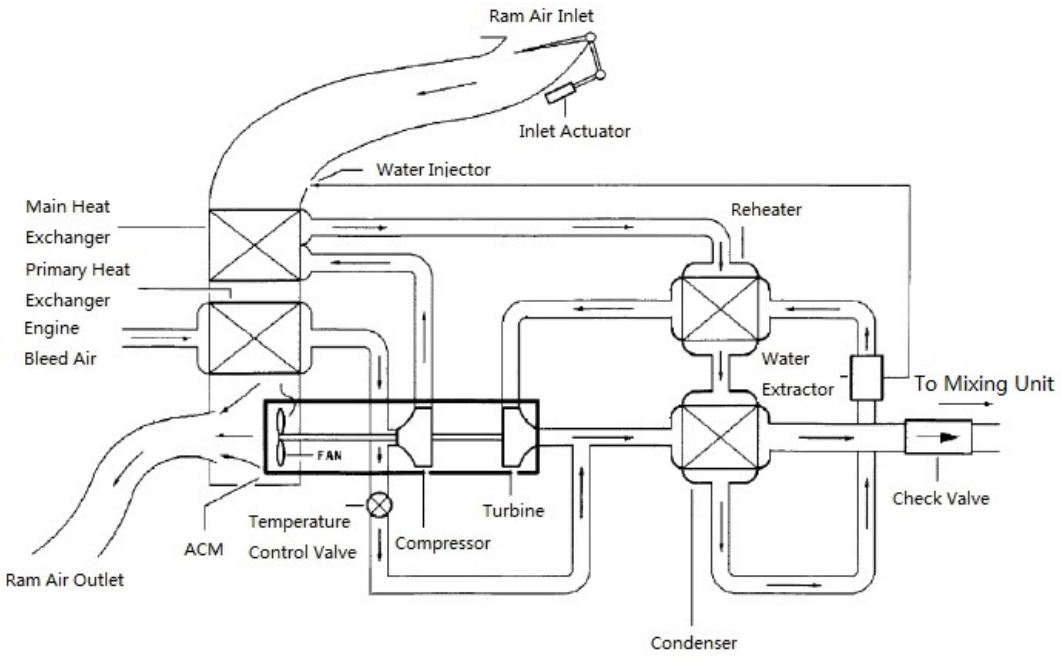

Figure 2- 10 Configuration of a typical three-wheel high pressure water separation system [12]

The high pressure water separation system consists of three components, reheater, condenser and water extractor. Bleeding air from the engine or APU firstly passes through the PHE. Then the ACM compressor compresses the air

to a higher pressure so that the downstream turbine would be more efficient. After be cooled again in the MHE, the airflow flows to the reheater. The first time the airflow goes through the reheater, it is cooled by the condenser outlet air. Then the condenser cools the air further by utilizing the cold air discharged from the turbine. Moisture is separated as droplets when the dew point is achieved after the two steps. After entering the water extractor, the droplets are extracted. Then the airflow passes through the reheater again. This time the airflow is reheated by the hot air comes from the MHX so that no free water is delivered into the turbine. After the temperature and pressure is decreased to appropriate values in the turbine through adiabatic expansion, the air then is delivered to the mixing unit.

Besides, there always is a Temperature Control Valve (TCV) in front of the compressor as shown in Figure 2-10. It is used to help adjust the turbine outlet temperature and remove the possible downstream ice.

2.3.3.2 Recirculation System

The recirculation system is to recycle part of cabin hot air from the under floor area to the mixing unit so that less airflow is required from the engines or APU. This configuration has been adopted by most of the modern civil transportation aircrafts because it leads to less fuel consumption. For example, more than 40 million gallons of fuel would have been wasted for the 767 fleet to date if the cabin was supplied with 100% engine bleed air [14]. At the same time, because of the low humidity at high altitude, to use the cabin recirculation air also helps the air conditioning system to improve the humidity in the cabin. Thirdly, utilization of the recirculation air can reduce the temperature difference between the cabin air and input fresh air so that passengers would feel more comfortable. At last but the most important, many studies have proved that this configuration can meet all the applicable safety and health regulations and standards [15].

The configuration of a typical recirculation system is shown in Figure 2-11. It can be seen that the recirculation system consists of just two components besides the ducts, which are the recirculation filter and the recirculation fan.

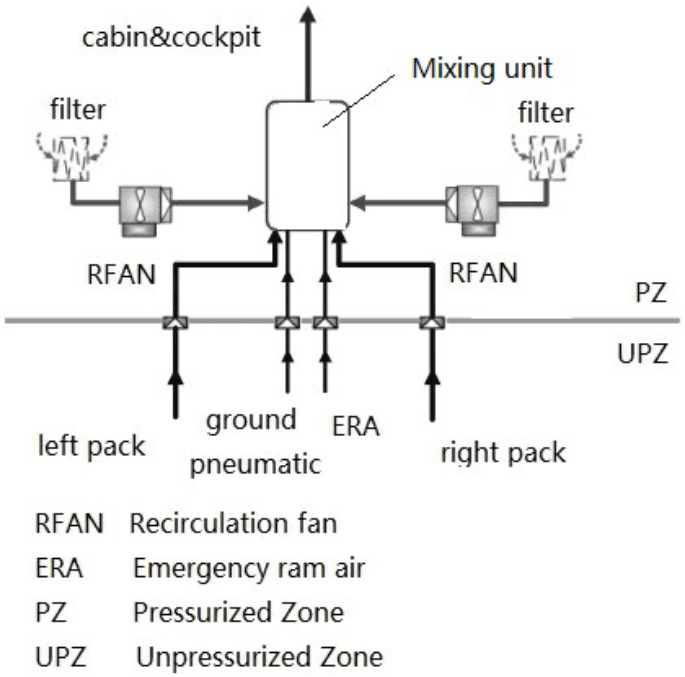

Figure 2- 11 Configuration of a typical Recirculation System [16]

After the airflow passes through the cabin, it is discharged to the under floor area. Then the recirculation fans extract the air from the cargo triangle area and deliver it to the mixing unit. Normally, the ratio between fresh air and recirculation air is from 40% to 60% in the mixing unit [17]. The recirculation filters are used to filtrate the recirculation air so that there would be no harmful and infectious substances spreading in the cabin.

2.3.3.3 Air Distribution System

After the mixture of fresh air and recirculated air in the mixing unit, the low temperature conditioned air can be delivered to the air distribution system. Before it enters the cabin, the Trim Air Valve (TAV) may add small among of hot air into the ducts so that the cabin inlet air temperature can be suitable, which are normally between 10℃ and 12℃ [11].

Normally, small civil transportation aircraft can be regarded as only consists of two zones. The air conditioning system supplies conditioned air to the cockpit and cabin respectively. For large civil transportation aircrafts, in order to control the cabin temperature more accurately, the cabin can be divided into two or

three zones like represented in Figure 2-6. The architecture of a typical air distribution system is shown in Figure 2-12.

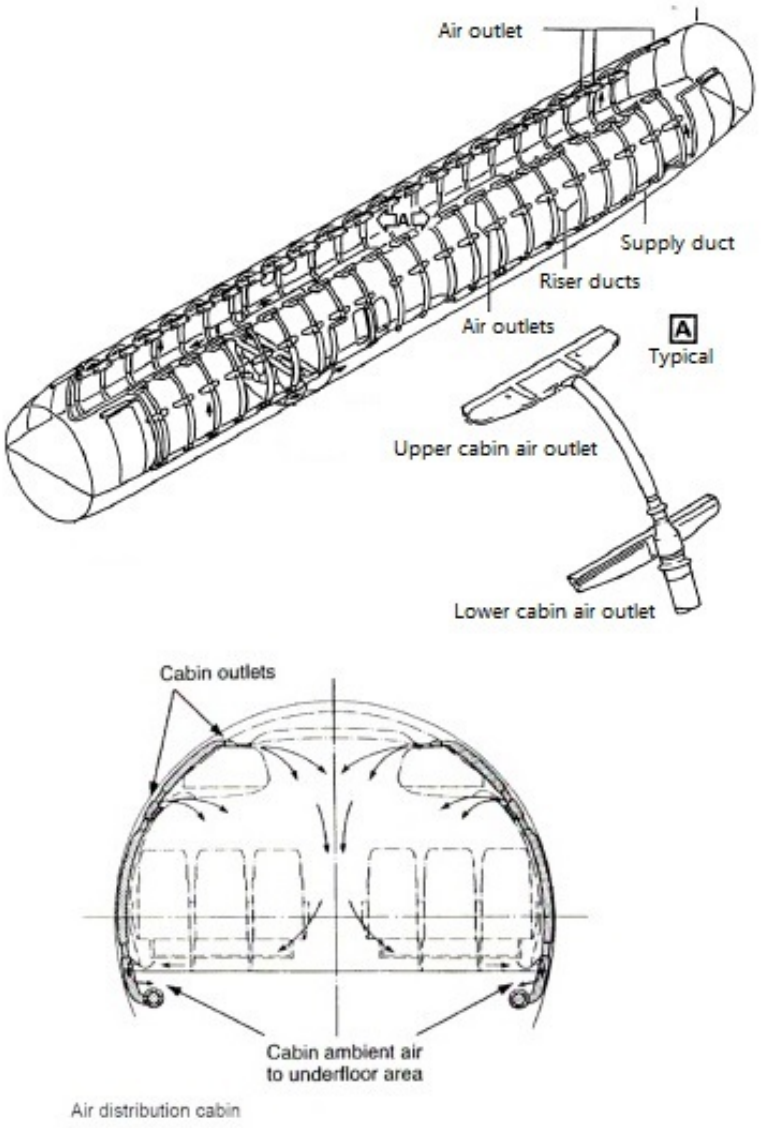

Figure 2- 12 Architecture of a typical air distribution system [12]

The air distribution system not only ensures that required airflow can be provided to the cabin, but also arranges how the airflow flows so that passengers could not feel obvious temperature variation, air movement and noise. At the same time, temperature in the Electronic-Electrical Bay should be regulated for keeping equipments work normally. The cargo temperature may be controlled when the aircraft transfers live animals. Ventilation of galley and

lavatory also should be provided. And the waste air should be discharged from the aircraft in time.

2.3.4 Cabin Pressure Control System

As mentioned in Section 2.1, the atmospheric pressure is about 19.4Kpa at an altitude of 12Km, where people would die in 5 minutes. On the other hand, aircraft structure may be damaged because of the over great inside and outside differential pressure during flight. Therefore, to maintain the cabin pressure in a suitable range is one of the most important tasks of the aircraft ECS.

Although there are no official requirement from US and European governments about the aircraft cabin pressure, there is certification requirement which requires the aircraft must be able to maintain a pressure equivalent to an altitude of 8,000ft when it is at the maximum flight altitude under normal operation conditions [17]. FAR Part 25.841 have the clear definition about this requirement. This value has taken both the cabin comfort and aircraft structure fatigue into consideration. With the development of new structural material, Boeing 787 has changed the value from 8,000ft to 6,000ft to improve the cabin comfort. This is a great improvement of aircraft cabin pressure control system.

The pressure regulating function is achieved by the Cabin Pressure Control Valve (CPCV) on most of the aircrafts, while some aircrafts use two valves to control the cabin pressure, like C919. The change of opening angels of CPCV modulates the rate of outlet airflow so that required cabin pressure and rate of pressure change can be satisfied. The CPCV always locates at the aircraft rear fuselage as shown in Figure 2-13.

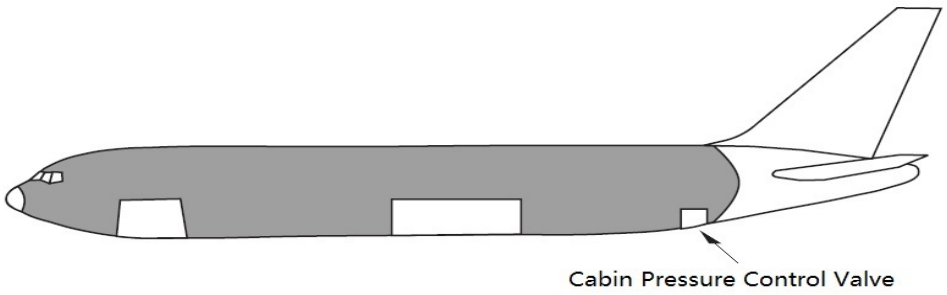

Figure 2- 13 A typical layout of a Cabin Pressure Control Valve [14]

There are two other cabin pressure control valves normally named as the Positive Pressure Release Valve and Negative Pressure Release Valve in the system. When the differential pressure between the outside and inside of the aircraft exceeds the bearing capability of the structure, corresponding valves will be fully open to prevent the aircraft from explosion.

2.4 Related Methodologies

The ECS can provide a life support environment to the passengers and crew members so that the aircraft can fly at a high altitude with relatively low specific fuel consumption. However, it indeed consumes much energy and influences the thrust performance of engines considerably. At the same time, the system needs to increase its cooling capability with more and more electronic devices being used in the aircraft systems that the heat load is increasing continually [18]. Therefore, to analyze and improve the system capability so that the aircraft can provide a more comfortable cabin, consume less energy and deal with the increased heat load becomes a significant engineering research project. Till now many researchers have done some work aiming at balancing the relationship among system configuration and corresponding influences. Among them two methodologies are introduced as follows.

2.4.1 FLECS

FLECS (Functional Mode Library of the Environmental Control System) offers a library with generic models from small ECS components up to the whole aircraft cabin [19]. The exact method of the FLECS is to simulate the ECS with Matlab/Simulink based on aircraft generalized volume, mass flow resistance and heat flow resistance.

Before the FLECS is set, a large number of investigations have been done on different types of aircrafts. Then a relative better ECS configuration is selected as the basic configuration according to the simulation and comparison results. After that, the system is analyzed in detail by separating each component into an individual part and a new ECS model is set based on the generalized and reassembled component models. Generally, the cabin model is simulated as a

combination of volume and heat transfer unit. Cabin heat transfer analysis is based on the heat convection, conduction and radiation activities. The ducts can be modelled with the help of a generalised flow resistance and volume element then the air distribution system can be assembled by these duct models. Other components in the system can be modelled based on mass flow resistance or heat flow resistance principles and the state equations for different flight phases must be defined clearly.

According to practical utilization of this methodology on Airbus 340-600, the simulation result of cabin inlet temperature had a good agreement with the measured values. Figure 2-14 shows the matching relationship.

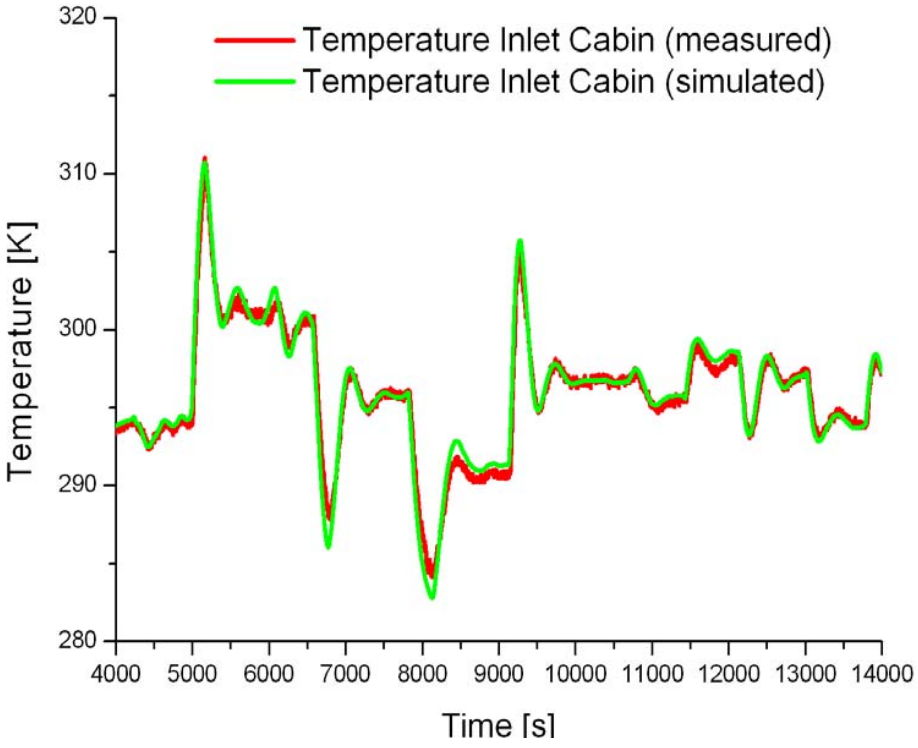

Figure 2- 14 Matching relationship between simulation and measurement [19]

But at the same time, the simulation result of cabin temperature did not match with the measured data. Figure 2-15 shows the deviations.

Therefore, at least two conclusions can be drawn in terms of the simulation. One is that simplification of the models of cabin or other components can help simulating and analyzing the system swiftly. But the final results would be

affected unpredictably. The other one is that the simulation results did not match with the measured data is partially because the methodology neglected the thermal capacities of the cabin skin and the cabin floor. This indicates that simulation can achieve accurate outputs only when all the related factors are taken into consideration. But it is unpractical to build all the simulation models at the same time since no accurate upstream inputs may leads to no required output. Thus some estimation has to be made in order to finish a complete system model.

The advantage of this methodology is that those component models form a very useful database and they can be cited directly by other researchers because they have no relationship with ambient conditions and only related with the parameters themselves. And with the database be updated continually, researchers can focus on improving the performance of the whole system rather than just on component level.

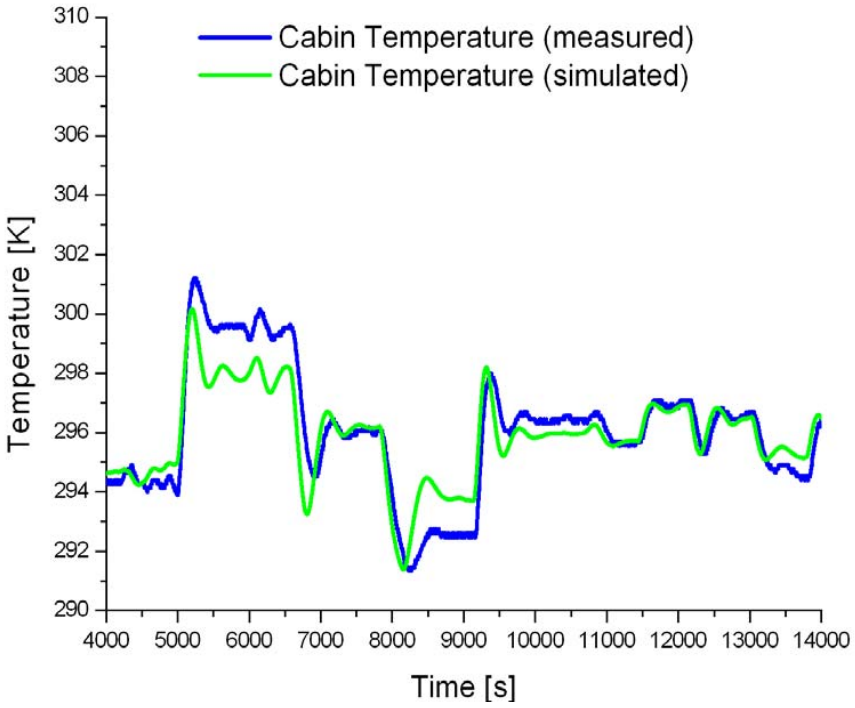

Figure 2- 15 Deviation of simulation results and measured data [19]

2.4.2 Mathematical Method

The ECS also can be optimized through establishing mathematical model [20]. The methodology is introduced as follows.

Before establishing the mathematical model, the system characteristics should be clarified. Then, several main components and related parameters should be taken into account and predefined simultaneously, such as the supply air mass flow, efficiency factors of the heat exchangers, the flow ratio and the thickness of the cabin insulation wall an so on. All these parameters are selected as the design variables. Thirdly, the parameters must have some constraints based on the system fundamental principles and current technology level. And all the design variables can be expressed by inequality. Such inequalities are used to limit the input data when the model is built.

Based on the system characteristics, the direct optimization method is adopted. In order to avoid possible variables distortion caused by the great difference of magnitudes during looking for the best values, the input design variables should be standardized. Then, the constraint issues can be transformed to unconstrained issues by the penalty function method or multiplier method. If the latter is selected as the optimization method, the object function gradient does not need be calculated and thus the alternate effects can be ignored.

Finally, the general sketch of system optimization program is shown in Figure 2-16. To quote subprogram of accelerating simplex method is used for calculating the constraints in terms of parameters about the system performance and components. To quote subprogram of generalized lagrange multiplier method is aiming at the best value for the object function. The corresponding configuration with minimum value of the object function is the best one.

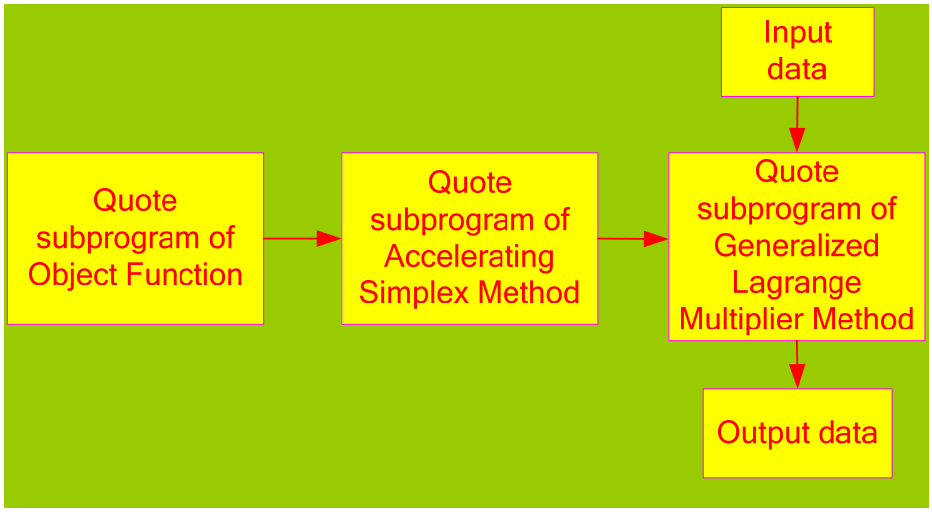

Figure 2- 16 System optimization general sketch [20]

This method is kind of static simulation and it has been proved to be reasonable and practicable. It is a method of analyzing the steady state performance of the ECS. Meanwhile, although the method is used for analyzing a military aircraft in the reference research, the analysis process about heat exchanger, turbine and compressor also can be shared when analyzing the ECS of civil transportation aircraft.

Combining the description shown in Section 2.4.1, the simulation software of Matlab/Simulink is selected as the research tool, and the static simulation is adopted since the cruise phase is regarded as a steady state.

3 METHODOLOGY

This research analyzes and compares the three-wheel low and high pressure water separation system. Since cruise phase is selected as the only research flight phase after analysis, where the ACS has been operating for a long time, static modeling and simulation method is enough in terms of the research target. The flow chart of analysis and comparison is shown in Figure 3-1.

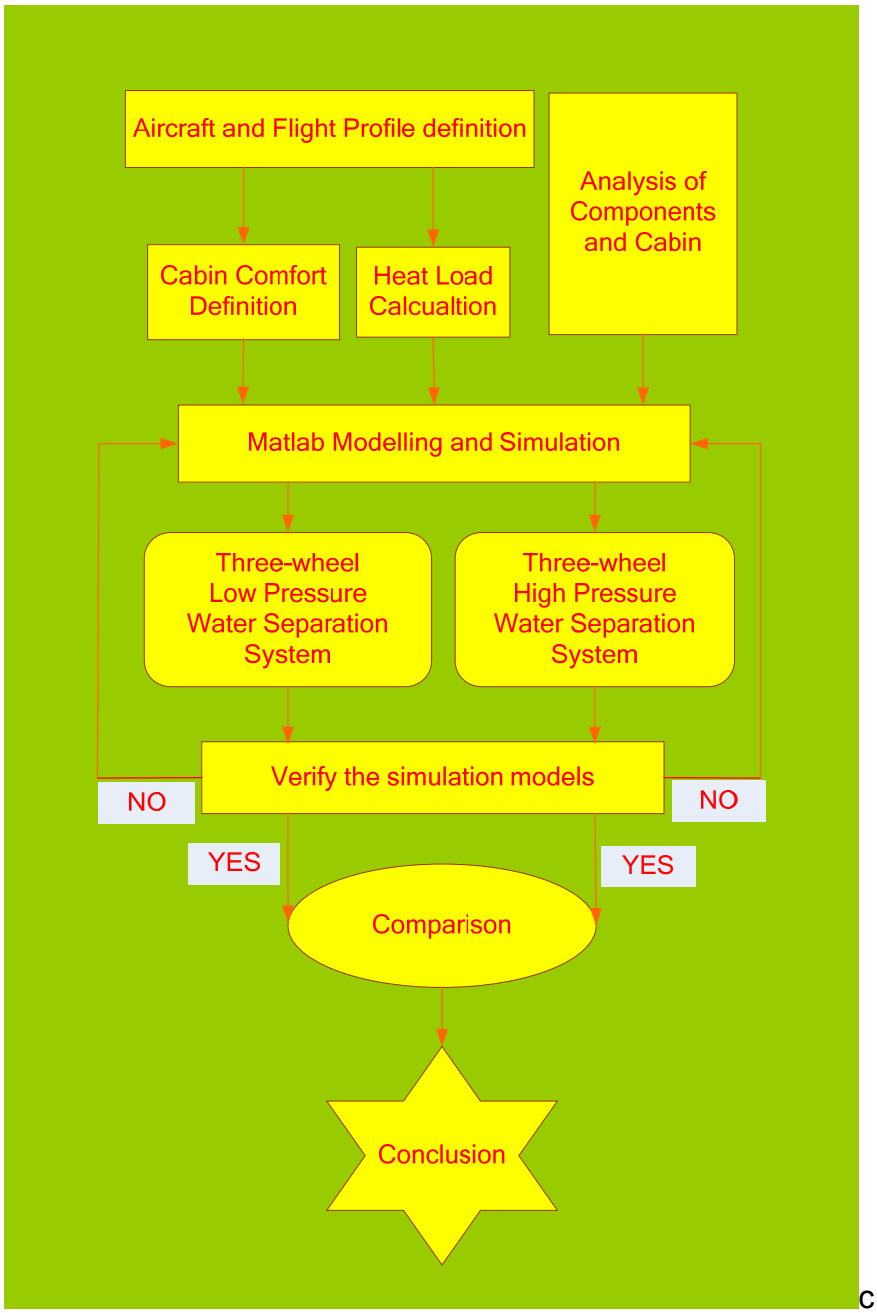

Figure 3- 1 Flow chart of research process

Aircraft definition is to define the parameters which are required for aircraft heat load calculation, such as the fuselage diameter and length, the thickness and materials of several layers of the fuselage wall, transparent area, number of aircraft occupants and so on.

In this research, flight profile definition is to get the flight altitude and speed during cruise so that the ambient environment condition indexes can be obtained and the fuselage skin temperature can be computed, which are necessary for aircraft heat load calculation.

Cabin performance definition is to express the cabin comfort by numerical numbers, which nominally includes the cabin temperature, pressure and humidity. Since the pressure almost keeps constant during cruise, humidity is decided by the number of aircraft occupants and the ratio of recirculated air, the temperature index is the key index here.

Aircraft heat load calculation is to compute the steady state heat load during cruise, which will be used to define the required aircraft ECS capability.

Matlab/Simulink modeling and analysis is the main part of this research. After the two different configurations are defined, the components in the system are analyzed one by one. Then corresponding models can be built. Finally, simulation models of the system of different configurations can be assembled.

Verifying the simulation models is to check whether the obtained temperature variation curve meets the one of Airbus 320 ECS and whether the relationship between engine bleed air mass flow and required ram air mass flow meets the related research. The variation trend and state point temperature values are checked and discussed. Confirming the validity is the precondition of analyzing and comparing the two configurations.

Comparison is to compare the different required inputs of the two configurations which are aiming at the same mix manifold inlet temperature, mainly about the \ ram air mass flow and turbine expansion ratio.

4 AIRCRAFT HEAT BALANCE

The nominal function of an aircraft Air Conditioning System is to regulate the temperature in the cabin, cockpit, cargo, and also ensure the environment of the EE Bay can keep the equipments operating normally. Actually, the function is achieved by managing the heat load in the aircraft. Thus the heat load of steady-state heat balance is the necessary input for designing an air conditioning system.

The cabin inlet airflow is focusing on removing the cabin heat load. The ventilation of EE bay and cargo is achieved by the blowing fans, which extract the cabin discharged air to remove the heat load. The blowing fans supply required air mass flow to EE bay and cargo so that the temperature can be controlled. Therefore, heat load in the cabin, which mainly produced by the fuselage wall, the cabin occupants and solar radiation, is selected to design the aircraft air conditioning system. The estimated heat load produced by the electronic-electrical equipments is only used for judging whether the cabin outlet airflow can remove the entire aircraft heat load successfully. Meanwhile, information from Airbus 320 ECS is referred since the author only focuses on a 150-seat civil transportation aircraft in this research and Airbus 320 is the typical aircraft at this level.

4.1 Aircraft Heat Load Calculation

Aircraft heat load can be regarded as coming from four aspects, the fuselage wall, the solar radiation, the aircraft occupants and the electronic-electrical equipments [7]. It is easy to describe these sources but difficult to finish a complete and precise calculation because there are so many factors should be taken into account at the same time. What is more, the exact flight altitude and speed also affect the calculation results. In this research, the common method is used to calculate the aircraft heat load in terms of the Airbus 320 structural parameters and cabin layout in the beginning. Then an estimation based on statistics is used to verify the calculation result.

4.1.1 Heat Load from the Fuselage Wall

Heat load due to the aircraft fuselage is decided by the ambient environment condition and aerodynamic heat. In order to obtain the value, first of all the aircraft outside skin temperature should be calculated.

When the aircraft is cruising at a high altitude, the fuselage skin temperature can be calculated by the following equation [11].

$$T_s = T_h\left(1 + r\frac{k-1}{2}Ma^2\right) \quad \textbf{(4- 1)}$$

Where

T_s = fuselage skin temperature, K

T_h = static temperature of the current atmosphere, K

r = recovery factor, r equals $Pr^{0.5}$ (laminar flow) or $Pr^{0.33}$ (turbulent flow)

k = isentropic factor of air, k =1.4

Ma = flight Mach number

After the fuselage skin temperature is calculated, the corresponding heat load can be computed by the following equation.

$$Q_f = \frac{\Delta T}{r_{cT}} \quad \textbf{(4- 2)}$$

Where

ΔT = temperature difference between the fuselage skin and cabin, K

r_{cT} = total thermal resistance

For Equation 4-2, it is easy to get the ΔT while the value of r_{cT} needs detailed analysis and calculation. Generally speaking, the civil transportation aircraft fuselage wall consists of three layers. The outside layer is the skin, the mediate layer is the insulation layer and the inside layer is the interior decoration layer.

In order to get an accurate heat load, the heat transfer coefficients, areas and thicknesses of these three layers are taken into account. The final r_{cT} is computed by adding the thermal resistances of the three layers.

$$r_{cT} = \sum_{i=1}^{i=3} r_{ci} \qquad \textbf{(4- 3)}$$

$$r_{ci} = \frac{x_i}{A_i K_{ci}} \qquad \textbf{(4- 4)}$$

Where

r_{cT} = total thermal resistance of the fuselage wall

r_{ci} = thermal resistance of the structural layer

x_i = thickness of the structural layer, m

A_i = area of the structural layer, m^2

K_{ci} = thermal conductivities of the material, W/m • K

4.1.2 Heat Load Caused by Solar Radiation

The increased heat load produced by solar radiation is absorbed mainly by the cockpit windshields and cabin observation windows. It can not be ignored because the great amount contributes to the aircraft inside environment, especially for the transparent area is increasing on the modern aircraft in order to improve the cabin comfort. According to related definition about heat transfer calculation, the radiative heat can be calculated by the following equation [21].

$$q_s = \tau G_s A_p \qquad \textbf{(4- 5)}$$

Where

τ = overall solar transmissivity of transparent area

G_s = total solar radiation, W/m^2

A_p = projected area of transparent area normal to suns rays, m^2

4.1.3 Heat Load Caused by Occupants

Aircraft heat load comes from passengers and crew members is the metabolic heat. The process of metabolism produces two kinds of heat load. One is the sensible heat and another one is the latent heat. The sensible heat spreads to the cabin through convection and radiation, which mainly depends on the cabin temperature and human activity levels. It increases the cabin temperature directly. The latent heat spreads in forms of breathe and sweat evaporation and it does not increase the cabin heat load even if the cabin discharged airflow is recirculated. It only influences the cabin relative humidity.

Table 4-1 shows the different thermal power when people at different physical conditions based on related research.

Table 4- 1 Thermal power of people at different physical conditions [7]

Physical condition	Thermal power (W)
Sleep	50
Sitting, at rest	70
Light manual work	100
Moderate manual work, walking	200
Heavy manual work	300

It can be seen that heat from human metabolism varies greatly from 50W to 300W in terms of different physical activities. Because the cabin flight attendants need to serve the passengers, passenger normally just sit and rest during flight, and the cockpit crew members are piloting the aircraft, the thermal power of passengers and crew members should be treated separately when doing the calculation. The detailed calculation please checks Appendix A.

4.1.4 Heat Load Caused by Electronic-Electrical Equipments

Aircraft heat load produced by the electronic-electrical equipments are mainly from the EE bay power utilization equipments, the cabin lighting and cockpit displayers. With the development of aviation industry and electronic technology, more and more electronic-electrical equipments are used on the civil transportation aircrafts in order to improve the system performance. For example, the Avionics System is likely to use more electronic equipments to achieve the highly automatic control function. The Electrical Power System (EPS) utilizes more electrical equipments than the past so that the power distribution system becomes smaller weight, less complexity but high automation, high reliability and maintainability. Thus the heat load caused by the electronic-electrical equipments is greater than the past.

But there is no equation can calculate the exact heat load before all the equipments are selected. Thus information from related research and known aircraft as shown in Table 4-2 can be referred. Then a preliminary value can be estimated, which includes the heat load produced by the power utilization equipments in the EE bay, the displayers in the cockpit, the galley heating and lighting in the cabin and so on.

Table 4- 2 Heat load values of some civil transportation aircrafts

Aircraft type	Passenger number	Heat load because of EE equipments
---	12	1700W [21]
CRJ700	70	3000W [10]
---	200	7101W [19]

4.2 Selection of Flight Phase

Because of the moisture in the engine bleed air, the main difference of HPWS and LPWS is that the high dew point temperature may limit the turbine outlet temperature in the LPWS sometimes that it could not be as low as that in the HPWS. And the condensation of residual moisture after the airflow passes

through the water extractor releases much heat to increase the turbine outlet temperature, which means reduction of cooling capability.

Meanwhile, the flight phases of a civil transportation aircraft consists of seven parts, ground, taxi, take off, climb, cruise, descent and landing. During cruise, the humidity is necessarily low because of the low temperature and pressure environment. Thus the effects from humidity to the LPWS can be ignored. But for the other flight phases, the influence from moisture to the turbine outlet temperature must be taken into consideration.

Hence, it can be stated that there are two different conditions should be considered when comparing the LPWS and HPWS. One is where there is much moisture which may affect the turbine outlet temperature and the other one is where the effect from moisture can be ignored.

And according to related research, the greatest cabin heat load happens in the extreme hot days when the aircraft is landing on the ground [22]. And normally the cruise phase takes the longest time during flight. Integrating above information, it can be concluded that the when the aircraft is on the ground, where the humidity and cabin heat load is greatest than other flight phases, and the cruise phase, which lasts the longest time but low humidity, can be selected as the research objects. But according to recent researches, the cruise phase is defined as the only research object in this research as explained as follows.

The cabin environment can be controlled by the APU bleed air or the ground air conditioning system when it is on the ground. Since the APU bleed air produces high levels of noxious emissions and fuel gas odors (e.g. 550 l/h of fuel are required for Boeing 747-400) and causes a noise of around 80 dB, life of APU is affected severely due to frequent start and shut off, the oil consumption brings more cost than using ground air conditioning system (the efficiency is between 10 and 12% while the ground air conditioning system can reach to 50%) [23], it can be predicted that civil transportation aircrafts will be willing to or even forced to use the ground air conditioning system rather than APU bleed air to control the cabin environment in the future. Actually, now some airports have already restricted the use of APU when the aircraft is on the ground, such as the Britain

Stansted Airport, America Nantucket Memorial Airport and Australia Innsbruck Airport. When the aircraft uses ground air conditioning system to control the cabin environment, the air conditioning packs do not need to work.

Therefore, it can be concluded that it is reasonable to select the cruise phase as the only research object in this research. The condition that the aircraft is on the ground can be done in future work or by other researchers.

4.3 Estimation of the Heat Load

The aircraft heat load can be calculated by the method as introduced in Section 4.1. Then, the obtained result should be verified. According to the statistics about the aircrafts performance parameters from 1954 to 2007 [24], a trend was discovered through analyzing 25 different kinds of civil transportation aircrafts as shown in Figure 4-1. It represents the relationship between the maximum aircraft heat load and number of passengers. It is stated that the maximum aircraft heat load and the number of passengers are in good linear relation.

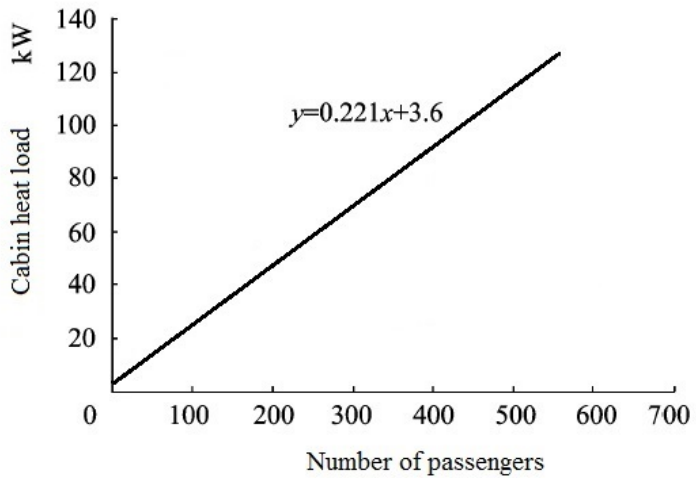

Figure 4- 1 Relation between aircraft heat load and the number of passengers [24]

Based on the diagram, taking ‘x’ as 150 into the equation ‘y=0.221x+3.6’, the maximum heat load of a 150-seat level aircraft should around 36.75kW. But this value only occurs in extreme hot days when the aircraft is on the ground. According to the analysis shown in Section 4.2, this research only focuses on the cruise phase that the calculated heat load must be less than the estimation value. The detailed calculation and analysis is shown in Appendix A.

5 AIRCRAFT DEFINITION

In this chapter, the purpose of defining a 150-seat aircraft is to help calculate the aircraft heat load. According to the required inputs mentioned in Chapter 4, the demanded structural parameters are shown in Table 5-1.

Table 5- 1 Aircraft structural parameters for heat load calculation

No.	Parameter	Function
1	Fuselage skin thickness, area and material	To calculate the heat load comes from fuselage wall
2	Fuselage insulation layer thickness, area and material	To calculate the heat load comes from fuselage wall
3	Cabin decoration layer thickness, area and material	To calculate the heat load comes from fuselage wall
4	Area of transparent area and thermal conductivity	To calculate the heat load caused by solar radiation
5	Number of passengers and crew members	To calculate the heat load caused by the occupants

5.1 Fuselage Skin Thickness and Material

For the airframe structure, the largest single item of the fuselage structure is the skin and its stiffeners. And because the skin/stiffener combination structure has been proved that it can meet the aircraft structural requirements perfectly since the earliest metal stressed skin airplanes, the structure just changed a little over so many years [25]. Therefore, related data from reference aircrafts can be quoted directly. And the effect of stiffeners is neglected through considering the good combination between the skin and insulation layer.

This research focuses on the civil transportation aircraft with 150 seats. As it is well known that Airbus 320 and Boeing 737 series are the most successful

aircrafts at this level, thus related data from these two aircrafts can be cited. This research chooses Airbus 320 as the reference aircraft.

Based on the description shown in Airbus 320 Structural Repair Manual, the fuselage skin is made of aluminium alloy and it is not thicker than 1.6mm (0.063inch), thus some researchers selected 1mm as design input [26] [27]. Besides, in terms of the information shown in Airbus Aircraft Characteristics Airport and Maintenance Panning, the fuselage cross section structural dimensions are illustrated in Figure 5-1. The fuselage length is 26.9m. Consequently, the area of the fuselage wall can be calculated as shown in Appendix A.

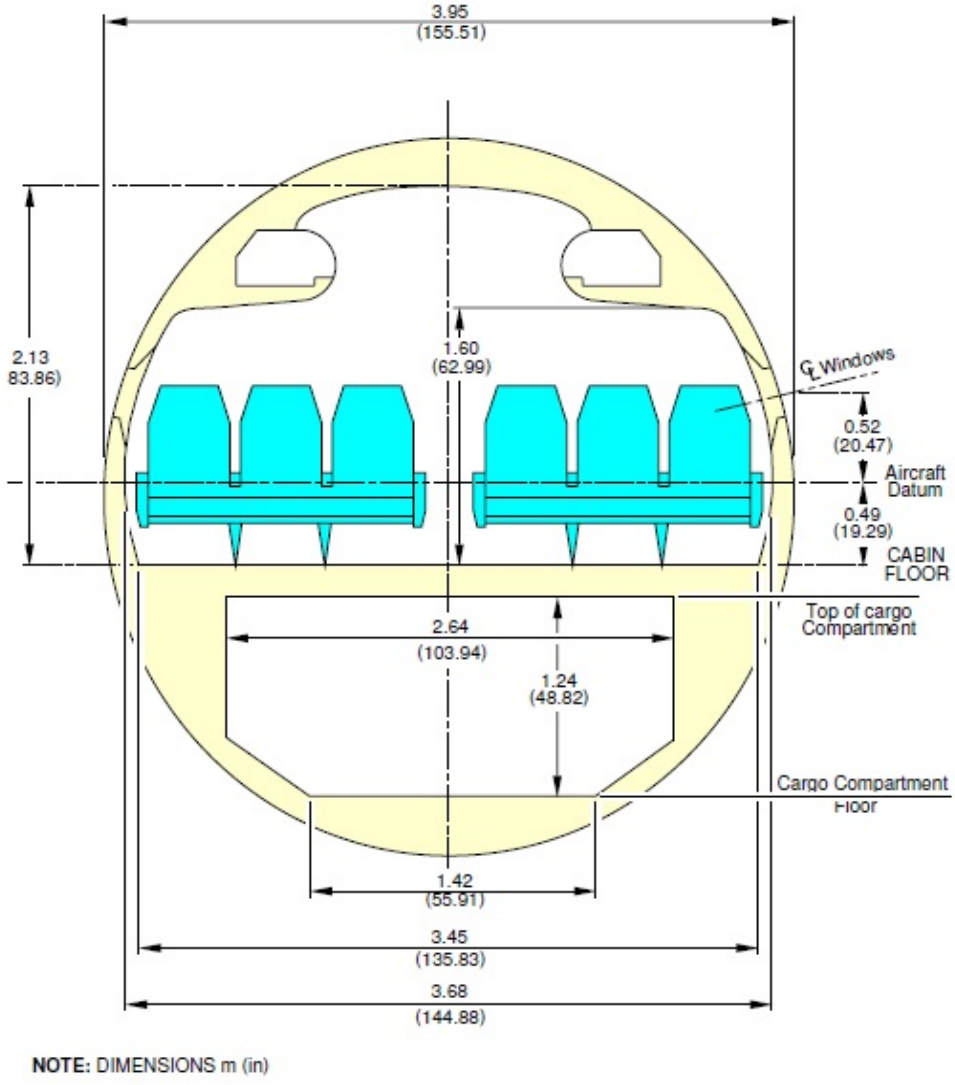

Figure 5- 1 Airbus 320 fuselage cross-section diagram [28]

5.2 Fuselage Insulation Layer Thickness and Material

In the civil transportation aircrafts, the cabin temperature should be kept around 20℃ in any flight phases. But the ambient environment temperature probably changes from -55℃ to +50℃ during flight which may creates a temperature difference of 75℃ to -30℃[27]. Therefore, an insulation layer is necessary for the fuselage wall to limit the thermal transmission between the aircraft outside and inside environment.

Normally, the aircraft heat insulation function is achieved by covering insulation blanket on the fuselage wall which has a thickness of a couple of inches. The insulation blankets are commonly made of fibreglass and the thickness can be selected as 50mm [29].

5.3 Cabin Decoration Layer Thickness and Material

The cabin decoration layer not only decorates the cabin wall so that the aircraft interior environment can be comfortable, but also has the function of limiting thermal transmission between the aircraft inside and outside environment. The thickness of Airbus 320 interior decoration layer is 35mm [30] and it is made of Nomex honeycomb core.

Combining the definition described in Section 5.1 and 5.2, structure of the fuselage wall can be expressed as follows.

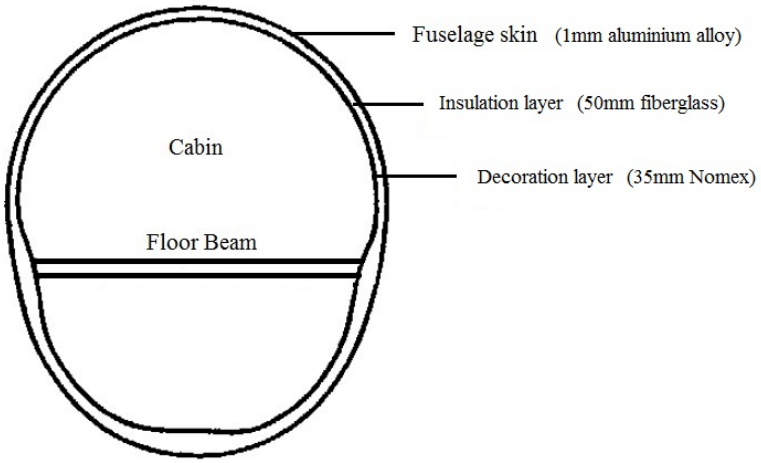

Figure 5- 2 Aircraft fuselage wall structure

5.4 Area of Transparent Area

Actually, the whole aircraft is surrounded by solar radiation during every flight phase. Compared with the fuselage skin, the aircraft transparent area, which includes the cockpit windshields and cabin observation windows, is more sensible when facing radiative heat. In order to calculate the heat load comes from the aircraft transparent area, it is inevitable to obtain the area of these two areas.

Based on the definition in FAR Part 25, the function of cockpit windshield is that, 'each pilot compartment must be arranged to give the pilots a sufficient extensive, clear, and undistorted view, to enable them to safely any maneuvers within the operating limitations of the airplane, including taxiing takeoff, approach, and landing'. Therefore it is indispensible although it may cause a big amount of solar heat enter the cockpit.

According to the description shown in Airbus 320 Flight Deck and Systems Briefing for Pilots, the areas of the three different windshields on each side of the aircraft are shown in Figure 5-3. Therefore, the total area of the cockpit windshields can be calculated as 2.36m^2.

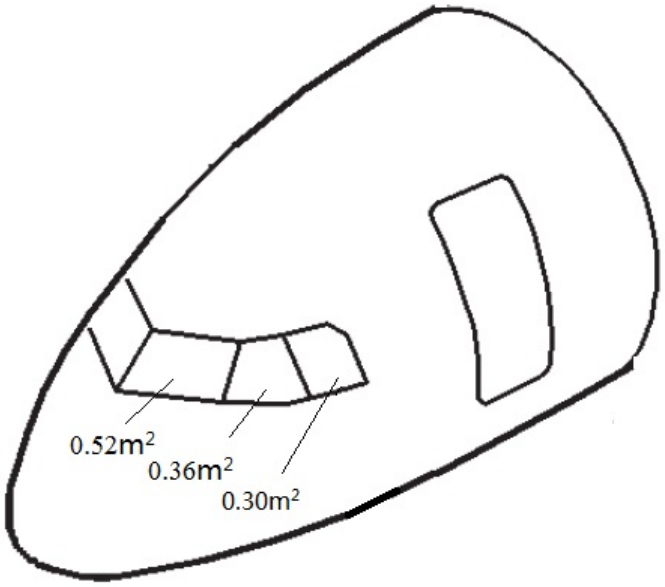

Figure 5- 3 Areas of the three cockpit windshields of Airbus 320

The observation windows make passengers can appreciate outside scenery and help adjust cabin brightness when the aircraft is landing on the ground. In terms of the definition from Airbus 320, the dimensions of each observation window are shown in Figure 5-4 that the area can be calculated as about 0.07m^2. And there are 82 windows based on the aircraft layout.

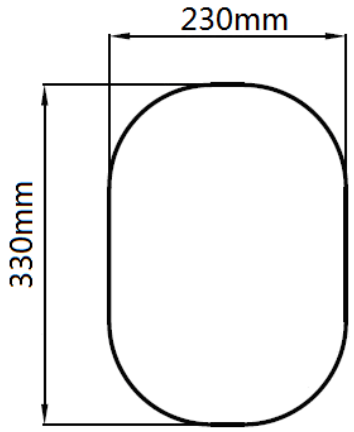

Figure 5- 4 Dimensions of Airbus 320 each cabin observation window

5.5 Number of Occupants

As mentioned before, this research focuses on the 150-seat level civil transportation aircraft. Airbus 320 standard type is the typical two class layout of this level. Therefore, the number of occupants and corresponding crew members can be chosen as the calculation inputs.

According to the definition in Airbus 320 Aircraft Characteristics Airport and Maintenance Panning, the cabin layout diagram is shown in Figure 5-5.

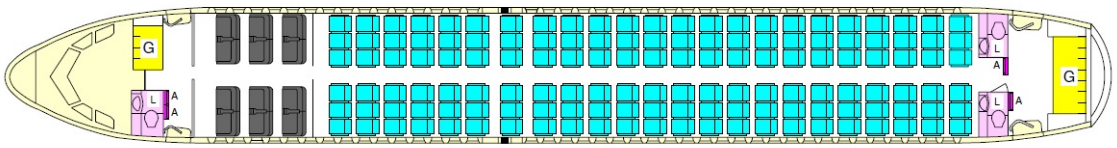

Figure 5- 5 Cabin layout diagram of Airbus 320 standard type [28]

Therefore, it can be defined that there are 150 passengers and 6 crew members, which includes 2 pilots and 4 flight attendants.

5.6 Cabin Performance Parameters Definition

In order to provide a comfortable environment to the passengers as well as preventing the aircraft structure from damaging because of over pressurization and depressurization, the aircraft ECS should meet some performance indexes, which are mainly about cabin pressure, temperature, air mass flow. Because the cabin humidity is determined by the performance of the recirculation system filters during cruise, it is not analyzed here. And since the cruise phase has been selected as the only research object, related performance parameters are shown as follows.

Table 5- 2 Cabin performance parameters definition

No.	Parameter name	Function Definition	Parameter
1	Temperature	a. Meet the cabin comfort requirement, normally from 19℃ to 24℃. b. Expressed by dry bulb temperature and represent the average temperature of the cabin.	21℃
2	Pressure	a. Cabin pressure altitude should keep constant and less than a specific value. b. The effects to the aircraft structure should be considered.	8,000ft
3	Air mass flow	a. Ensure required cabin fresh air mass flow based on FAR Part 25 b. Keep the cabin heat balance c. Maintain the cabin pressure	>250g/min/person

5.7 Flight Profile Definition

The aircraft flight profile is a map which combines the flight altitude and speed that the aircraft has been designed to operate [31]. It limits the aircraft operation environment and extreme performance to make sure the aircraft can operate safely during its lifespan as the initial design purpose.

In this research, to define a flight profile is mainly aiming at getting the cruise altitude and speed, which will be used to get the environmental parameters and calculate the fuselage skin temperature.

For a typical civil transportation aircraft, the flight phases consists of seven parts, ground, taxi, take off, climb, cruise, descent and landing. Because this research only focuses on the cabin environment at cruise phase, the altitudes and speeds of other six flight phases do not need be defined here.

Figure 5-6 shows a typical flight profile for a civil transportation aircraft.

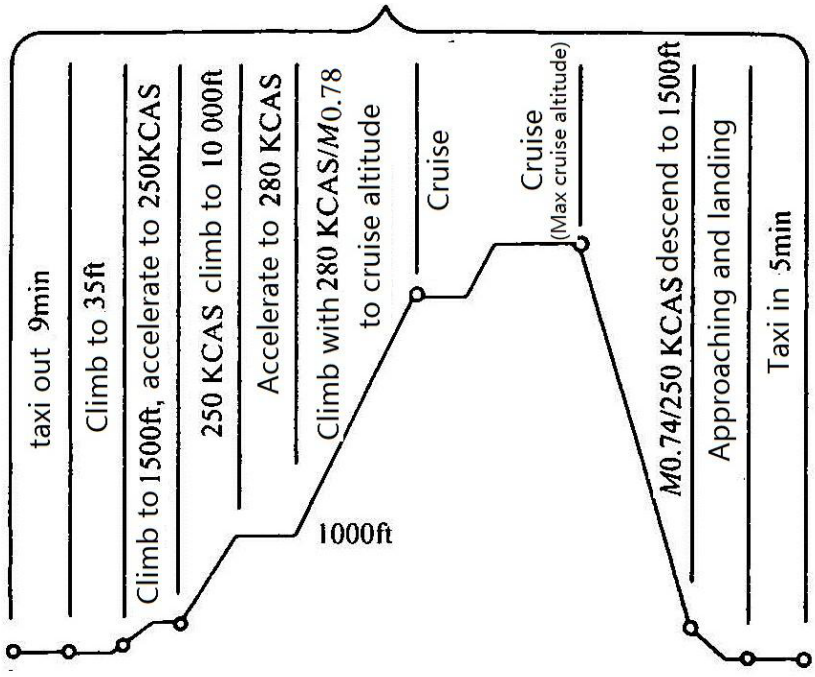

Figure 5- 6 Typical flight profile for a civil transportation aircraft [32]

Based on the description shown in Airbus 320 performance definition, the economical cruise altitude is 37,000ft and the cruise speed is 0.78Mach. These two information is what only be used in is research.

6 ANALYSIS OF ECS COMPONENTS

In order to analyze the system performance and start related research, corresponding simulation models for each of the components should be built at first, which means to find out the relationship between input and output temperature and pressure. The basis of this analysis includes the fundamental knowledge of heat transfer and aerodynamics, working principles and mechanical dimensions of the components, ambient environment condition, system configuration and data from Airbus 320. Finally, the simulation model of the whole ACS can be assembled by integrating all the component models. And the temperature model and pressure model are built respectively in order to simplify the analysis.

In terms of the system configurations which are shown in Figure 2-9 and 2-10, the components to be simulated are listed in Table 6-1.

Table 6- 1 Component list for simulation

item	List of components
1	Main Heat Exchanger
2	Primary Heat Exchanger
3	Compressor
4	Turbine
5	Reheater and Condenser
6	Mix Manifold
7	Cabin
8	Duct

Then, taking an air conditioning pack as research object, the parameters to be analyzed can be defined as shown in Figure 6-1.

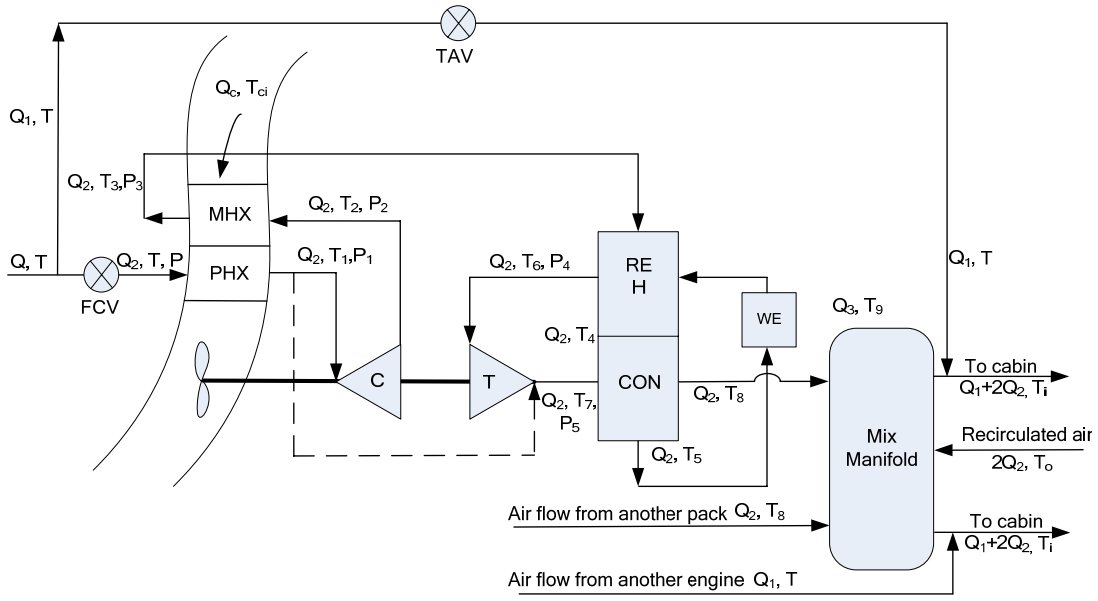

Figure 6- 1 Variables in the air conditioning system

Consequently, the variables can be defined based on the schematic diagram, which are the engine bleed air temperature T, pressure P and mass flow Q_2, the ram air temperature T_{ci} and mass flow T_c, the compressor compression ratio π_c and the turbine expansion ratio π_t. Since the performances of heat exchangers (MHE, PHE, Reheater and Condenser) are unchangeable once the structural dimensions are fixed, there are no variables about them. At the same time, according to the definition from Airbus 320 ECS training manual as shown in Figure 6-2, T can be defined as 205℃ (473.15K), P is about 44 psi (0.30MPa). The compressor compression ratio is 1.3. T_{ci} can be calculated based on the ambient atmosphere and cruise speed.

Therefore, there are only three variables needs analysis in the system, which are the engine bleed air mass flow Q_2, the ram air mass flow Q_c and turbine expansion ratio π_t. The relationship between Q_c and π_t can be discovered if Q_2 is assumed to be constant. The amount of trim air Q_1 can be calculated after Q_2 is confirmed in terms of the requirement of removing cabin heat load.

And based on the definition of Airbus 320 ECS, the normal fresh air mass flow to the cabin is 0.818kg/s during cruise and the maximum mass flow can reach

120% of the normal one. Thus Q_2 can be defined as from 0.3kg/s to 0.5kg/s for each air conditioning pack.

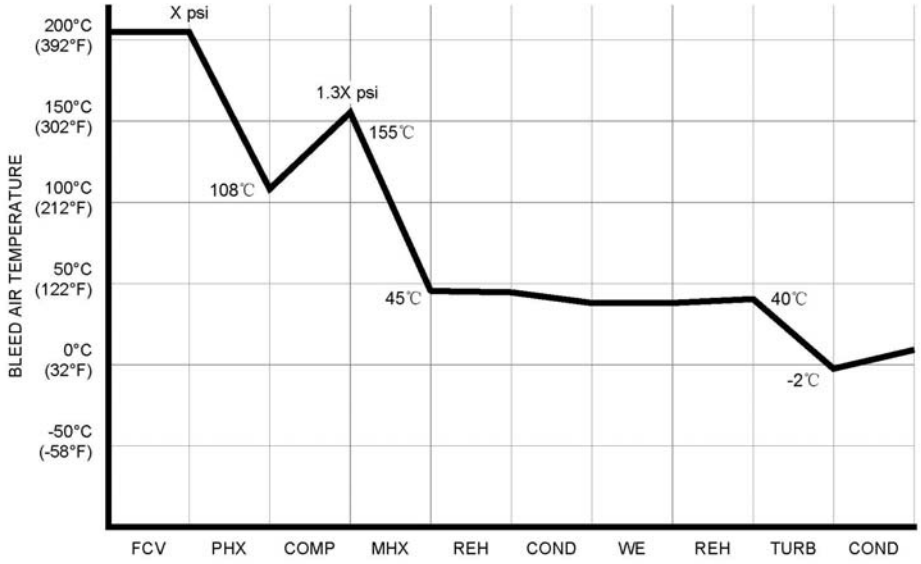

Figure 6- 2 Parameters of the air conditioning pack on Airbus 320 [33]

6.1 Main Heat Exchanger

Heat exchanger is one kind of mechanical equipment which is quite efficient for heat transfer. Although it has several different kinds of configurations, such as the counter flow type, the parallel flow type and the cross flow type, the cross flow type tube-fin heat exchanger as shown in Figure 6-3 is the most common choice for the aircraft air conditioning pack. Normally, it consists of four parts, the inlet and outlet pipes, the tubes and fins.

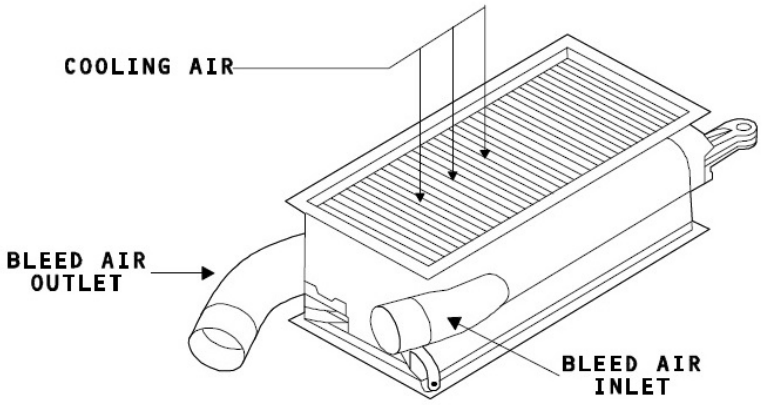

Figure 6- 3 ECS main heat exchanger [33]

The function of main heat exchanger is to cool the high temperature airflow which is discharged from the ACM compressor. Neglecting possible leakage in the equipment, the component can be simplified by the following diagram.

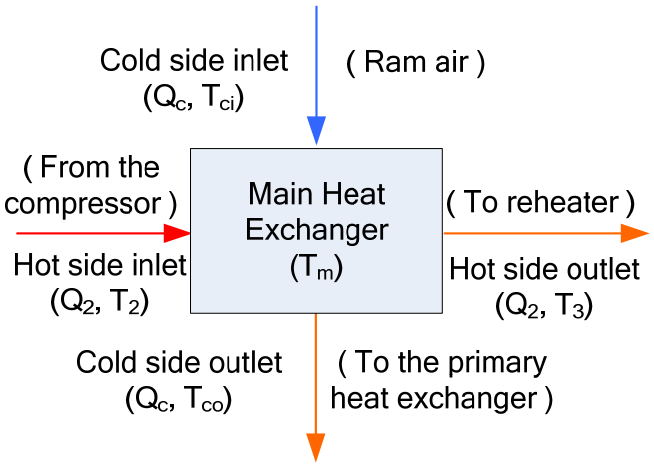

Figure 6- 4 Schematic of main heat exchanger

In Figure 6-4, where Q is the mass flow and T is the temperature of the airflow, whose units are kg/s and K respectively.

When the hot airflow is moving forward in the main heat exchanger, it is cooled by the ram cold air, thus the temperature decreases continually. The general temperature variation curve is shown in Figure 6-5, where the X-axis is the contact area of heat exchanger and Y-axis is the temperature of airflow.

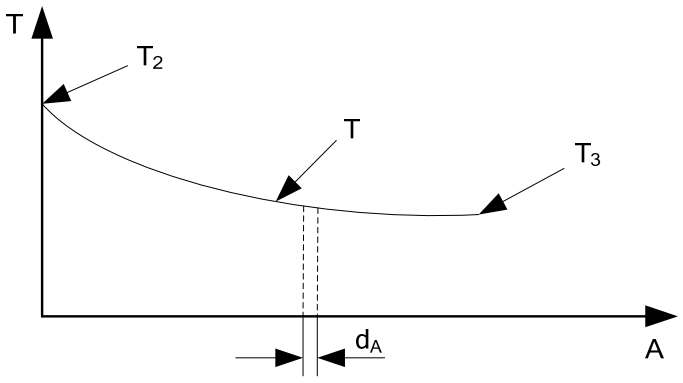

Figure 6- 5 General temperature variation curve of hot airflow

Heat exchange between the hot airflow and cold airflow is actually relying on the heat exchanger as intermediate material. And heat transferred from the hot

air to the cold equals to that transfer between the hot air and heat exchanger core. Thus based on the theory of forced convection, the heat transfer can be calculated as follows.

$$Q = \mathrm{h}_h A \Delta T \quad \textbf{(6- 1)}$$

Where

Q = heat loss of the hot airflow, W

h_h = hot air side heat transfer coefficient, W/m^2.K

A = heat exchange area of the main heat exchange hot air side, m^2

ΔT = temperature difference between the hot airflow and MHE core, K

And because heat transfer varies in terms of the area of the heat exchanger, then Equation 6-1 can be expressed in the differential form as follows.

$$dQ = \mathrm{h}_h \left(T - T_m\right) dA \quad \textbf{(6- 2)}$$

Where

T = temperature of the hot airflow, K

T_m = temperature of the MHE core, K

Meanwhile, temperature change of the hot side airflow also can be expressed in terms of the ideal gas specific heat equation as follows.

$$dT = T_{out} - T_{in} = \frac{-dQ}{cm} \quad \textbf{(6- 3)}$$

Where

T_{in} = MHE inlet hot air temperature, K

T_{out} = MHE outlet hot air temperature, K

c = specific heat at constant pressure c_p, 1,005J/kg • K

m = MHE inlet hot air mass flow, kg/s

Combining Equation 6-2 and Equation 6-3, the following three equations can be obtained step by step.

$$-cmdT = h_h\left(T - T_m\right)dA \quad \textbf{(6- 4)}$$

$$\frac{\mathrm{d}T}{T - T_m} = -\frac{h_\mathrm{h} dA}{cm} \quad \textbf{(6- 5)}$$

$$\int \frac{dT}{T - T_m} = -\int \frac{h_\mathrm{h} dA}{cm} \quad \textbf{(6- 6)}$$

The MHE hot air outlet temperature would keep at T_2 if there is no heat exchanger or T_3 when the contact area of the heat exchanger is A. Therefore, the integral formula of Equation 6-6 can be written in the following form.

$$\left[\ln\left(T - T_m\right)\right]_{T_2}^{T_3} = -\frac{h_h A}{cm} \quad \textbf{(6- 7)}$$

$$\ln\frac{T_3 - T_m}{T_2 - T_m} = -\frac{h_h A}{cm} \quad \textbf{(6- 8)}$$

$$e^{\frac{-h_h A}{cm}} = \frac{T_3 - T_m}{T_2 - T_m} \quad \textbf{(6- 9)}$$

In Equation 6-9, m is the hot air mass flow, which is Q_2 in terms of the definition shown in Figure 6-1. A is the total heat transfer area, which includes the tubes outside surfaces and the fins. The fin efficiency factor η_f should be taken into consideration based on the heat transfer principle. Thus Equation 6-9 can be written as follows.

$$T_3 = \left(T_2 - T_m\right)exp\left(-\eta_f h_h A / c_p Q_2\right) + T_m \quad \textbf{(6- 10)}$$

Thus the MHE hot airflow lost heat can be expressed as follows.

$$Q_h = cm\Delta T = cm\left(T_2 - T_3\right) = c_p Q_2 \left(T_2 - T_m\right)\left[1 - \exp\left(-\eta_f h_h A / c_p Q_2\right)\right] \quad \textbf{(6-11)}$$

Where

T_3 = temperature of the MHE outlet hot airflow, K

T_2 = temperature of the MHE inlet hot airflow, K

T_m = temperature of the MHE core, K

η_f = fin efficiency factor

h_h = hot air side heat transfer coefficient, W/m^2 • K

A = heat exchange area of the MHE hot air side, m^2

Q_2 = MHE hot air side inlet mass flow, kg/s

In Equation 6-10, Q_2 is the parameter which needs computation. T_2 is the temperature of ACM compressor discharged airflow. A is determined by the heat exchanger structural dimensions. T_m is a function determined by the mass flow and temperature of both the hot airflow and cold airflow based on the energy conservation law. The expression will be shown later since heat transfer condition of the cold airflow is unknown yet here.

The Reynolds number should be represented at first in order to calculate the Nusselt number N_{uD}.

$$\mathrm{Re} = \frac{\rho V D}{\mu} \quad \textbf{(6- 12)}$$

Where

ρ = density of the hot airflow, kg/m^3

v = velocity of the hot airflow, m/s

D = hydraulic diameter of the tube, m

μ = dynamic viscosity, kg/m • s

In this equation, v can be demonstrated by the following equation in terms of the mass flow and tube area.

$$\mathrm{V} = \frac{\dot{m}}{\rho A} \qquad \textbf{(6- 13)}$$

Where

$\dot{m}$ = mass flow in each tube, kg/s

ρ = density of the hot air in the tubes, kg/m^3

A = the inside cross sectional area of the tube, m^2

$\dot{m}$ can be expressed as $\frac{Q_2}{33}$ because the MHE has 33 tubes and the total inlet mass flow is Q_2. Therefore, Equation 6-12 can be written in the following form.

$$\mathrm{Re} = \frac{Q_2 D}{33\mu A} \qquad \textbf{(6- 14)}$$

Here, D can be calculated by the hydraulic diameter equation.

$$D_H = \frac{4A}{P} \qquad \textbf{(6- 15)}$$

Where

A = the inside cross sectional area of the tube, m^2

P = the wetted perimeter of the cross-section, m

Consequently, Equation 6-14 can be expressed as the following form by taking Equation 6-15 into it.

$$\mathrm{Re} = \frac{4Q_2}{33\mu P} \qquad \textbf{(6- 16)}$$

Based on the dimensions of the specific main heat exchanger, the cross sectional area A is about 0.002m^2 for each tube and the perimeter P is around 0.54m. Thus the hydraulic diameter D_H can be calculated as 0.015m.

μ is the viscosity of air, which is determined by the airflow temperature. The relationship is expressed as follows according to the Sutherland formula.

$$\frac{\mu}{1.79\times10^{-5}}=\left(\frac{T}{288.15}\right)^{1.5}\times\frac{288.15+110.4}{T+110.4} \qquad \textbf{(6- 17)}$$

Since the temperature decreases continually when the airflow passes through the heat exchanger, it is difficult to catch the exact temperature at each state point. Thus the average temperature of the hot airflow can be selected for calculation. And because normally the ratio of engine bleed air and ram air mass flow is less than 0.5, literally the hot airflow average temperature t_{mh} should be used to calculate the viscosity μ based on the definition of log mean temperature difference as follows.

$$t_{mh}=\frac{T_{ci}+T_{co}}{2}+\frac{\left(T_2-T_{ci}\right)-\left(T_3-T_{co}\right)}{\ln\dfrac{T_2-T_{ci}}{T_3-T_{co}}} \qquad \textbf{(6- 18)}$$

But it has been proved that this method is impractical. Since there are too many unknown parameters, it is quite difficult to complete the system model. And the algebraic loops also makes the model can not run successfully. As a result, estimation has to be made to calculate the Reynolds number without causing much deviation from the actual situation based on the information from Airbus 320. On the one hand, it has been found that the exact value of t_{mh} in a specific range (±10℃) only changes the value of μ a little. On the other hand, the system stable condition should be almost consistent with the information shown in Figure 6-2.

In terms of the information shown in Figure 6-2, it can be seen that the MHE inlet airflow temperature is about 428K and the outlet temperature is around

318K. Thus an average temperature of 367K is selected to calculate the μ. Consequently, Equation 6-16 can be simplified as follows.

$$\mathrm{Re} = 1.04 \times 10^4 Q_2 \qquad \textbf{(6- 19)}$$

The value of Q_2 can be estimated as around 0.35kg/s from each engine based on the requirement defined in FAR Part 25.831. Then, the Reynolds number can be calculated as 3640, which proves the airflow is transitional turbulent flow when it passes through the main heat exchanger. Thus the Gnielinski equation can be used to calculate the Nusselt Number [34].

$$N_{uD} = \frac{(f/8)(\mathrm{Re}-1000)\mathrm{Pr}}{1+12.7(f/8)^{1/2}\left(\mathrm{Pr}^{2/3}-1\right)} \qquad \textbf{(6- 20)}$$

In Equation 6-20, f is expressed as $(0.790\ln \mathrm{Re} - 1.64)^{-2}$ for the smooth surface and Pr can be defined as 0.707 under the condition of 3.9bar and 367K.

At the same time, since the empirical correlation $N_{uD} = \frac{h_h D}{k}$ also can be used to calculate the Nusselt number, so that the MHE hot air side heat transfer coefficient can be represented by the following equation.

$$h_h = \frac{N_{uD} k}{D} \qquad \textbf{(6- 21)}$$

Where

h_h = MHE hot air side heat transfer coefficient, W/m^2 • K

N_{uD} = Nusselt number

k = air thermal conductivity, W/m • K

D = hydraulic diameter of the tube, m

According to related research, the air thermal conductivity k can be calculated by the following equation [35]. Since the hot airflow average temperature in the MHE has been defined as 367K, k can be computed as 0.031.

$$k = 1.52\times10^{-11}T^3 - 4.86\times10^{-8}T^2 + 1.02\times10^{-4}T - 3.93\times10^{-4} \quad \textbf{(6- 22)}$$

Based on the definition about heat exchanger heat transfer area calculation, the total heat transfer area A mentioned in Equation 6-10 can be computed by the following equation [36].

$$A = A_p + A_f = 2N_1L_1L_2\left[\left(s_f - \sigma_f\right) + 2h_1\right] / s_f \quad \textbf{(6- 23)}$$

Where

A = MHE hot air side total heat transfer area, m^2

A_p = primary heat transfer area, m^2

A_f = secondary heat transfer area, m^2

N_1 = the pass number of hot airflow

L_1 = length of the MHE, m

L_2 = width of the MHE, m

h_1 = fin height, $h = \sqrt{s^2 + s_f^2}\ / 2$, m

The definition of other parameters in this equation is shown in Figure 6-6.

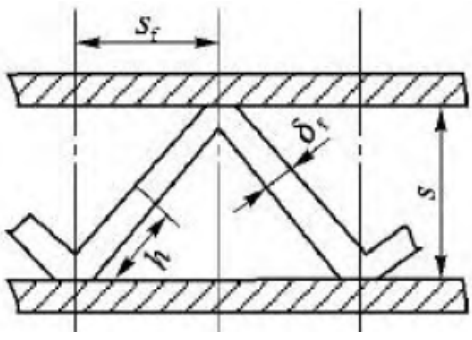

Figure 6- 6 Parameters for calculating the heat transfer area [36]

Therefore, the value of A can be calculated as follows based on the dimensions of the specific MHE.

$$A = A_p + A_f = 2N_1L_1L_2\left[\left(s_f - \sigma_f\right) + 2h_1\right] / s_f$$

$$= 2 \times 33 \times 0.27 \times 0.169 \times [(0.002 - 0.0002) + 2 \times 0.006] / 0.002$$

$$= 20.78m^2$$

Meanwhile, the temperature of the fin between two tubes is varying because of heat loss, thus the fin efficiency factor η_{f} should be taken into consideration. And since aluminium alloy is the most common material for the fin because of obvious benefits of cost and weight, the corresponding thermal conductivity around 177 W/m • K is used for the calculation [34]. The thickness of the fin can be defined as 0.0002m. Finally, the fin efficiency factor mentioned in Equation 6-10 can be calculated as follows [36].

$$\eta_{\mathrm{f}} = \frac{\tanh(mh)}{mh} \quad \textbf{(6- 24)}$$

Where

$m = \sqrt{\frac{2h_h}{\lambda_f \delta_f}}$, h_h is the MHE hot air side heat transfer coefficient (W/m^2 • K), λ_f is the fin thermal conductivity (177W/M • K), δ_f is the fin thickness (0.0002m)

$h = \sqrt{s^2 + s_f^2} / 2$ fin height, 0.006m

At the same time, there will be pressure drop when the airflow goes forward in the main heat exchanger because of friction. The total pressure drop in the system will affect the air speed when the airflow enters the cabin, and consequently it influences whether enough airflow can be supplied to the cabin. Thus pressure drop caused by the MHE should be calculated. The Darcy-Weisbach equation is selected to analyze the pressure drop in this system.

$$\Delta P = \lambda \frac{L}{D} \frac{\rho V^2}{2} \quad \textbf{(6- 25)}$$

Where

ΔP = pressure drop, pa

λ = Darcy friction factor

L = length of the airflow pass, m

ρ = density of the airflow, kg/m^3

V = velocity of the airflow, m/s

D = (hydraulic) diameter of the pipe and tube, m

λ can be found from the Moody diagram in terms of the Reynolds number and relative pipe roughness.

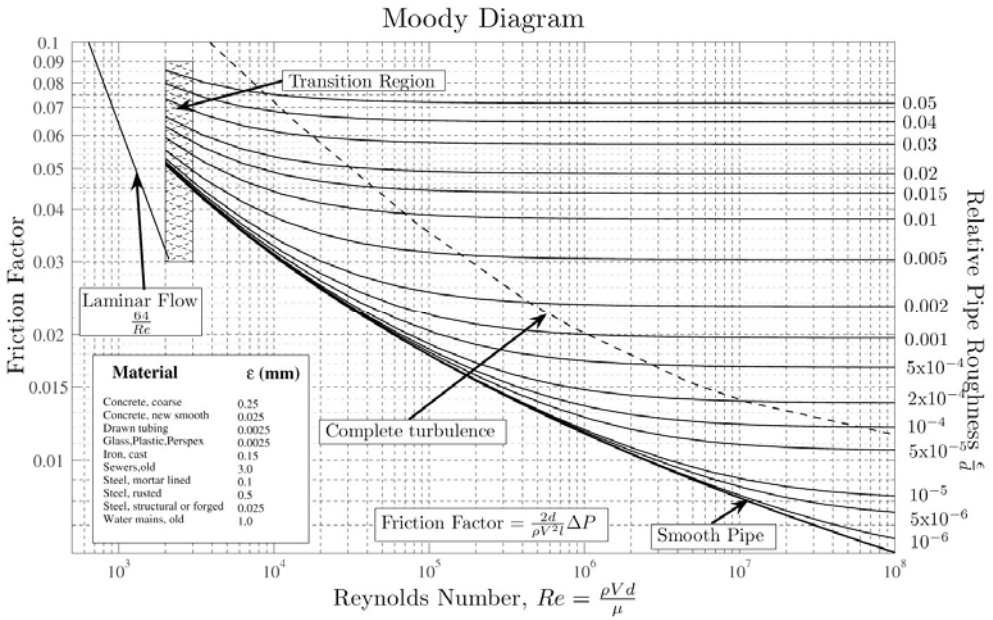

Figure 6- 7 Moody Diagram [37]

Normally, the absolute roughness coefficient ε of aluminium alloy pipe is around 1.5×10^{-6}m.

Then, the pressure drop should be calculated separately because the airflow temperature in the ducts and the diameters of the pipes are different.

When the airflow is going through the inlet pipe, with a diameter of 3.5inch (0.089m), the relative roughness (ε / D_H) can be calculated as 1.7×10^{-5}. The

Reynolds number is represented as $\frac{Q_2 D_1}{\mu_1 A}$, then λ can be found from the Moody Diagram. Similarly, the relative roughness of the tube can be calculated as 10^{-4} because D_H is 0.015m, and the Reynolds number can be demonstrated as $\frac{4Q_2}{33\mu_2 P}$. The relative roughness of the outlet pipe can be calculated as 1.5×10^{-5} since the diameter D_2 is 4inch (0.1m), and the Reynolds number is expressed as $\frac{Q_2 D_2}{\mu_3 A}$. It should be noted that the values of μ in these three equations are different because the airflow temperature at different state points are different.

For the specific MHE, the length of both the inlet pipe and outlet pipe is about 0.8m. The length of the tubes is 0.17m.

The density of airflow ρ is dependent on the current pressure and temperature. The value can be expressed by the ideal gas state equation.

$$\rho = \frac{MP}{RT} \qquad \textbf{(6- 26)}$$

Where

M = molar mass of air, 29

P = pressure of the airflow, bar

R = constant, 0.0831J/mol • K

T = temperature of the airflow, K

In Equation 6-25, the airflow speed V in the inlet pipe can be expressed as $\frac{Q_2}{0.006\rho_1}$ by taking the cross sectional area into Equation 6-13, while the values are $\frac{Q_2}{0.066\rho_2}$ and $\frac{Q_2}{0.008\rho_3}$ respectively when it is in the tubes and outlet pipe.

Finally, taking all the above data into Equation 6-25, the pressure drop from the MHE inlet pipe till the outlet port can be calculated by adding them together as follows.

$$\Delta P = \sum_{i=1}^{3} \Delta P_{\mathrm{i}} \qquad \textbf{(6- 27)}$$

The outlet temperature T_{co} of the MHE cold side can be represented similarly as shown in Equation 6-10.

$$T_{co} = \left(T_{ci} - T_m\right) exp\left(-\eta_f h_c A / c_p Q_c\right) + T_m \qquad \textbf{(6- 28)}$$

Consequently, the cold airflow gained heat can be expressed like Equation 6-11 as follows.

$$Q_c = cm\Delta T = cm\left(T_{co} - T_{ci}\right) = c_p Q_c \left(T_{ci} - T_m\right)\left[\exp\left(-\eta_f h_c A / c_p Q_c\right) - 1\right] \qquad \textbf{(6- 29)}$$

Where

T_{co} = temperature of the MHE outlet cold airflow, K

T_{ci} = temperature of the MHE inlet cold airflow, K

η_{f} = fin efficiency factor

h_c = heat transfer coefficient of the MHE cold air side, W/m^2 • K

A = heat transfer area of the MHE cold air side, m^2

Q_c = MHE cold air side inlet mass flow, kg/s

In this equation, T_{co} needs computation because the MHE outlet cold airflow will be used for cooling the PHE hot airflow. T_{ci} is the temperature of the ram air T_R, which can be calculated as follows.

$$T_{ci} = T_R = T_a \times \left(1 + 0.2M^2\right) \qquad \textbf{(6- 30)}$$

Where

T_R = temperature of the ram air, K

T_a = ambient temperature at the cruise altitude, K

M = Mach number of cruise speed, Mach

Since the ambient temperature T_a is 216.65K at the altitude of 37,000ft and the cruise speed is 0.78 Mach, the value of T_{ci} can be computed as follows.

$$\mathrm{T_{ci}} = \mathrm{T_a} \times \left(1 + 0.2\mathrm{M}^2\right) = 216.65 \times (1 + 0.2 \times 0.78^2) = 243.01\mathrm{K}$$

Based on Equation 6-11, Equation 6-29 and the energy conservation law, the MHE core temperature T_m can be demonstrated by the following equation. This equation indicates that the MHE hot air side lost heat equals to the cold air side gained heat. Consequently, T_m can be expressed for building model.

$$Q_h = Q_c \tag{6- 31}$$

$$T_m = T_{ci} - \frac{Q_2\left(T_2 - T_3\right)}{Q_c\left[\exp\left(-\eta_f h_c A / c_p Q_c\right) - 1\right]} \tag{6- 32}$$

Then, in order to calculate the Reynolds number which will be used to express the Nusselt number, the calculation method from related textbook is referred as the following equation [36].

$$\mathrm{Re} = \frac{g_m d_e}{\mu} \tag{6- 33}$$

Where

g_m = mass flow, kg/m^2 • s

d_e = equivalent diameter of the fin, m

The equation used to calculate the mass flow is as follows [36].

$$g_m = \frac{Q_m}{A_e} = \frac{Q_m}{N_c\left(L_h - 1.5b_s\right)\left(s - \frac{2h\delta}{s_f}\right)} \quad \textbf{(6- 34)}$$

Where

Q_m = air mass flow, kg/s

A_e = air circulation area, m^2

N_h = pass number of the cold airflow

L = length of the fin, m

b_s = width of the cover strip, m

h = $\sqrt{s^2 + s_f^2}$ / 2 , m

Other parameters can be found from the Figure 6-6.

Then, taking the dimensions of the specific MHE into Equation 6-34, g_m can be represented as follows.

$$g_m = \frac{Q_m}{A_e} = \frac{Q_m}{N_c\left(L_h - 1.5b_s\right)\left(s - \frac{2h\delta}{s_f}\right)}$$

$$= \frac{Q_c}{34\left(0.29 - 1.5\times 0.005\right)\left(0.011 - \frac{2\times 0.006\times 0.0002}{0.002}\right)} = \frac{Q_c}{0.094}$$

And the d_e mentioned in Equation 6-33 is calculated as follows.

$$D = \frac{2(s_f s - 2h\delta_f)}{s_f + 2h} = 0.003m \quad \textbf{(6- 35)}$$

Where

s_f = fin pitch, 0.002m

δ_f = fin thickness, 0.0002m

Therefore, finally the Reynolds number can be expressed by the following equation.

$$\mathrm{Re} = \frac{3Q_c}{94\mu} \qquad \textbf{(6- 36)}$$

In order to choose corresponding equation for calculating the Nusselt number, the Reynolds number should be estimated at first. Based on engineering experience, Q_c can be defined as 0.8kg/s preliminarily. And the cold airflow average temperature in the MHE can be estimated as 267K based on the energy conservation law. Consequently, the Reynolds number can be calculated as 1362 by Equation 6-36. It proves the cold airflow is laminar flow in the MHE. Then, the airflow Nusselt number NuD can be obtained as 7.54 [34]. Consequently, the heat transfer coefficient h_c can be calculated by Equation 6-21 combing the definition of k which is shown in Equation 6-22 and D is 0.003m.

Then, the fin efficiency factor η_{f} can be obtained by taking the value of h_c and fin height into equation 6-24.

At the same time, the value of A mentioned in Equation 6-28 can be computed by using Equation 6-23.

$$A = A_p + A_f = 2N_2L_1L_2\left[\left(s_f - \sigma_f\right) + 2h_1\right] / s_f$$

$$= 2\times 34\times 0.169\times 0.27\times[\left(0.002 - 0.0002\right) + 2\times 0.006] / 0.002$$

$$= 21.39m^2$$

6.2 Primary Heat Exchanger

The structure of a primary heat exchanger is similar with the main heat exchanger as shown in Figure 6-8, but the thickness is smaller because it has a lower capability requirement.

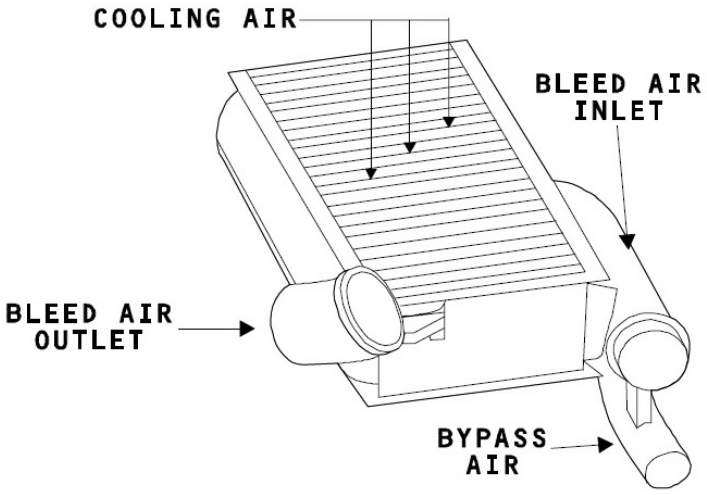

Figure 6- 8 ECS primary heat exchanger [33]

The inlet cooling air of the PHE is the airflow discharged from the MHE cold side. Similar with the simplified schematic shown in Figure 6-3, the schematic of the PHE is depicted as follows.

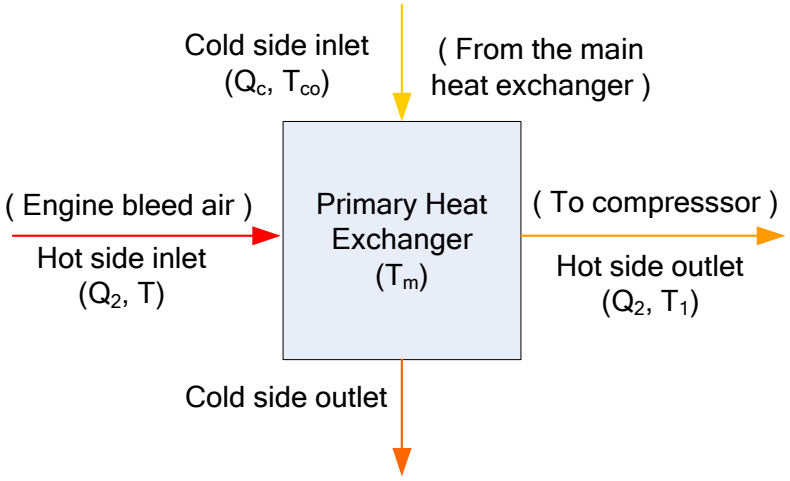

Figure 6- 9 Schematic of primary heat exchanger

Similar with the description shown in Section 6.1, temperature of the engine bleed air can be demonstrated as follows after it passes through the PHE.

$$T_1 = (T - T_m)\,exp\left(-\eta_f h_h A / c_p Q_2\right) + T_m \qquad \textbf{(6- 37)}$$

Then, the PHE hot airflow lost heat can be expressed as follows.

$$Q_h = cm\Delta T = cm\left(T - T_1\right) = c_p Q_2 \left(T - T_m\right)\left[1 - \exp\left(-\eta_f h_h A / c_p Q_2\right)\right] \qquad \textbf{(6- 38)}$$

Where

T_1 = temperature of the PHE outlet hot airflow, K

T = temperature of the PHE inlet hot airflow, 478K (205℃)

T_m = temperature of the PHE core, K

η_f = fin efficiency factor

h_h = PHE hot air side heat transfer coefficient, W/m^2 • K

A = area of the PHE hot air side, m^2

In this equation, Q_2 is the variable needs be analyzed. T is the temperature of the airflow discharged from the engine, which has been regulated to 478K (205℃) by the precooler.

According to the Airbus ECS definition, the engine bleed air mass flow is 0.818kg/s during cruise. This means each engine provides about 0.4kg/s fresh air to the aircraft. Therefore, Q_2 can be expressed as 0.3+ 0.2sin (u) kg/s combing the requirements defined in FAR Part 25.831. The maximum value of Q_c can be estimated as 3.3 kg/s according to the dimension of the Ram Air Valve, the cruise altitude and speed.

The Reynolds number should be calculated in order to choose corresponding equation to compute the heat transfer coefficient h_h. Similar with the description shown in Section 6.1, the following equation is obtained since there are 34 tubes.

$$\mathrm{Re} = \frac{2Q_2}{17\mu P} \qquad \textbf{(6- 39)}$$

Based on the dimensions of the specific PHE, the cross sectional area A is about 0.0005m^2 for each tube and perimeter P is around 0.175m. Thus the hydraulic diameter can be calculated as 0.012m.

Like discussed in Section 6.1, the average temperature of the airflow in the PHE can be estimated as 426K. Thus Equation 6-39 can be written in the following form.

$$\mathrm{Re} = 2.73\times10^{4} Q_2 \qquad \textbf{(6- 40)}$$

Taking Q_2 as 0.35kg/s into above equation, the Reynolds number can be calculated as 9555, which proves that hot airflow in the PHE is fully turbulent. Then, the Nusselt number can be calculated by the Colburn equation and Prandtl number, which will be used to calculate the heat transfer coefficient h_h.

$$N_{uD} = 0.023\,\mathrm{Re}^{3/4}\,\mathrm{Pr}^{0.3} \qquad \textbf{(6- 41)}$$

In this equation, the Prandtl number can be computed as 0.705 by taking the average temperature as 426K and pressure as 3bar into calculation. The air thermal conductivity k can be calculated as 0.035 by Equation 6-22.

The area A which mentioned in Equation 6-37 can be calculated by taking all the related data in Equation 6-23.

$$A = A_p + A_f = 2N_1L_1L_2[(s_f - \delta_f) + 2h_1]/s_f$$

$$= 2\times34\times0.086\times0.27\times[(0.002-0.0002)+2\times0.005]/0.002$$

$$=9.32\mathrm{m}^2$$

Of course, the fin efficiency factor η_f also needs consideration as discussed in Section 6.1. Taking all the related parameters in Equation 6-24, the fin efficiency factor η_f can be expressed by the following equation.

$$\eta_{\mathrm{f}}=\frac{\tanh(mh)}{mh}=\frac{\tanh\left(\sqrt{\frac{2h_h}{177\times 0.0002}}\times 0.005\right)}{\sqrt{\frac{2h_h}{177\times 0.0002}}\times 0.005}\approx\frac{\tanh\left(\sqrt{\frac{h_h}{0.018}}\times 0.005\right)}{\sqrt{\frac{h_h}{0.018}}\times 0.005}$$

The pressure drop when the airflow passes through the PHE can be calculated by the Darcy-Weisbach equation, which is introduced in Equation 6-25.

λ can be found from the Moody diagram in terms of the Reynolds number and the relative roughness of pipes and tube.

As mentioned in Section 6.1, the absolute roughness coefficient of an aluminium alloy pipe is around 1.5×10^{-6}m. Because the diameters and lengths of the inlet pipe, the tubes and outlet pipe are different, the pressure drop in these ducts should be calculated separately.

When the airflow goes through the inlet pipe, the relative roughness (ε / D_H) can be calculated as 1.5×10^{-5} since the pipe diameter is 4inch (0.1m). After the Reynolds number is calculated through using equation $\frac{Q_2 D_1}{\mu_1 A}$, k can be found from the Moody diagram. Similarly, the relative roughness of the tube can be calculated as 1.67×10^{-4} since the hydraulic diameter is 0.012m, and the Reynolds number is $\frac{2Q_2}{17\mu_2 P}$. The relative roughness of the outlet pipe can be calculated as 1.5×10^{-5} because the diameter is 4inch (0.1m), and the Reynolds number is expressed as $\frac{Q_2 D_2}{\mu_3 A}$. The values of u totally depend on the current airflow temperature.

For the specific PHE, length of both the inlet pipe and outlet pipe is 0.65m. The length of the tubes is 0.27m.

The air density ρ is dependent on the current temperature and pressure, which can be calculated by Equation 6-26.

The airflow speed V in the inlet pipe can be expressed as $\frac{Q_2}{0.008\rho}$, while the values are $\frac{Q_2}{0.014\rho}$ and $\frac{Q_2}{0.008\rho}$ in the tubes and outlet pipe.

Taking all the above data into Equation 6-25 and 6-27, the total pressure drop in the PHE can be obtained.

Then, the PHE cold air outlet temperature can be demonstrated by the similar form like Equation 6-37 as follows.

$$T_o = (T_{co} - T_m)\, exp\left(-\eta_f h_c A / c_p Q_c\right) + T_m \qquad \textbf{(6- 42)}$$

The PHE cold airflow gained heat can be expressed as follows which is similar with Equation 6-38.

$$Q_c = cm\Delta T = cm(T_o - T_{co}) = c_p Q_c (T_{co} - T_m)\left[\exp\left(-\eta_f h_c A / c_p Q_c\right) - 1\right] \qquad \textbf{(6- 43)}$$

Where

T_o = temperature of the PHE outlet cold airflow, K

T_{co} = temperature of the PHE inlet cold airflow, K

T_m = temperature of the PHE core, K

η_f = fin efficiency factor

h_c = PHE cold side heat transfer coefficient, W/m^2 • K

A = heat transfer area of the PHE cold air side, m^2

Q_c = PHE cold air side inlet mass flow, kg/s

In this equation, T_{co} has been expressed by Equation 6-28.

The PHE core temperature T_m can be demonstrated by the following equation based on the energy conservation law.

$$Q_h = Q_c \tag{6- 44}$$

$$T_m = T_{co} - \frac{Q_2\left(T - T_1\right)}{Q_c\left[\exp\left(-\eta_f h_c A / c_p Q_c\right) - 1\right]} \tag{6- 45}$$

Similar with the analysis shown in Section 6.1, the cold airflow in the PHE can be confirmed as laminar flow after checking the preliminary Reynolds number. Then the Nusselt number can be selected as 7.54. Consequently, the heat transfer coefficient h_c can be calculated.

Finally, the fin efficiency factor η_f can be computed by taking all the above parameters into Equation 6-24. And the value of A mentioned in Equation 6-42 can be computed by using Equation 6-23.

$$A = A_p + A_f = 2N_2 L_1 L_2\left[\left(s_f - \sigma_f\right) + 2h_1\right] / s_f$$

$$= 2 \times 35 \times 0.086 \times 0.27 \times [\left(0.002 - 0.0002\right) + 2 \times 0.005] / 0.002$$

$$= 9.59 m^2$$

6.3 Compressor

As mentioned in Section 2.3.3, the Air Cycle Machine (ACM) is a 3-wheel air bearing Machine, which connects the fan, compressor and turbine in one rotating shaft. The compressor is driven by the turbine expansion force so that the engine bleed air is compressed to a high pressure, thus a high expansion ratio can be achieved in the downstream turbine and an enough low outlet temperature can be achieved.

Based on the information shown in Figure 6-1, the parameters about the ACM compressor are depicted in Figure 6-10.

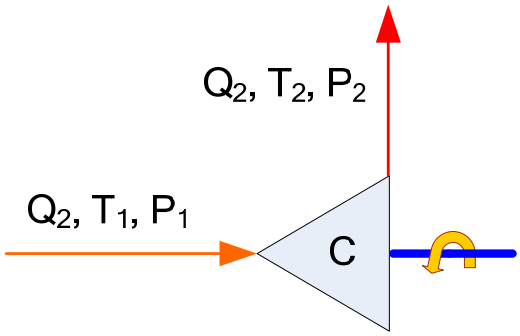

Figure 6- 10 Parameters about the compressor

Assuming that there is no heat gain or lost during compression, and all the energy produced by the compressor is used to compress the airflow, the whole work stage can be regarded as adiabatic (isentropic) process. Thus the following equation can be cited.

$$PV^{\gamma} = Constant \qquad \textbf{(6- 46)}$$

$$i.e.\ P_1V_1^{\gamma} = P_2V_2^{\gamma} \qquad \textbf{(6- 47)}$$

Where

P = pressure of the airflow, pa

V = volume of the airflow, m^3

γ = ratio of specific ration C_p and C_v, 1.4

Meanwhile, the airflow is regarded as ideal gas in order to use corresponding thermodynamics equation. Consequently, the ideal gas state equation can be selected as the basis of deduction.

$$PV = mRT \qquad \textbf{(6- 48)}$$

$$P_1V_1 = mRT_1 \Rightarrow V_1 = mRT_1 / P_1 \qquad \textbf{(6- 49)}$$

$$P_2V_2 = mRT_2 \Rightarrow V_2 = mRT_2 / P_2 \qquad \textbf{(6- 50)}$$

Combining the Equation 6-47, the following two equations can be obtained step by step.

$$P_1\left(mRT_1 / P_1\right)^{\gamma} = P_2\left(mRT_2 / P_2\right)^{\gamma} \quad \textbf{(6- 51)}$$

$$T_2 = T_1\left(\frac{P_2}{P_1}\right)^{\frac{\gamma-1}{\gamma}} \quad \textbf{(6- 52)}$$

Where

T_2 = compressor outlet temperature, K

T_1 = compressor inlet temperature, K

P_1 = compressor inlet pressure, pa

P_2 = compressor inlet pressure, pa

$\frac{P_2}{P_1}$ = compressor compression ratio, π_c

Thus the temperature difference between the compressor inlet port and outlet port can be demonstrated as follows.

$$\Delta T_s = T_2 - T_1 = T_1\left(\left(\frac{P_2}{P_1}\right)^{\frac{\gamma-1}{\gamma}} - 1\right) \quad \textbf{(6- 53)}$$

However, the compressor outlet temperature is higher than the value calculated by the isentropic equation because of the compressor efficiency η_c .The definition of η_c is shown as follows.

$$\eta_c = \frac{h_{2s} - h_1}{h_{2a} - h_1} \quad \textbf{(6- 54)}$$

Where

h_{2s} = enthalpy of isentropic process at the exit, KJ/Kg

h_{2a} = enthalpy of actual process at the exit, KJ/Kg

h_1 = enthalpy at the inlet, KJ/Kg

Then, the equation can be written in the follow form step by step.

$$\eta_c = \frac{h_{2s} - h_1}{h_{2a} - h_1} = \frac{c_p\left(T_2 - T_1\right)}{c_p\left(T_{2a} - T_1\right)} = \frac{\left(T_2 - T_1\right)}{\left(T_{2a} - T_1\right)} = \frac{\Delta T_s}{\Delta T} \qquad \textbf{(6- 55)}$$

Where

T_2= outlet temperature based on isentropic process, K

T_{2a}= actual outlet temperature, K

T_1= inlet temperature, K

Finally, the compressor actual outlet temperature can be demonstrated by the following equation combining Equation 6-53 and 6-55.

$$T_2 = T_1 + \Delta T = T_1 + \frac{1}{\eta_c}\Delta T_s = T_1\left\{1 + \frac{1}{\eta_c}\left[\left(\frac{P_2}{P_1}\right)^{\frac{\gamma-1}{\gamma}} - 1\right]\right\} \qquad \textbf{(6- 56)}$$

In the equation, the value of compressor adiabatic efficiency η_c is always between 0.7 and 0.8 for the centrifugal compressor. Thus 0.75 can be selected for the preliminary calculation. And based on engineering experience on the single-aisle civil transportation aircraft, the compressor compression ratio is normally from 1.0 to 1.8 for the classic ECS, though the value can reach 5 for the compressor used on Boeing 787 ECS air conditioning pack. Finally, the value of π_c is selected as 1.3 at stable condition in terms of the information shown in Figure 6-2.

6.4 Turbine

After the airflow is delivered into the turbine, the temperature will decrease due to expansion. At the same time, air expansion produces mechanical power to drive the shaft which connects the fan and compressor.

The parameters related with the turbine are shown in Figure 6-11.

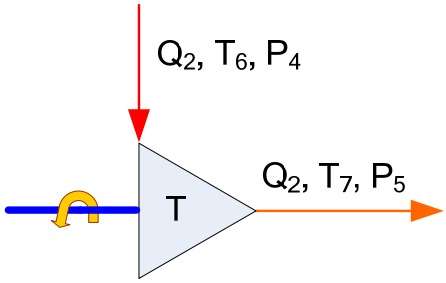

Figure 6- 11 Parameters about the turbine

The relationship between turbine inlet temperature T_6 and outlet temperature T_7 can be demonstrated by using the similar method for analyzing the compressor. Thus the following equation is derived.

$$T_7 = T_6 - \Delta T = T_6 - \eta_t \Delta T_s = T_6 \left\{ 1 - \eta_t \left[1 - \left(\frac{P_5}{P_4} \right)^{\frac{\gamma - 1}{\gamma}} \right] \right\} \qquad \textbf{(6- 57)}$$

Where

T_7 = turbine outlet temperature, K

T_6 = turbine inlet temperature, K

η_t = turbine efficiency, 0.75 for axial turbine

P_4 = turbine inlet pressure, pa

P_5 = turbine outlet pressure, pa

$\frac{P_5}{P_4}$ = reciprocal of turbine expansion ratio, $\frac{1}{\pi_t}$

In this equation, P_4 is decided by the engine bleed air pressure, the compressor compression ratio and the pressure drop when the airflow passes through the heat exchangers. P_5 can be computed by adding the entire downstream pressure drop and the cabin pressure together as shown in Equation 6-58. Then, the required expansion ratio π_t can be obtained.

$$P_5 = P_c + \sum \Delta P \qquad \textbf{(6- 58)}$$

Where

P_c = cabin pressure, pa

$\sum \Delta P$ = the total pressure drop from the turbine to the cabin, pa

The value of cabin pressure can be defined as 0.08Mpa since the cabin altitude is kept around 8,000ft during cruise. In order to calculate $\sum \Delta P$, all the downstream equipments should be taken into consideration in theory, including the condenser, the mix manifold and the ducts. This issue will be analyzed later.

6.5 Reheater and Condenser

Reheater and condenser are the typical equipments in the three-wheel high pressure water separation system. They are used to decrease the temperature of the airflow so that more moisture in the airflow can be condensed and then be extracted. In order to build corresponding models, the main parameters related to these two equipments are defined in Figure 6-12.

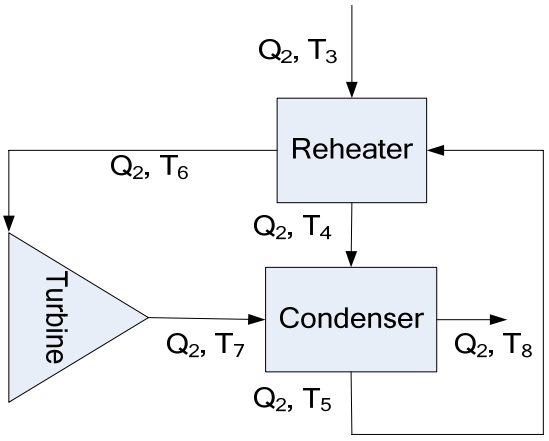

Figure 6- 12 Parameters about reheater and condenser

Here, information from Airbus 320 is adopted since it is difficult to find detailed structural parameters about the two equipments.

First of all, the efficiency of reheater can be obtained based on the information shown in Figure 6-2 as follows.

$$\varepsilon_R = \frac{T_3 - T_4}{T_3 - T_5} = \frac{318 - 317}{318 - 312} = 0.17 \quad \textbf{(6- 59)}$$

Thus the value of T_4 can be expressed by the following equation.

$$T_4 = 0.83T_3 + 0.17T_5 \quad \textbf{(6- 60)}$$

And based on the energy conservation law, the value of T_6 can be represented as follows.

$$T_6 = T_3 - T_4 + T_5 \quad \textbf{(6- 61)}$$

Similarly, corresponding data about the condenser can be got as follows.

$$\varepsilon_C = \frac{T_4 - T_5}{T_4 - T_7} = \frac{317 - 312}{317 - 271} = 0.11 \quad \textbf{(6- 62)}$$

$$T_5 = 0.89T_3 + 0.11T_5 \quad \textbf{(6- 63)}$$

$$T_8 = T_4 - T_5 + T_7 \quad \textbf{(6- 64)}$$

Consequently, the simulation model of HPWS can be achieved as shown in Figure B-12 of Appendix B. In the LPWS, T_8 can be regarded as T_7 because the influence from the water extractor can be ignored.

Besides, it can be stated that the humidity will increase the condenser outlet temperature due to the released heat because of condensation if there is much moisture in the airflow. Thus the actual condenser outlet temperature is higher than the ideal value. During cruise, this situation would not happen because of the nearly zero humidity so that the energy conservation law can be used to calculate the condenser outlet temperature.

At the same time, the pressure drop when the airflow passes through the reheater and condenser can be estimated by using Equation 6-25. Finally, the total pressure drop ΔP can be obtained by adding them together.

6.6 Cabin

In this research, the main aim of simulating the cabin is to check whether the inlet air mass flow can remove the cabin heat load and keep the cabin pressure altitude. Since the cruise phase has been selected as the only research object, the cabin pressure can be satisfied once the outlet air mass flow equals to the inlet air mass flow. Thus the only target here is to check whether the input air mass flow can remove the aircraft heat load. And because there is only one Cabin Pressure Control Valve (CPCV) in the aircraft, the whole aircraft, including the cockpit and cabin, can be regarded as one part. Thus the cabin model can be built as illustrated in Figure 6-13.

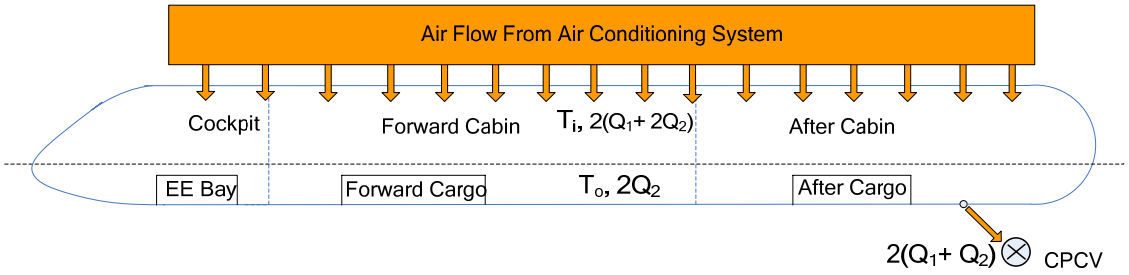

Figure 6- 13 Sketch of the cabin model

The CPCV keeps slightly open to maintain the cabin pressure during cruise, thus the outlet air mass flow can be regarded as equal to the inlet mass flow from the engines, which is $2(Q_1+Q_2)$. Then, the temperature of cabin inlet airflow can be defined as T_i, and the heat load used to calculate T_i can be computed as 13587W based on the calculation shown in Appendix A. It is caused by the occupants and solar radiation. Meanwhile, defining the ratio between fresh air and recirculated air in the mix manifold as 50%, the following equation can be obtained in terms that all the heat load in the cabin should be exhausted in order to keep the cabin temperature always around 21℃.

$$Q=\mathrm{W}c_p\left(T_c-T_i\right) \quad \textbf{(6- 65)}$$

Where

Q = total heat load in the cabin, W

W = inlet mass flow rate, kg/s

T_c = cabin temperature, K

T_i = cabin inlet airflow temperature, K

Taking related parameters in Equation 6-63 so that T_i can be expressed as follows.

$$T_i = 294.15 - \frac{13.52}{2\left(Q_1 + 2Q_2\right)} \quad \textbf{(6- 66)}$$

Since T_i always is no less than 10℃ in order to create comfortable airflow to the cabin, the relationship between Q_1 and Q_2 can be expressed by the following equation by taking it as 11℃ (284.15K) [38].

$$Q_1 + 2Q_2 = 0.676 \quad \textbf{(6- 67)}$$

At the same time, the temperature of CPCV outlet airflow can be calculated based on the whole heat load by the following equation.

$$T_o = 294.15 + \frac{Q}{2c_p\left(Q_1 + Q_2\right)} \quad \textbf{(6- 68)}$$

In Equation 6-68, Q is 7,000W based on the calculation shown in Appendix A.

6.7 Mix Manifold

The mix manifold is a simple mechanical component where the engine bleed fresh air and recirculated air mix with each other.

Based on the energy conservation law, the total input energy to the mix manifold can be computed by the following equation.

$$E = \sum_{i=1}^{n} Q_i \mathrm{h}_i \quad \textbf{(6- 69)}$$

Where

E = total input energy of the mix manifold, KJ

Q = air mass flow of each pass, Kg/s

h = enthalpy of each pass, KJ/kg

While the enthalpy value h can be calculated by the following equation.

$$h_i = c_p T_i \tag{6- 70}$$

Since c_p is constant as 1,005J/kg • K, the output temperature can be computed by the following equation.

$$T_O = \frac{\sum Q_i T_i}{\sum Q_i} \tag{6- 71}$$

In terms of the air conditioning system configuration and the definition of T_i shown in Section 6.6, the mix manifold inlet and outlet airflow parameters can be illustrated by the following figure.

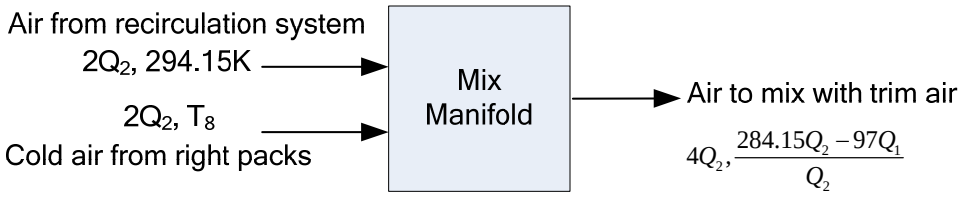

Figure 6- 14 Schematic of the mix manifold

Consequently, T_8 can be represented as follows.

$$T_8 = \frac{274.15Q_2 - 194Q_1}{Q_2} \tag{6- 72}$$

Till now, analysis about the system components and cabin has been finished. Consequently, corresponding simulation models can be built as shown in Appendix B. The next step is to check the validity of the models.

7 Validation of Models

In order to validate the simulation models, first of all the required ram air mass flow is calculated based on the parameters comes from Airbus 320. It should meet related published research result. Then, the temperature variation trend and values of the state points are checked.

The ECS provides 0.818kg/s fresh air to the aircraft during cruise on Airbus 320, thus it can be speculated that each air conditioning pack is responsible for about 0.4kg/s. Meanwhile, based on the information shown in Figure 6-2, the turbine outlet temperature should be around 271K (-2℃) under such a condition. Therefore, the required ram air mass flow can be obtained as 0.868kg/s through iterative calculation in terms of the simulation models as shown in Appendix B. This value meets the engineering experience and related research [3].

Besides, the temperature variation trend and values of the state points which are obtained based on the assembled model should be checked in order to verify the validity.

7.1 Primary Heat Exchanger

According to the analysis shown in Section 6.2, the variables related to the PHE and need demonstration are the heat transfer coefficient h_h, the fin efficiency fact η_{f} and the outlet temperature T_1.

The analysis about the heat transfer coefficient is shown in Section 6.2. It can be stated that h_h is a variable mainly related with the engine bleed air mass flow. Based on FAR Part 25.831, the air conditioning system should provide 250g/min fresh air to each of the passenger during flight. At the same time, the supplied air should remove the cabin heat load in time. Combining the information comes from Airbus 320, the value of engine bleed air Q_2 is defined as from 0.3kg/s to 0.5kg/s as discussed at the beginning of Chapter 6.

Since Q_c has been determined as 0.868kg/s, the curve depicted in Figure 7-1 is achieved by running the simulation model shown in Figure B-5 of Appendix B.

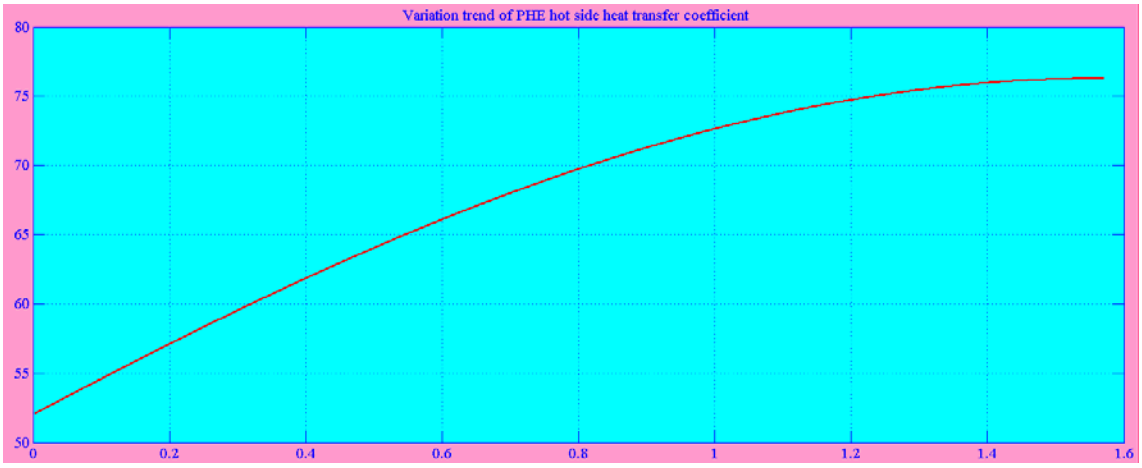

Figure 7- 1 Variation trend of PHE hot side heat transfer coefficient h_h

It can be seen that the value of heat transfer coefficient h_h increases with the increase of engine bleed air mass flow. This meets the actual condition. Combining the heat transfer area A and the fin efficiency factor η_f, the total heat transfer coefficient of the PHE hot air side can be calculated as around 600W/m^2 • K when Q_2 is 0.4kg/s. Based on engineering experience, this value is a little low but can be acceptable.

The value of heat transfer coefficient is not the key parameter which can be used to judge the validity of the simulation model. The final judgement will be made later based on whether the PHE have enough capability to cool the engine bleed air to required temperature as what shown in Figure 6-2.

The fin efficiency factor η_f of triangular fin is always between 0.3 and 1 and the higher the better [34]. This information can be used to check the simulation result of η_f. At the same time, it can be stated that the value of η_f will decrease with the increase of heat transfer coefficient h_h based on the definition shown in Equation 6-24. These two points are used to check the validity of simulation model about η_f.

The created variation curve of η_f is shown in Figure 7-2 in terms of the simulation model shown in Figure B-3.

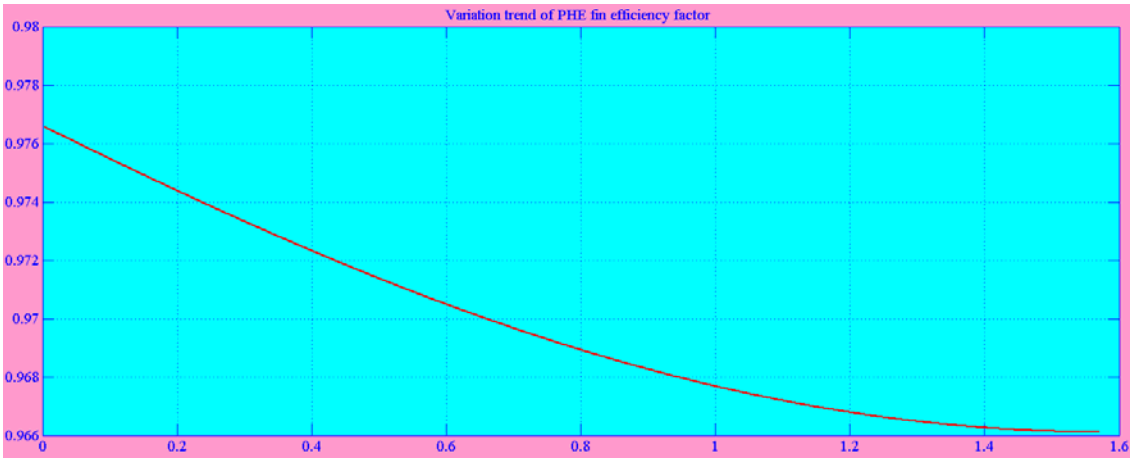

Figure 7- 2 Variation trend of PHE hot side fin efficiency factor η_{f}

It can be seen that the variation trend and range of the PHE fin efficiency factor η_{f} fully meets previous description. The values are between 0.966 and 0.977, which proves the fins are of high efficiency. Thus the simulation model of η_{f} is regarded as acceptable.

Meanwhile, the variation curve of PHE outlet temperature T_1 can be obtained based on the simulation model shown in Figure B-5. The value of Q_2 is also listed in order to help finding out corresponding temperature value.

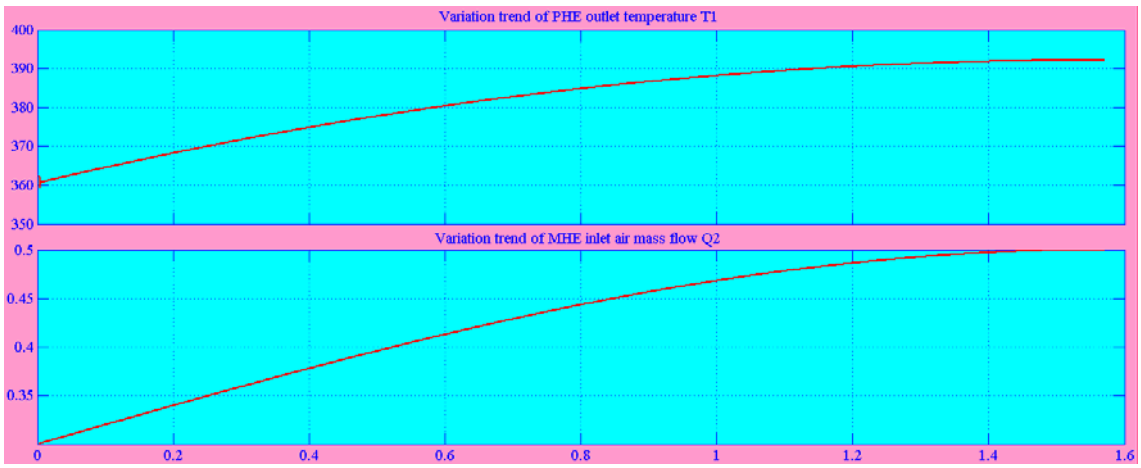

Figure 7- 3 Variation trend of PHE outlet temperature T_1

First of all, it can be seen that the PHE outlet temperature increases with the increase of engine bleed air mass flow when the inlet ram air mass flow is

0.868kg/s. This meets the actual condition. It also can be found that the temperature T_1 is 378K when engine bleed air mass flow is 0.4kg/s. It is only 3K lower than corresponding temperature value as shown in Figure 6-2. This proves that the heat transfer performance of the PHE is similar with the one used on Airbus 320.

At the same time, it also proves that the estimated parameters which are used to calculate the Reynolds number as shown in Section 6.2 are acceptable. A temperature difference of 3k would not affect the result of calculating the heat transfer coefficient based on Equation 6-21. And the small temperature difference can be regulated by the downstream equipments easily.

7.2 Compressor

Compressor determines the relationship between PHE outlet temperature T_1 and MHE inlet temperature T_2 . Defining the compression ratio as 1.3 and adiabatic efficiency as 0.75 as described in Section 6.3, the variation curve of compressor outlet temperature T_2 can be obtained as follows.

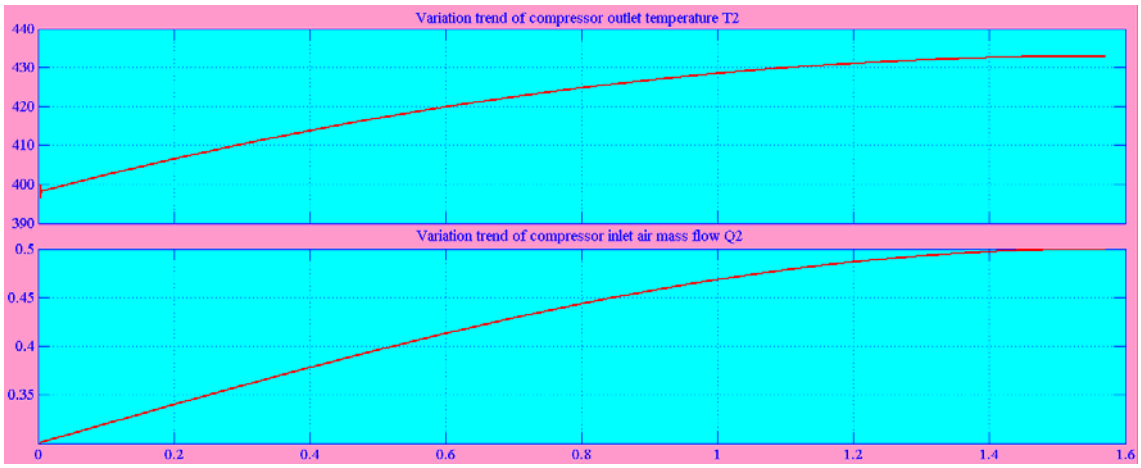

Figure 7- 4 Variation trend of compressor outlet temperature T_2

It is confirmed that the compressor outlet temperature is only influenced by the inlet temperature when the efficiency factor and compression ratio are constant as defined in Equation 6-56. And it is absolutely that the compressor inlet temperature increases with the increased engine bleed air. Thus it can be

stated that the compressor outlet temperature variation curve shown in Figure 7-4 meets the actual physical condition. At the same time, the value of T_2 can be found as 418K when the engine bleed air mass flow is about 0.4kg/s, while the temperature at this state point is 428K according to the information shown in Figure 6-2. It can be seen that there is a temperature difference of 10K, which is possibly caused by the lower PHE outlet temperature as mentioned in Section 7.1 and the indefinite adiabatic efficiency.

Based on above data and the simulation model, the outlet temperature can reach a value of 428K if the compression ratio increases to 1.38. But since the downstream equipments will continue to regulate the temperature, there is no need to do such modification now.

7.3 Main Heat Exchanger

The performance of MHE affects the reheater inlet temperature T_3 directly. Once the mechanical dimensions and ram air mass flow are fixed, the engine bleed air mass flow determines the outlet temperature.

The MHE simulation model is built as shown in Figure B-6 of Appendix B. Similar with the description shown in Section 7.1, the MHE hot side heat transfer coefficient h_h is analyzed. The created curve is shown as follows.

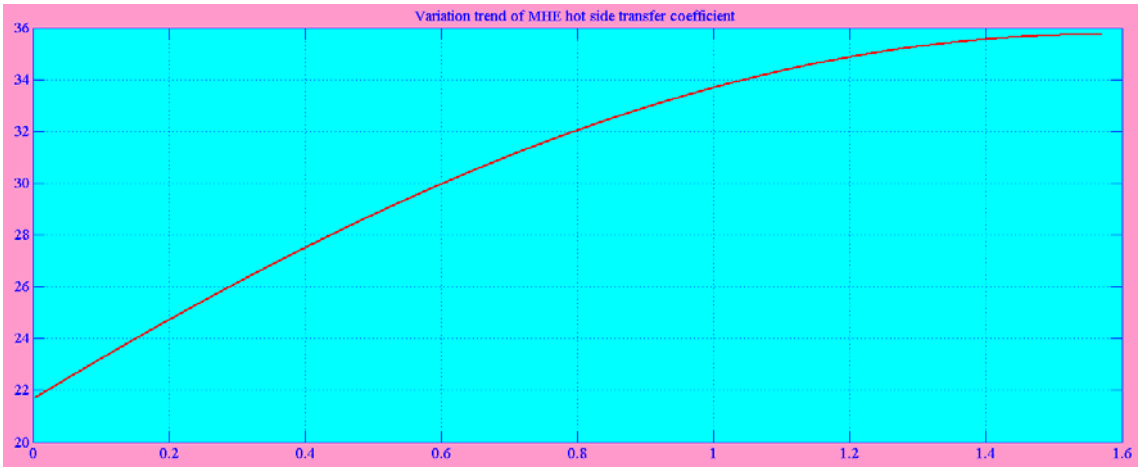

Figure 7- 5 Variation trend of the MHE hot side heat transfer coefficient h_h

It can be seen that the heat transfer coefficient h_h increases with the increase of engine bleed air. But the value at corresponding point is much less than that of the PHE. The MHE heat transfer coefficient of hot air side is 29W/m^2 • K while corresponding value is 65 W/m^2 • K of the PHE when the engine bleed air mass flow is 0.4kg/s. Based on the heat transfer area A and the fin efficiency factor η_f, the total heat transfer coefficient of the MHE hot air side can be calculated as 600W/m^2 • K, which is almost the same as that of PHE hot air side.

As mentioned in Section 7.1, the fin efficiency factor of triangular fin is normally between 0.3 to 1 and the higher the better. Based on the simulation model shown in Figure B-8 of Appendix B, the following curve is achieved, which illustrates the variation trend and range of MHE fin efficiency factor.

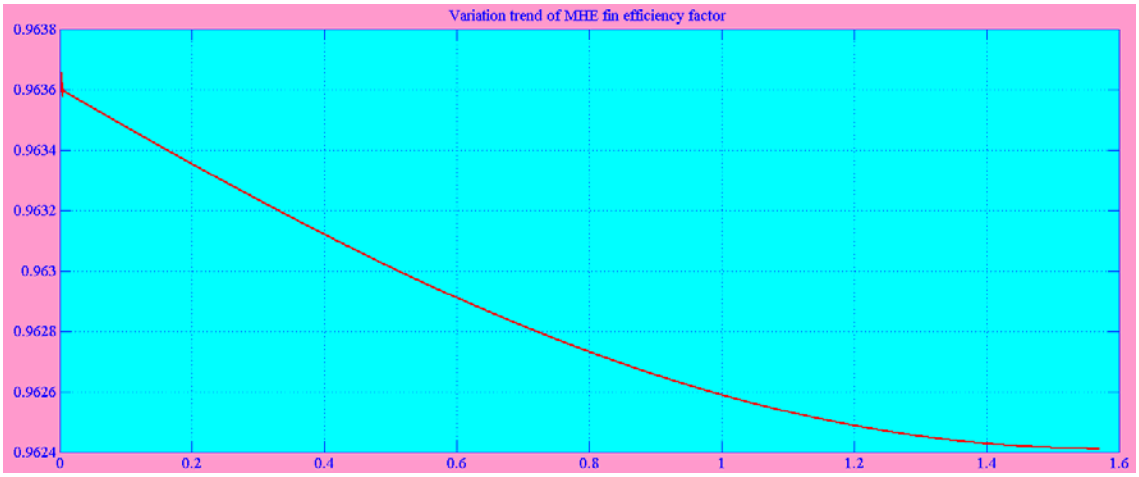

Figure 7- 6 Variation trend of the MHE fin efficiency factor η_f

It can be seen that the MHE fins are of high efficiency that the efficiency factor is from 0.962 to 0.964, which is similar with that of the PHE fins. Similar with the analysis about the PHE fins, it can be stated that the estimated dimensions about the MHE structure and fins are acceptable.

At the same time, the simulation curve of the MHE outlet temperature T_3 can be achieved as shown in Figure 7-7. It can be seen that MHE outlet temperature increases with the increased engine bleed air when the ram air mass flow is constant. This meets the actual physical condition.

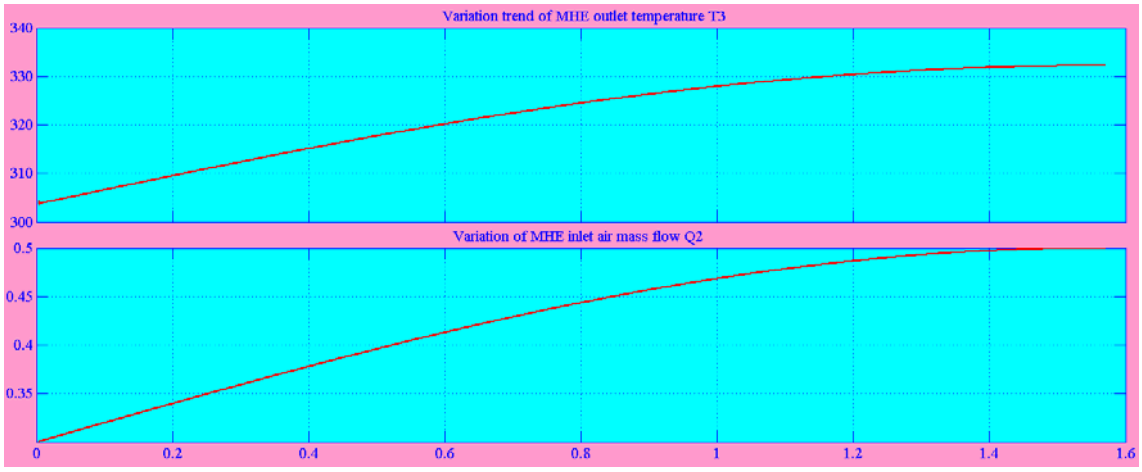

Figure 7- 7 Variation trend of the MHE outlet temperature T_3

Meanwhile, the temperature is 319K when the engine bleed air mass flow is 0.4kg/s, which is just 1K higher than that of Airbus 320. This means the estimated parameters about the heat exchanger and fins are acceptable. The simulation model can be used for next research.

7.4 Turbine

The inlet temperature, the adiabatic efficiency and the expansion ratio determines the turbine outlet temperature together. The initial adiabatic efficiency is selected as 0.75 for axial turbine as discussed in Section 6.4. The expansion ratio can be obtained as 2.0 by taking the inlet temperature as 313K and outlet temperature as 271K into Equation 6-57 according to the information shown in Figure 6-2 from Airbus 320. These data are used as the preliminary input for the turbine simulation model. Consequently, the turbine simulation model can be built as shown in Figure B-11 of Appendix B. And the created curve of turbine outlet temperature is shown in Figure 7-7.

It can be seen that the variation trend meets the actual physical process. Besides, the temperature is 271K when the inlet engine bleed air mass flow is 0.4kg/s, which perfectly meets the information shown in Figure 6-2. Since the turbine outlet temperature is a key value in the system, it is selected to calculate required ram air mass flow.

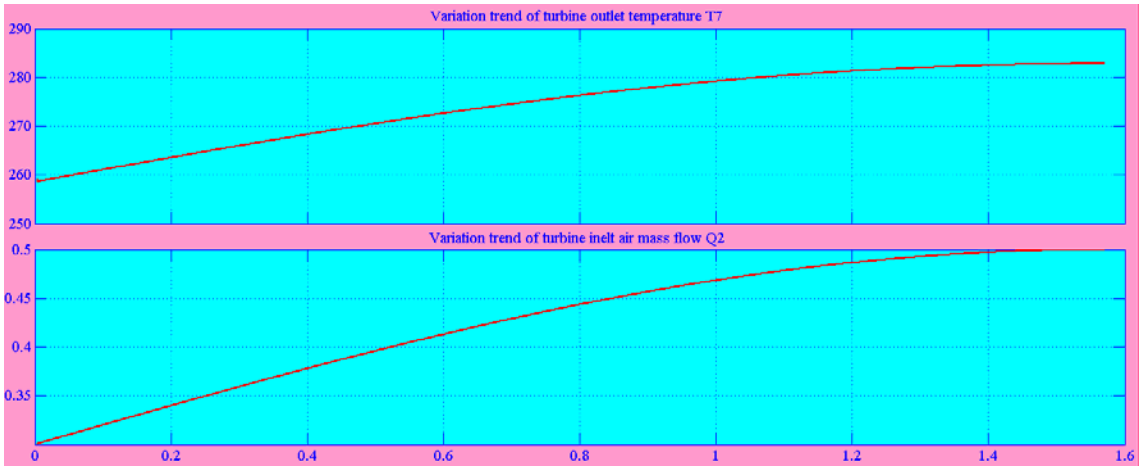

Figure 7- 8 Variation trend of turbine outlet temperature T_7

7.5 High Pressure Water Separation System

Through using the data comes from Airbus 320, the efficiencies of the reheater and condenser have been obtained as 0.17 and 0.11 respectively. Thus the simulation model is built as shown in Figure B-12 of Appendix B. Consequently, the variation trend of condenser outlet temperature can be created as shown as follows.

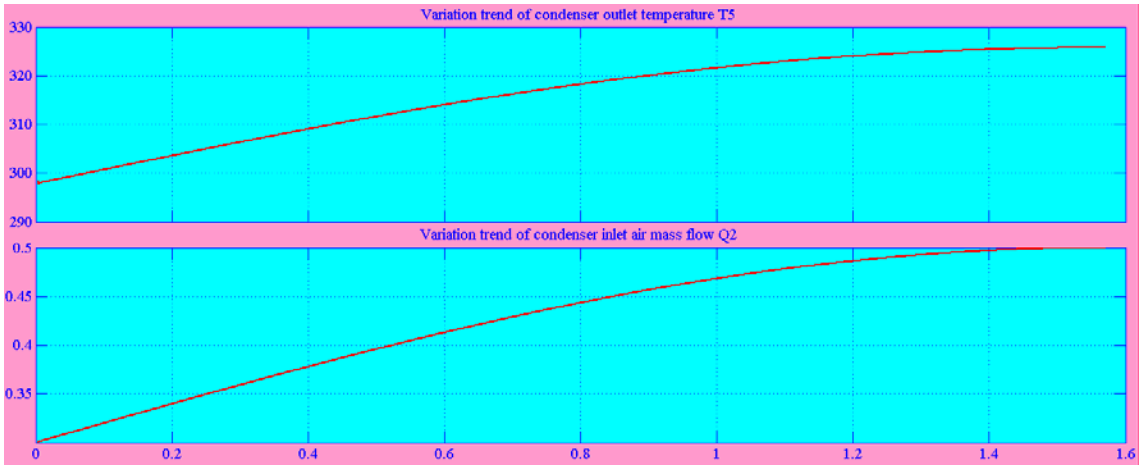

Figure 7- 9 Variation trend of condenser outlet temperature T_5

It can be seen that the variation trend meets the actual physical condition. And the temperature is 312.5K when the engine bleed air mass flow is about 0.4kg/s, which just has a deviation of 0.5K compared with the information shown in Figure 6-2. Thus the simulation model is regarded as valid.

Similarly, the variation trend curve of reheater outlet temperature can be created as follows.

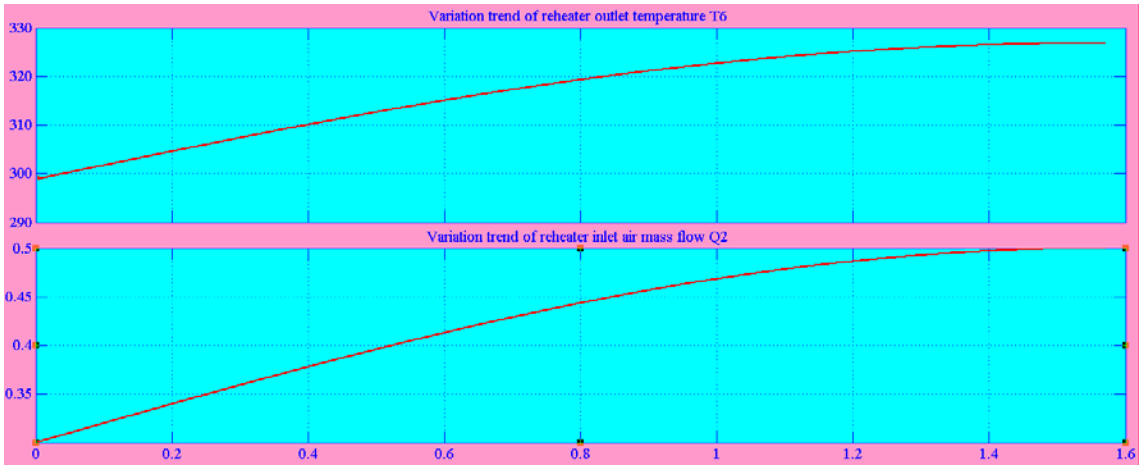

Figure 7- 10 Variation trend of reheater outlet temperature T_6

It can be seen that the variation trend meets the actual physical condition. And the temperature is 313.5K when the engine bleed air mass flow is about 0.4kg/s, which is only 0.5K higher than that of Airbus 320 as shown in Figure 6-2. Thus the simulation model is regarded as valid.

Till now, it can be stated that the simulation model of HPWS is acceptable because the created curves of the components fit the information shown in Figure 6-2 perfectly. Thus consequent simulation and analysis can be done.

7.6 Low Pressure Water Separation System

Since the LPWS just has a water extractor, it does not create temperature difference between the turbine outlet and mix manifold inlet. The effect from the water extractor to the system is ignored. The mix manifold inlet temperature can be regarded as equal to the turbine outlet, which is shown in Figure 7-8.

Till now, the HPWS model has been built and validated. In order to show how good it fits the reality based on the information comes from Airbus 320, both of the created temperature variation curve and that on Airbus 320 are illustrated in one picture as follows. In conclusion, the simulation model can be used for later research because of the small deviations. The LPWS model can be obtained by just removing the models of reheater and condenser.

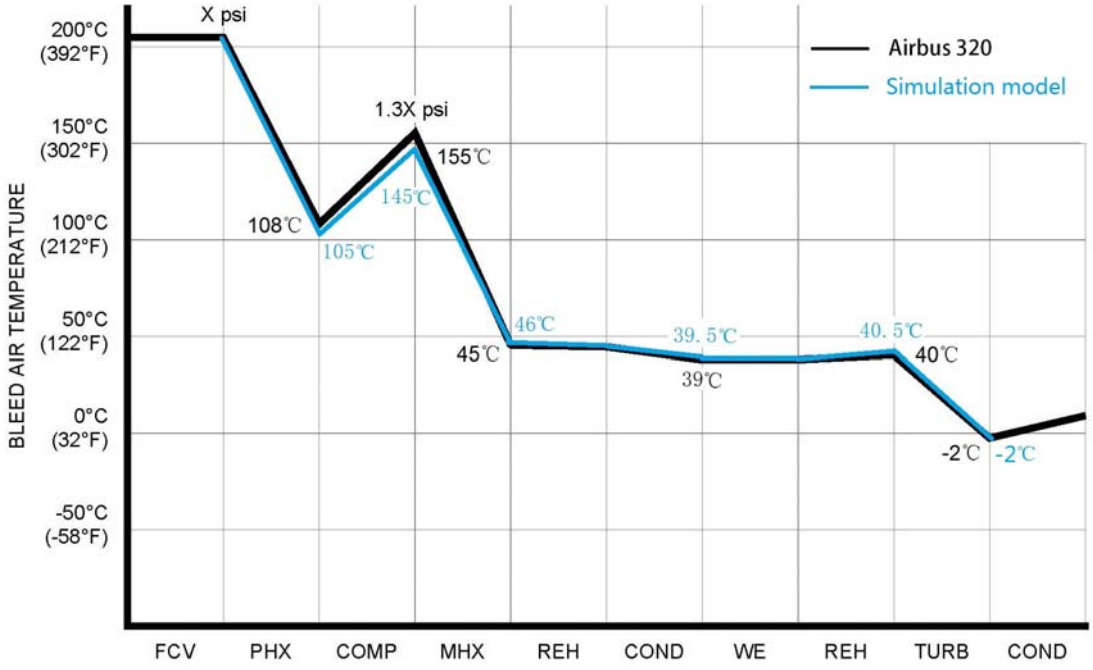

Figure 7- 11 Simulation results of the air conditioning pack

8 Analysis and Comparison

Based on the analysis shown in Section 6.6, because the cabin inlet air temperature is almost constant in order to meet the comfort requirements, it can be stated that the cabin inlet air mass flow decides whether the cabin heat load can be extracted fully. Then, related temperature values can be expressed by the mass flow.

Since the quantity of engine bleed air has been defined in Equation 6-67 and the maximum Q_2 is 0.338kg/s, the mix manifold inlet temperature T_8 can not exceed 274K based on Equation 6-72. Thus the following table is obtained.

Table 8- 1 Relationship between T_8 and required engine bleed air mass flow

No.	T_8 (K)	Q_1 (kg/s)	Q_2 (kg/s)	Q_1+Q_2 (kg/s)
1	270	0.008	0.334	0.342
2	271	0.006	0.335	0.341
3	272	0.004	0.336	0.340
4	273	0.002	0.337	0.339
5	274	0	0.338	0.338

It can be seen that higher T_8 requires less engine bleed air. Literally, T_8 of 274K can be selected for research. But the trim air is necessary because it probably be used to control the temperature of some areas. And Q_1 of 0.002kg/s is too low for the flow control and pressure regulation in the air supply ducts. Therefore, T_8 of 272K, corresponding Q_1 of 0.004kg/s and Q_2 of 0.336kg/s are selected as the research basis.

It is obviously that the turbine outlet temperature equals the mix manifold inlet temperature in the LPWS, while the latter is higher than the turbine outlet temperature in the HPWS since it gets heat from the condenser. This is the

main difference between these two configurations, which may cause different requirement about engine bleed air mass flow and ambient ram air mass flow, or requires different turbine expansion ratios. Therefore, the value of T_7 and T_8 demonstrated in Section 6.4 and 6.5 are selected as research objects.

Meanwhile, there is one point should be clarified again. It has been stated in many documents that the airflow moisture content in the HPWS and LPWS is different. This brings different dew point temperature. Normally, the dew point temperature is higher in the LPWS than that in the HPWS, which means the airflow is easier to condense and even get icing. Ice in the airflow must be avoided because it may block or damage the downstream equipments. Therefore, the turbine outlet temperature in the LPWS can not be decreased to as low as that in the HPWS. But in this research, the cruise phase is selected as the only research object, where the environment absolute humidity is nearly zero at an altitude of higher than 6,700m [8]. This means the moisture content in the engine bleed air is not a factor which will limit the turbine outlet temperature. Thus the turbine outlet temperature can be lower than 0℃ for both of the two configurations.

8.1.1 Constant turbine expansion ratio

As analyzed in the above section, once the engine bleed air mass flow is confirmed, the ram air mass flow and turbine expansion ratio determines the mix manifold inlet temperature. In order to keep the cabin comfort and remove the heat load successfully, the required fresh air to each of the air conditioning pack has been defined as 0.336kg/s. This is the basis for later analysis.

As mentioned in Section 7.4, the turbine expansion ratio π_t is 2.0 during cruise on Airbus 320 and the efficiency is 0.75. These two values are selected as the preliminary inputs in this section. And in order to find out possible regular pattern, similar expansion ratios, like 1.6, 1.8, 2.2 and 2.4 are also selected to calculate corresponding ram air mass flow.

In the LPWS, the required turbine outlet temperature, which is the same as the mix manifold inlet temperature, has been defined as 272K. Consequently, the

required ram air mass flow Q_c can be obtained as 0.781kg/s based on the simulation model.

In the HPWS, according to the simulation model shown in Figure B-12, the required ram air mass flow can be got as 0.793kg/s in order to get a mix manifold inlet temperature of 272K. And the turbine outlet temperature can be obtained as 267K.

Finally, the following table can be obtained by summarizing all the above information.

Table 8- 2 Required Q_c in the LPWS and HPWS under the same η_t

No.	Turbine expansion ratio π_t	Required Q_c in the LPWS (kg/s)	Required Q_c in the HPWS (kg/s)	Mass flow difference (kg/s)
1	1.6	1.052	1.061	0.009
2	1.8	0.891	0.902	0.011
3	2.0	0.781	0.793	0.012
4	2.2	0.701	0.713	0.012
5	2.4	0.639	0.650	0.011

It can be seen that the LPWS requires less ram air compared with the HPWS when the turbine expansion ratio is the same. The difference of required ram air mass flow is quite similar as shown in Table 8-2, which is about 0.012kg/s (43.2kg/h) no matter what the turbine expansion ratio is. And based on the information shown in Table 8-2, the following figure can be obtained, which illustrates the variation trend of Q_c with the increased π_t and the difference of Q_c under the same π_t.

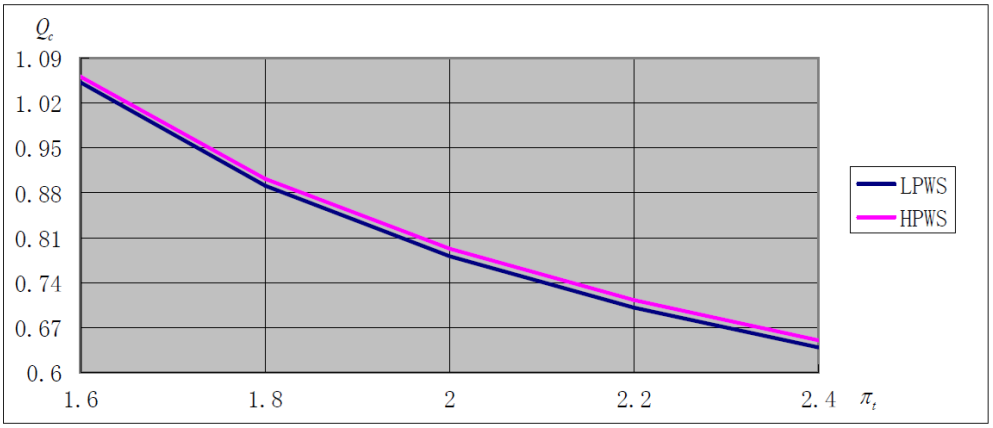

Figure 8- 1 Variation trend of Q_c with increased π_t

It can be stated that higher expansion ratio leads to less ram air mass flow. And the two curves are almost parallel, which means the difference of ram air mass flow in the LPWS and HPWS keeps constant in spite of the increased η_t.

8.1.2 Constant ram air mass flow

When the engine bleed air mass flow is defined, the ram air mass flow and turbine expansion ratio decide the mix manifold inlet temperature together. Section 8.1.1 has discussed the different ram air mass flow requirement when the turbine expansion ratios are the same for the low and high pressure water separation system. This section will analyze the difference of turbine expansion ratios when the ram air mass flow is the same.

The ram air mass flow which can be used to do the analysis in this section is based on what are shown in Table 8-2. Consequently, corresponding required turbine expansion ratios can be obtained based on the simulation model of HPWS and LPWS. The detailed data is shown as follows.

Table 8- 3 Required π_t in the LPWS and HPWS under the same Q_c

No.	Ram air mass flow	Required π_t for the LPWS	Required π_t for the HPWS	Expansion ratio difference
1	0.6kg/s	2.55	2.61	0.06
2	0.7 kg/s	2.20	2.24	0.04
3	0.8 kg/s	1.96	1.98	0.02
4	0.9 kg/s	1.78	1.80	0.02
5	1.0 kg/s	1.66	1.67	0.01

It can be seen that the turbine in the HPWS reaches a slightly higher expansion ratio than that in the LPWS when the ram air mass flow is the same when it aims at the same mix manifold inlet temperature. The required π_t decreases with the increase of ram air mass flow. And the difference of required π_t between the LPWS and HPWS decreases with the increased ram air mass flow. Figure 8-2 shows the variation trend.

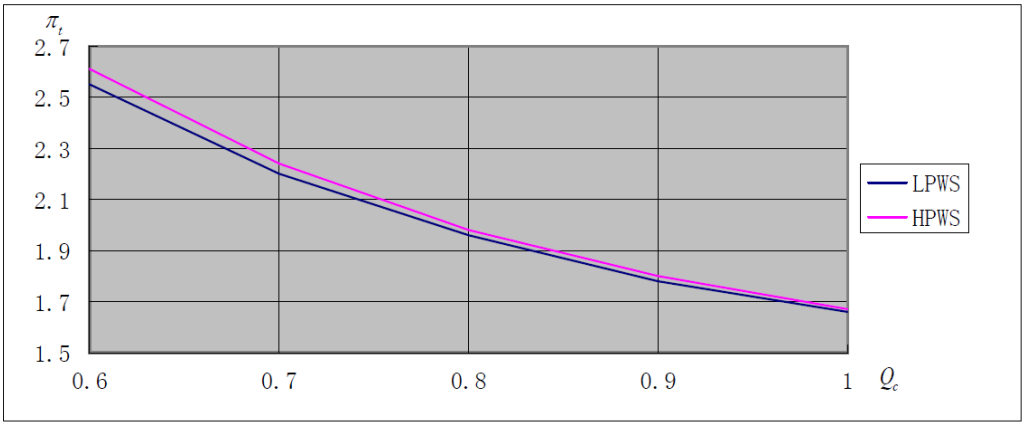

Figure 8- 2 Variation trend of π_t with increased Q_c

8.1.3 Results and discussion

There are mainly two points can be drawn based on what are shown in the above two sections. The precondition is that the same mix manifold inlet temperature is satisfied and effects from the humidity are ignored.

- The LPWS requires about 0.012kg/s ram air less than the HPWS when the turbine expansion ratio is the same (around 2.0). And the difference almost keeps constant with the variation of turbine expansion ratio.
- The HPWS requires a turbine expansion ratio of about 0.02 higher than that in the LPWS when the ram air mass flow is the same (around 0.8kg/s). And the difference decreases with the increase of ram air mass flow. When the ram air mass flow reaches to about 1kg/s, the required turbine expansion ratio of the LPWS and HPWS are almost the same.

Therefore, it can be stated that the required inputs is quite similar for both of the LPWS and HPWS which are aiming at the same cabin comfort requirements. The LPWS has advantage but it is not so apparent. But according to related research, the LPWS has some other obvious advantages, such as it has less accessories (82% of HPWS), lower mass (63% of HPWS), lower cost (83% of HPWS) and higher reliability (140% of HPWS) [11]. Therefore, it is reasonable to choose the LPWS for the aircraft ECS during cruise.

Meanwhile, it can be seen the calculated mix manifold inlet temperature is 272K in this research, which is less than 0℃. The LPWS may not reach such a low temperature if there is moisture in the engine bleed air because it should avoid the risk of getting ice. Thus the temperature of cabin inlet airflow would be higher than what defined in this research (11℃), which leads to consume more engine bleed air. This condition always happens at the flight phases except cruise and it should be analyzed individually. The HPWS has advantage under such conditions.

In the HPWS, the water extractor is located at the upstream of the turbine. Thus the moisture content in the turbine inlet airflow is quite low. Consequently, the low dew point can satisfy a low turbine outlet temperature, which normally can

below 0℃. Meanwhile, because of the low moisture content, the heat due to water condensation in the HPWS is obviously smaller than that in the LPWS when the airflow is discharged from the turbine. The heat because of water condensation can not be ignored. For example, it can be calculated that the heat due to 1g of condensation water may increase the temperature of turbine outlet airflow by 2.5℃ when the engine bleed air mass flow is around 0.4kg/s [11]. This condition can be selected as a special research topic.

Besides, it is found that the percentage of recirculated air in the mix manifold also affects the demanded turbine outlet temperature apparently in this research. More recirculated air is recycled leads to lower required turbine outlet temperature. Actually the percentage of recirculated air is around 35% on Airbus 320. Thus the required turbine outlet temperature is higher than 0℃ and the LPWS can meet such requirement.

8.2 Analysis of Pressure Variation

Analysis of pressure variation trend in the system helps to judge the system configuration feasibility assistant with the temperature simulation model. Based on the simulation and analysis shown in Section 8.1.3, the LPWS is better for the aircraft during cruise. Thus this configuration is analyzed.

The main aim of analyzing the pressure condition when the airflow is going forward in the air conditioning system is to make sure that there is appropriate pressure difference between the cabin air supply duct outlet port and cabin. Enough fresh air mass flow and limited air speed should be satisfied.

In the aircraft ECS, the pressure of cabin inlet airflow mainly decided by four aspects, which are the pressure of turbine outlet airflow, the pressure of trim airflow, the pressure of cabin and the pressure drop in the air supply ducts.

The pressure of the turbine outlet airflow is decided by three aspects, which are the compressor compression ratio, the turbine expansion ratio and the pressure drop in heat exchangers.

Since the engine bleed air mass flow Q_2 has been defined as 0.336kg/s, the ram air mass flow Q_c can be obtained as 0.639kg/s in order to satisfy a mix manifold inlet temperature of 272K. Consequently, all the temperature values of the state points can be got. First of all, the pressure drop due to the MHE can be calculated based on the description shown in Section 6.1.

$$\Delta P_1 = \lambda \frac{L}{D} \frac{\rho V^2}{2}$$
$$= 0.017 \times \frac{0.8}{0.089} \times \frac{3.19 \times 17.55^2}{2} = 75\text{pa}$$

$$\Delta P_2 = \lambda \frac{L}{D} \frac{\rho V^2}{2}$$
$$= 0.05 \times \frac{0.17}{0.015} \times \frac{3.36 \times 1.52^2}{2} = 2\text{pa}$$

$$\Delta P_3 = \lambda \frac{L}{D} \frac{\rho V^2}{2}$$
$$= 0.017 \times \frac{0.8}{0.01} \times \frac{4.17 \times 10.07^2}{2} = 284\text{pa}$$

$$\Delta P = \Delta P_1 + \Delta P_2 + \Delta P_3 = 361 pa$$

Similarly, the pressure drop happens in the PHE can be calculated as 420pa according to the analysis shown in Section 6.2. Based on above calculation, it can be concluded that the pressure drop in the heat exchangers can be ignored because it is so little when compared with the effects from compressor and turbine. The turbine outlet temperature is only relying on the compressor compression ratio and turbine expansion ratio.

The pressure of trim air can be computed based on the cabin pressure and pressure drop in the air supply ducts. Based on the system configuration, the pressure model can be built as the following figure.

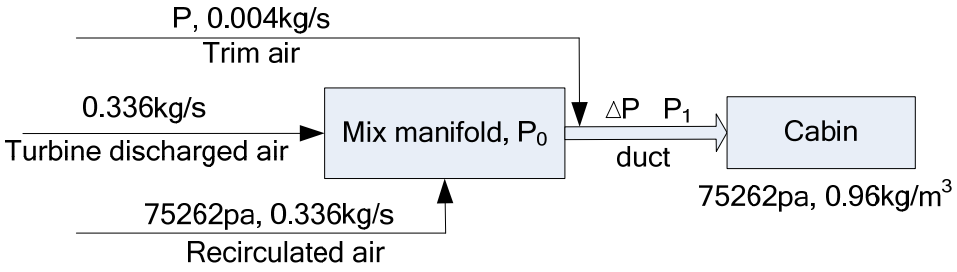

Figure 7- 12 Cabin pressure model

Since the cabin pressure is kept at an altitude of 8,000ft (75262pa), the air density can be calculated as 0.96kg/m^3. Once the speed of cabin inlet airflow is defined, the required pressure of the air supply duct outlet port can be calculated as follows by the Bernoulli equation.

$$P_1 = \frac{1}{2}\rho v^2 + P_c \qquad \textbf{(7- 1)}$$

Where

P_1 = pressure of cabin air supply duct outlet port, pa

ρ = density of cabin inlet airflow, kg/m^3

v = speed of cabin inlet airflow, m/s

p_c = cabin pressure, pa

Then, the Reynolds number of the airflow in the air supply duct should be calculated by Equation 6-12. The only required input is the diameter of the air supply ducts, since the temperature has been defined as 284K (11℃) and the pressure can be regarded as equal to the cabin pressure roughly.

Consequently, the friction factor can be found from the Moody diagram. Then, the pressure drop in the duct can be calculated by the Darcy-weisbach equation. Thus value of P_o can be obtained roughly by adding P_1 and ΔP together. Finally, the required pressure of the trim air can be computed by the following equation.

$$P \approx \frac{1}{2}\rho v^2 + P_0 \qquad \textbf{(7- 2)}$$

Where

P = pressure of trim airflow, pa

ρ = density of trim air, kg/m^3

v = speed of trim air, m/s

The main variables of affecting the pressure analysis are the duct diameters. Since there are no parameters about the ducts are found and it is better to analyze the pressure model based on a specific aircraft, thus here just introduced the method.

9 CONCLUSION

9.1 General Conclusion

Based on the simulation and analysis, it can be stated the LPWS is better for the specific aircraft during cruise than the HPWS. About 0.012kg/s of ram air is saved when the turbine expansion ratio is 2.0 and it keeps such an advantage not matter what the turbine expansion ratio is. The turbine expansion ratio just has a difference of 0.02 when the ram air is the same (around 0.8kg/s). And it becomes smaller and smaller with the increased ram air mass flow. Beyond the technical advantage, the LPWS has less accessories (82% of HPWS), lower mass (63% of HPWS), lower cost (83% of HPWS) and higher reliability (140% of HPWS). Thus the conclusion is drawn.

In the research, the author uses a new method to build simulation models for the PHE and MHE. The heat exchangers are considered as the intermediate equipment, which means heat transfer is between the airflow and heat exchangers, instead of between the hot airflow and cold airflow. And since it is difficult to deal with a number of variables in the simulation model, an estimation of the airflow average temperature when it passes through the heat exchangers is made based on the information comes from Airbus 320. Temperature of the heat exchanger themselves are expressed in terms of the energy conservation law. Meanwhile, the simulation models of compressor and turbine are built based on the isentropic process and adiabatic efficiency factor, and that of the reheater and condenser are based on the heat exchanger efficiencies. The simulation models of the cabin and mix manifold are built according to the cabin heat balance requirement and energy conservation law.

Then, since the required ram air mass flow meets engineering experience and related research, the created temperature variation curves just has small deviations compared with that of Airbus 320, conclusion is drawn that the simulation models can meet the Airbus 320 ECS performance curve quite well. Thus the simulation model is confirmed. Therefore, the model can be used for related research about aircraft ECS analysis based on a specific aircraft.

At the same time, since the cruise phase is selected as the only research object during flight, the aircraft flight altitude is about 37,000ft, where the absolute humidity is nearly zero. The moisture content in the engine bleed air is quite low. Consequently, the turbine outlet temperature can be lower than 0℃ since the risk of getting ice does not exist. This is the precondition on building and analyzing the simulation model.

The required fresh air mass flow can be calculated based on the cabin heat load and cabin inlet airflow temperature. Then, there are only two parameters influencing the system performance, which are the ram air mass flow and turbine expansion ratio.

In order to find out possible variation trend of the ram air mass flow when the turbine expansion ratio is the same in the low and high pressure water separation system, the author analyzes five different values of π_t. It can be concluded that the LPWS requires less ram air in all these conditions.

When the ram air mass flow is constant, corresponding turbine expansion ratio in the low and high pressure water separation system are different. π_t in the HPWS is just slightly higher than that in the LPWS, and the difference gets smaller and smaller with the increased ram air mass flow .

Finally, since the pressure at the cabin inlet port is decided by four aspects, which are the pressure of the turbine outlet air, the cabin recirculated air, the trim air and the pressure drop caused by the air supply ducts, the pressure model can be built. But since no parameters about the air supply ducts are found, there is no need to estimate many data to do the detailed calculation, thus only the method is introduced.

9.2 Future Work

Due to the insufficient data about the tubes and fins of heat exchangers, the author made some estimation about the dimensions of the fins based on related research. This may caused some deviation from the practical heat exchanger

structure. Therefore, some data may be updated later if more precise parameters are obtained, which will make the simulation more accurate.

Actually, the main difference of LPWS and HPWS are caused by the moisture in the airflow. The HPWS can remove more moisture from the system thus the turbine outlet temperature and heat due to moisture condensation are lower than that in the LPWS. This issue can be selected as a special topic for future research.

And based on the simulation model, it is found that the compressor and turbine adiabatic efficiencies affect the performance of the system performance apparently. This can be selected as one topic for later researchers.

Finally, due to lack of parameters about the air supply ducts, the author just introduced the method about calculating the pressure drop. The truth is that there are several different diameters of ducts in the system. Moreover, the bending radius of the duct junctions will also affect the pressure drop apparently. Thus the simplified method may cause deviation on pressure drop calculation. The best way of analyzing the ducts is to build calculation model based on a specific aircraft.

REFERENCES

[1] Vega Diaz, R. (2011), "Analysis of an electric environmental control system to reduce the energy consumption of fixed-wing and rotary-wing aircraft", Cranfield University.

[2] Mahindru, D. and Mahendru Sr, P. (2011), "Environmental Control System for Military and Civil Aircraft", *Global Journal of Research Engineering,* vol. 11, no. 5_D.

[3] Isidoro, M. (1995-2013), *Aircraft Environmental Control*. http://webserver.dmt.upm.es/~isidoro/tc3/Aircraft%20ECS.pdf

[4] Cavcar, M. (2000), "The International Standard Atmosphere (ISA)", *Anadolu University, Turkey.*

[5] Sinnett, M. (2007), "787 No-bleed systems: saving fuel and enhancing operational efficiencies", *Aero Quarterly*, pp. 6-11.

[6] Airbus (January 2013), *Airbus_Summary_Results_1989-2012-update_Jan2013*, available at: *http://www.airbus.com/no_cache/company/market/orders-deliveries/* (accessed March 2013).

[7] Paolo, A. (2009), *Numerical Models for Aircraft Systems – lecture notes, Chapter 6 – Environmental Control System*, Politecnico Di Milano.

[8] *Civil Aviation Regulation of China, Part 25 Airworthiness Standards: Transport Category Airplanes* (2011), R4, CAAC.

[9] *http://ozten.net/aviation/Airbus 320/images/Wingaicejpeg.*

[10] Omer Majeed, P. E. (November, 2010), *Aircraft Environmental Control Systems, A Presentation of Current Systems and New Developments,* AERO 4003, Carleton University.

[11] Shou, R. and He, H. (2004), *Flight Vehicle Environmental Control,* Press of Beijing University of Aeronautics and Astronautics.

[12] Mathieu, K. (2006), "Simulation of Components from the Environmental Control System". http://www.fzt.haw-hamburg.de/pers/Scholz/arbeiten/TextKwiatkowski.pdf

[13] Janardhana, S. (2012), "Cabin Heat Loads Modeling and Dynamic Simulation of ECS for a Single Seater Fighter Aircraft".

[14] Hunt, E. H., Reid, D. H., Space, D. R. and Tilton, F. E. (1995), "Commercial airliner environmental control system: Engineering aspects of cabin air quality", *Aerospace Medical Association annual meeting.*

[15] Elwood H. Hunt and David R. Space (1994), "The airplane cabin environment", available at: http://citeseerx.ist.psu.edu/viewdoc/download?doi=10.1.1.304.7321&rep=rep1&type=pdf

[16] Nan, G. and Sun, X. (2012), "Analysis of the Recirculation Impact to Aircraft Air Conditioning Performances", *Civil Aircraft Design & Research,* No.4, pp. 42.

[17] Andreas, B. (2009), "Environmental Control Systems", *ICE International Aviation Conference*, 9-10 March.

[18] Zhao, H., Hou, Y., Zhu, Y., Chen, L. and Chen, S. (2009), "Experimental study on the performance of an aircraft environmental control system", Applied Thermal Engineering, vol. 29, no. 16, pp. 3284-3288.

[19] Müller, C., Scholz, D. and Giese, T. (2007), "Dynamic simulation of innovative aircraft air conditioning", available at: http://www.mp.haw-hamburg.de/pers/Scholz/FLECS/FLECS_Paper_CEAS_07-09-10.pdf

[20] He, H. and Hao, J. (1996), "Optimum Design for Environmental Control System of Aircraft Cabin", Journal of Beijing University of Aeronautics and Astronautics, vol. 22, no. 5.

[21] SAE Aerospace, Applied Thermodynamics Manual, (2004), Air Conditioning Load Analysis, Society of Automotive Engineers, USA.

[22] Tang, C. (2011), Environment Control System for All Electric Aircraft Flying Crane, Cranfield University.

[23] Sikorski, E. (2010), "Air-Conditioning of Parked Aircraft by Ground-Based Equipment", International Refrigeration and Air Conditioning Conference.

[24] Zhang, X., Yang, C. and Yuan, X. (December, 2009), "Engineering estimation methods of thermal load of airplane", Journal of Beijing University of Aeronautics and Astronautics.

[25] Niu, C. (1999), Airframe structural design: practical design information and data on aircraft structures, Conmilit Press Limited.

[26] Krakers, L. (2009), Parametric fuselage design, Integration of mechanics and acoustic & thermal insulation (Doctor of Philosophy thesis), Delft University of Technology.

[27] Van Tooren, M. and Krakers, L. (2007), "Multi-disciplinary Design of Aircraft Fuselage Structures", 45th AIAA Aerospace Sciences Meeting and Exhibit.

[28] Airbus (2005), "Airbus 320 Aircraft Characteristics - Airport and Maintenance Planning", available at: http://www.airbus.com/fileadmin/media_gallery/files/tech_data/AC/Airbus-AC-A320-Jun2012.pdf

[29] Zhang, T. T., Tian, L., Lin, C. and Wang, S. (2012), "Insulation of commercial aircraft with an air stream barrier along fuselage", Building and Environment, Volume 57, pp. 97-109.

[30] Liu, J. (2000), *Civil Transportation Aircraft Configuration Preliminary Design and Propulsion System Integration Design, Volume 7 of Aircraft Design Manual, Aviation Industry Press, Beijing.*

[31] Raymer, D. P. (2006), *Aircraft design: a conceptual approach,* American Institute of Aeronautics and Astronautics, Inc.

[32] Wang, A. (2005), *Civil Transportation Aircraft General Design, Volume 5 of Aircraft Design Manual, Aviation Industry Press, Beijing.*

[33] Liebherr. (2004), Airbus A319/AIRBUS 320/A321 ECS Training Manual.

[34] Incropera, F. P., Lavine, A. S. and DeWitt, D. P. (2011), Fundamentals of heat and mass transfer, John Wiley & Sons Incorporated, pp. 545.

[35] *http://bouteloup.pierre.free.fr/lica/phythe/don/air/air_k_plot.pdf*

[36] Yu, J. (2006), Heat Exchanger Principle and Design [M], Press of Beijing University of Aeronautics and Astronautics.

[37] *http://en.wikipedia.org/wiki/File:Moody_diagram.jpg*

[38] Dipartimento Di Ingegneria Aerospaziale, Aircraft systems - lec*ture notes, Chapter 9 – Environmental Control System*, Politecnico Di Milano, available at: http://www.aero.polimi.it/~ls072645/bacheca/dispense/01-AircSyst.pdf

[39] Chaudhuri, S., Bhattacharyya, D., Maity, A. and Pal, A. (1997), "Surface coatings for solar application", *Materials science forum,* Vol. 246, Trans Tech Publ, pp. 181.

Appendix A Cabin Heat Load Calculation

According to the methods introduced in Chapter 4, the aircraft heat load can be calculated from four aspects.

The first one is that comes from the fuselage wall. First of all, the fuselage skin temperature can be calculated by Equation 4-1 as follows.

$$T_s = T_h\left(1 + r\frac{k-1}{2}Ma^2\right)$$

Table A-1 shows the values definition of the parameters.

Table A- 1 Values definition of the parameters

No.	Parameter name	Explanation	Value
1	T_h (K)	Ambient temperature of the altitude 37,000ft	216.65K
2	r	Recovery factor, where for the turbulent flow is $Pr^{0.33}$, Pr is 0.7	0.89
3	k	Isentropic factor of air	1.4
4	Ma	Cruise Mach number	0.78

Therefore, the fuselage skin temperature can be calculated as follows.

$$T_s = T_h\left(1 + r\frac{k-1}{2}Ma^2\right) = 216.65 \times \left(1 + 0.89 \times \frac{1.4-1}{2} \times 0.78^2\right) = 240.11K$$

Then the calculation of thermal resistance is calculated as follows based on the description shown in Section4.1.1.

$$r_{cT} = \sum_{i=1}^{i=3} r_{ci}$$

$$r_{ci} = \frac{x_i}{A_i K_{ci}}$$

Based on the aircraft definition shown in Chapter 5, the required parameters in Equation A-3 are shown in Table A-2.

Table A- 2 Values definition of Equation A-3

No.	Parameter name	Explanation	Value
1	x_i (m)	Thickness of the layer	Fuselage skin x_1: 0.001 Insulation layer x_2: 0.05 Decoration layer x_3: 0.035
2	A_i (m^2)	Area of the layer	Fuselage skin A_1:195.83 Insulation layer A_3: 191.23 Decoration layer A_4: 187.91
3	K_{ci} (W/m • K)	Thermal conductivities of the material	Fuselage skin K_1: 140 Insulation layer K_2: 0.03 Decoration layer K_3: 0.25

Where

$$A_1 = \frac{\pi L(r_4 - r_3)}{\ln\left(\frac{r_4}{r_3}\right)} + 2 \times 0.5 \times 26.9 = \frac{3.14 \times 26.9 \times (1.975 - 1.974)}{\ln\left(\frac{1.975}{1.974}\right)} + 26.9 = 195.83 m^2$$

$$A_2 = \frac{\pi L(r_3 - r_2)}{\ln\left(\frac{r_3}{r_2}\right)} = \frac{3.14 \times 26.9 \times (1.974 - 1.924)}{\ln\left(\frac{1.974}{1.924}\right)} + 2 \times 0.5 \times 26.9 = 191.23 m^2$$

$$A_3 = \frac{\pi L(r_2 - r_1)}{\ln\left(\frac{r_2}{r_1}\right)} = \frac{3.14 \times 26.9 \times (1.924 - 1.889)}{\ln\left(\frac{1.924}{1.889}\right)} + 2 \times 0.5 \times 26.9 = 187.91 m^2$$

K_1= 140 W/m • K (Aluminium alloy)

K_2= 0.03 W/m • K (Fiberglass)

K_3= 0.28 W/m • K (Nomex)

Then by using Equation 4-4, the total thermal resistance r_{cT} can be calculated as follows.

$$r_{cT} = \sum_{i=1}^{i=3} r_{ci} = \frac{0.001}{195.83 \times 140} + \frac{0.05}{191.23 \times 0.03} + \frac{0.035}{187.91 \times 0.25} = 0.009$$

Finally, since the cabin temperature is 294.15K (21℃) and the temperature of fuselage skin is 240.11K, the heat transfer between the aircraft fuselage skin and cabin can be calculated as follows.

$$Q_f = \Delta T / r_{cT} = (240.11 - 294.15) / 0.009 = -6{,}004W$$

It can be seen that the heat load is minus, which indicates the fuselage skin does not play role on increasing the cabin heat load during cruise. Actually, the cabin is losing heat because of the heat transfer between fuselage wall and ambient environment.

The second step is to calculate the heat load because of the solar radiation. According to the description shown in Section 4.1.2 and assuming that there is just around half of the observation windows are exposed to the sunshine directly, the radiative heat can be calculated as follows.

$$Q_s = \tau G_s A_p = 0.66 \times 1367 \times (1.18 + 0.07 \times 40) = 3{,}591W$$

Where

q_s = area factor, 0.66 [21]

G_s= 1367W/m^2 [39]

A_p= 1.18m^2 (each side windshield) and 0.07m^2 (each cabin observation window)

The third step is to calculate the heat load due to the aircraft occupants. During flight, defining the pilots and most of the passengers are in light manual work condition, the attendants are in moderate manual work condition, the heat load

comes from the occupants can be calculated as follows based on the definition shown in Section 4.1.3.

$$Q_o=152\times100+4\times200=16{,}000W$$

The last step is to calculate heat load comes from the electronic-electrical equipments. According to the referred information from related aircrafts which is shown in Table 4-2, the value of 7KW is selected as the input in this research.

Till now, the total heat load in the aircraft can be computed as 20,587W by adding all of the four items. It can be seen that it is about 16KW less than 36.75KW as section 4.3 described. Two points can be used to explain the difference.

The first point is that the estimated value of 36.75KW is the maximum aircraft heat load when the aircraft is landing on the ground as section 4.3 described. The temperature of the fuselage skin can reach to about 50 ℃ at that time, while the value is about -33℃ during cruise. The temperature difference of 83℃ causes a heat load difference of 9,226W in terms of the Equation 4.4.

The second point is that influence from the cabin floor is ignored in this calculation because lacks of structural parameters. And the calculation result must be smaller if taking the cabin floor into consideration since it causes cabin heat load loss during cruise phase. But when the aircraft is landing on the ground during hot days, the ambient high temperature will increase the cabin heat load through the cabin floor. This may cause a heat load of several kilowatts.

Therefore, it is stated that the final calculation result 20,587W is suitable as design input for the air conditioning system.

Appendix B Simulation Models of ECS Components

Based on the analysis shown in Chapter 6, the simulation models of classic ECS which uses three-wheel low or high pressure water separation system can be built step by step.

B.1 Model of the Primary Heat Exchanger

First of all, the input engine bleed air mass flow Q_2 should be simulated.

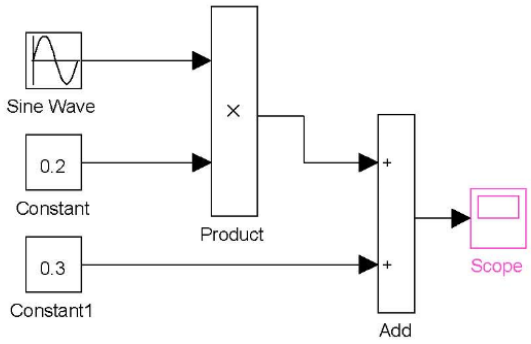

Figure B- 1 Simulation model of Q_2

Then, According to the analysis shown in Section 6.2, the simulation model of PHE can be built as shown in Figure B-5. The compressed model of 'subsystem' is as following picture.

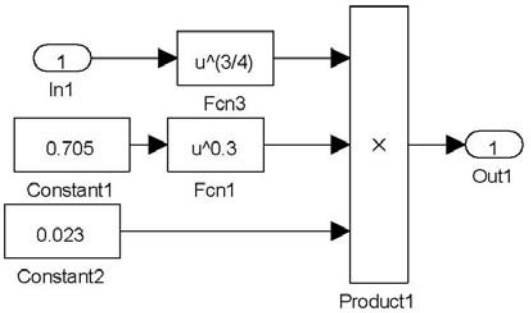

Figure B- 2 Simulation model of 'Subsystem'

The compressed model of 'subsystem1' is shown as follows.

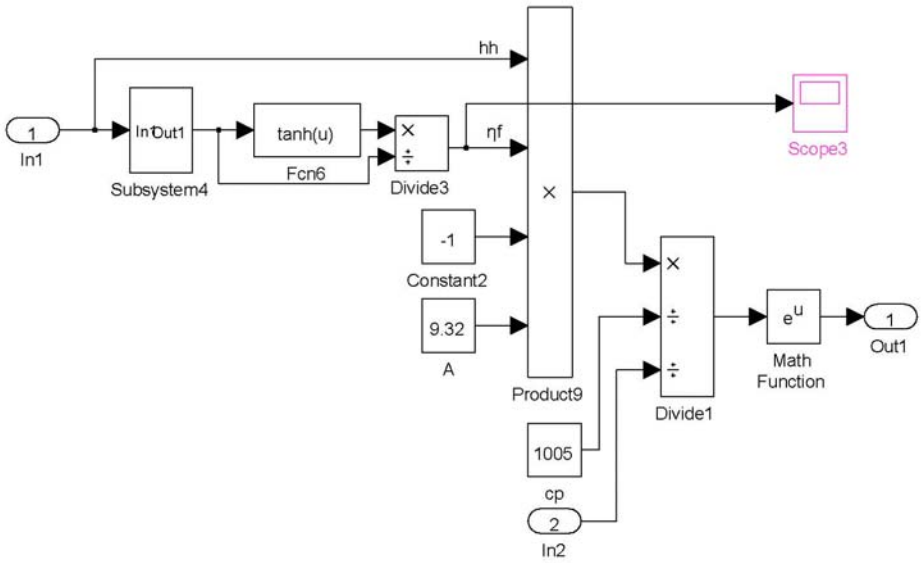

Figure B- 3 Simulation model of 'Subsystem1'

The compressed model of 'subsystem4' is shown as the following picture.

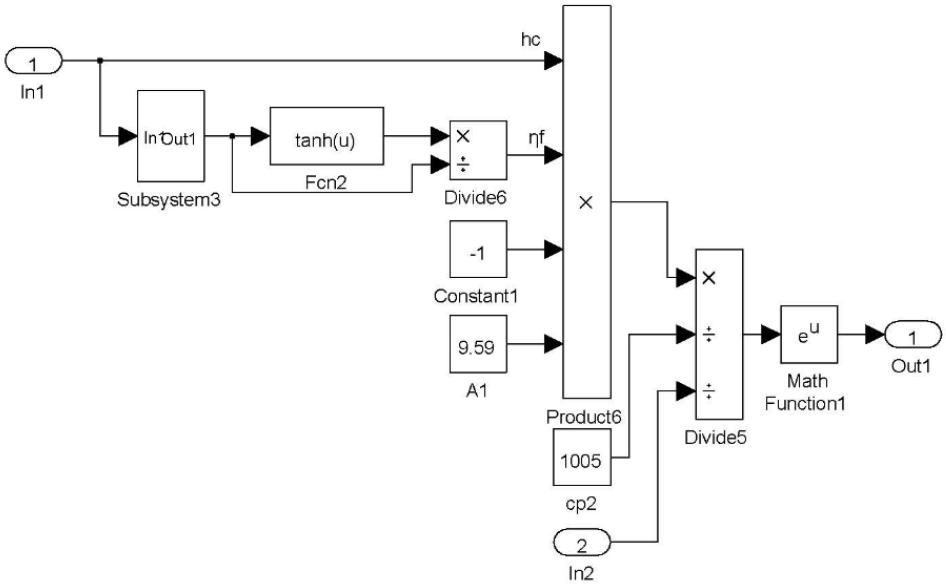

Figure B- 4 Simulation model of 'Subsystem4'

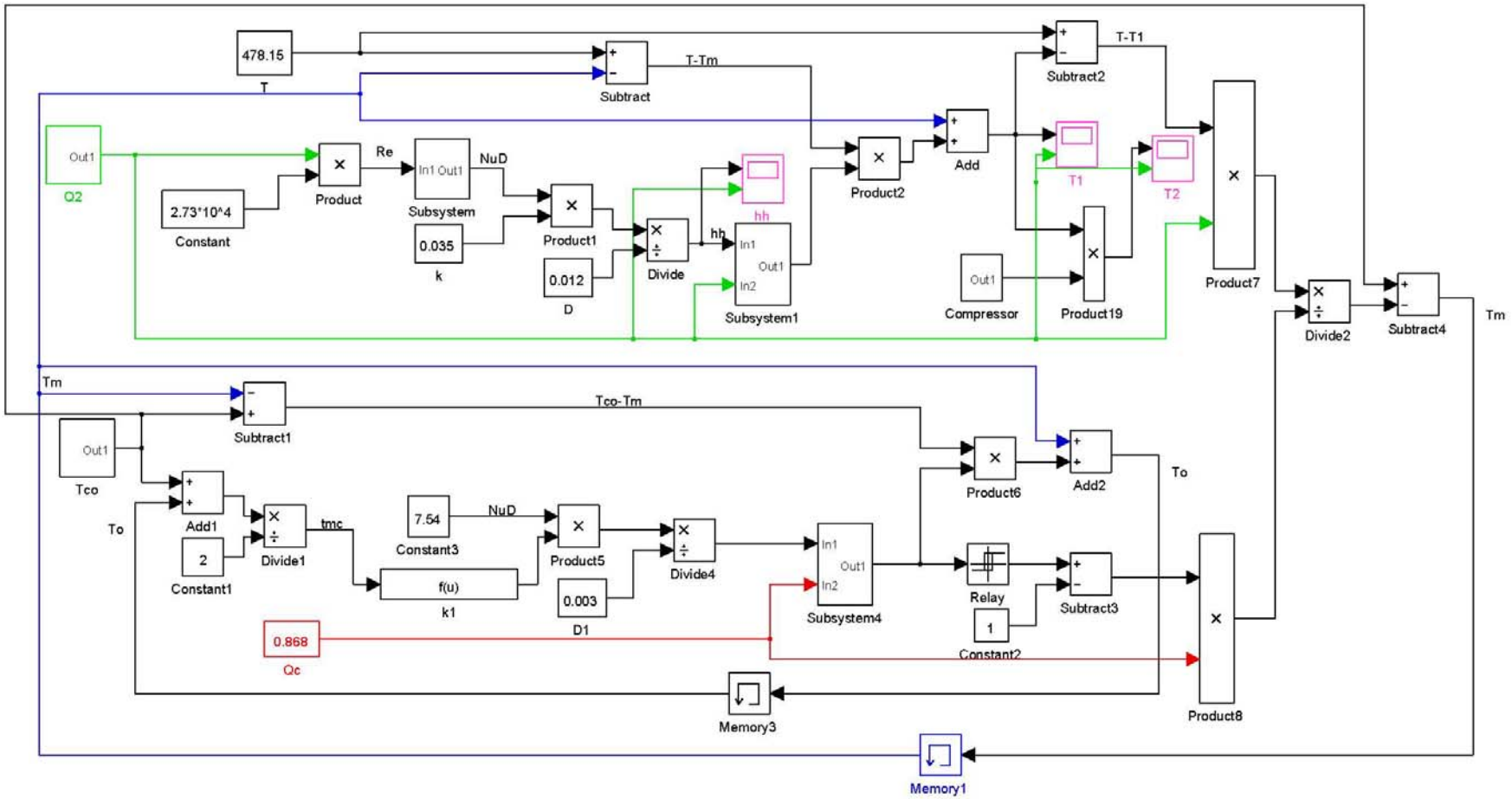

Figure B- 5 Simulation model of PHE

B.2 Model of the Main Heat Exchanger

According to the analysis shown in Section 6.1, the simulation model of the MHE is depicted as follows.

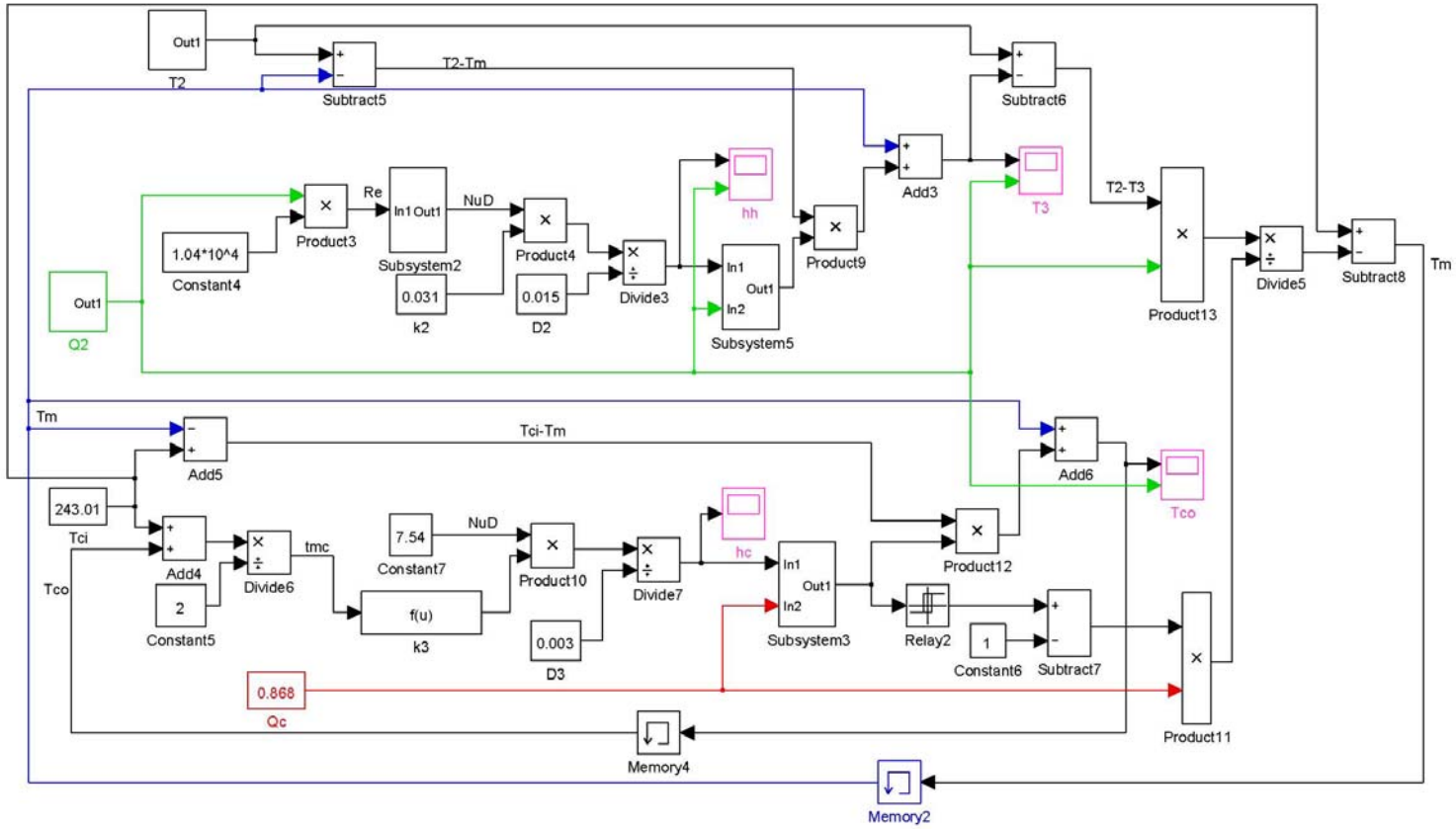

Figure B- 6 Simulation model of MHE

The compressed model of ‘subsystem’ is shown as following picture.

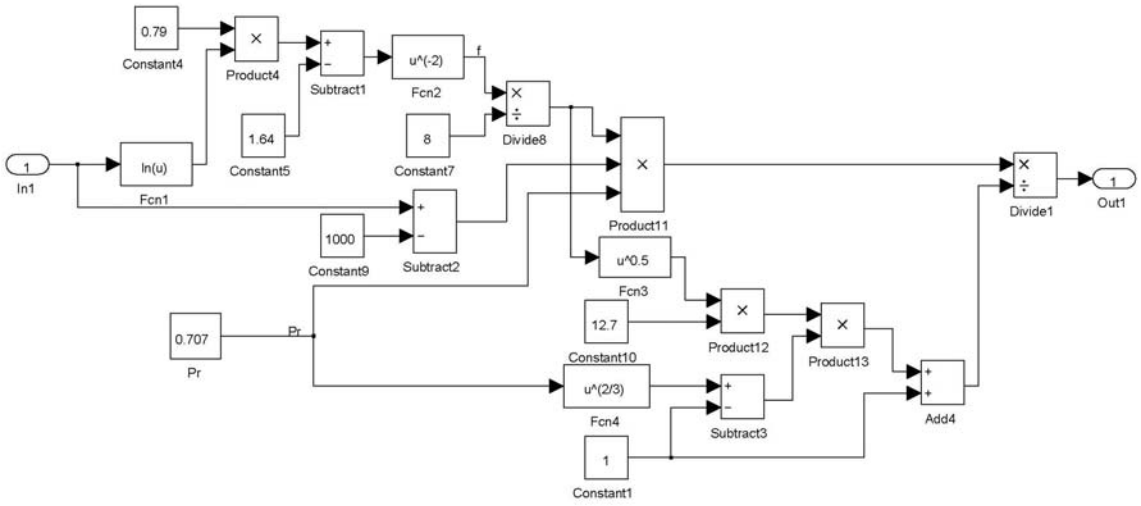

Figure B- 7 Simulation model of ‘Subsystem’

The compressed model of ‘subsystem2’ is depicted as following picture.

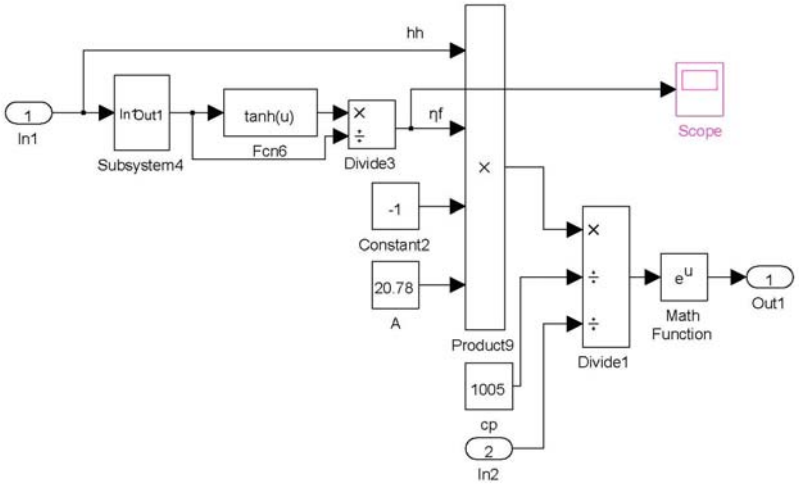

Figure B- 8 Simulation model of ‘Subsystem2’

The compressed model of ‘subsystem3’ is shown as follows.

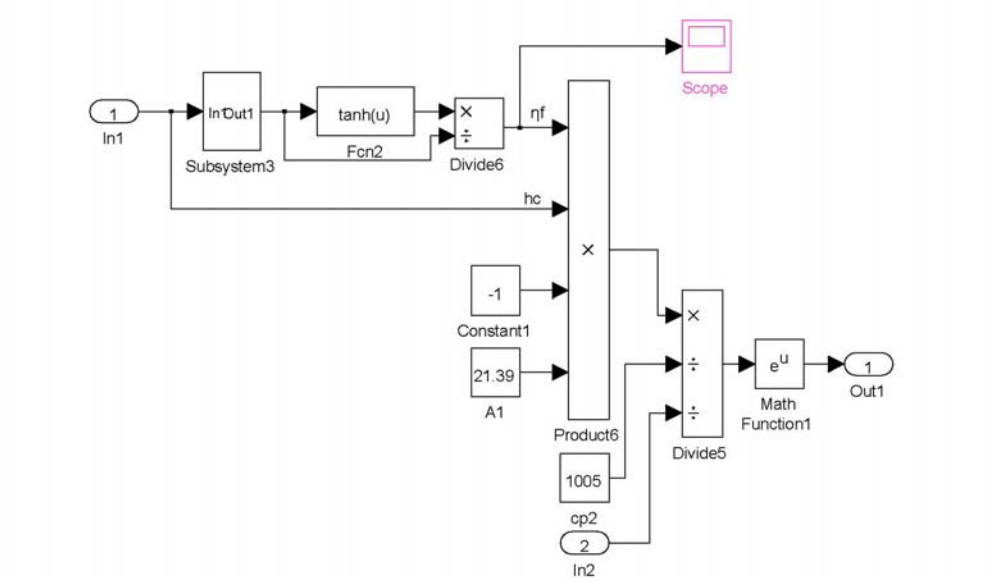

Figure B- 9 Simulation model of 'Subsystem3'

B.3 Model of the Compressor

Based on the analysis shown in Section 6.3, the compressor simulation model can be built as follows.

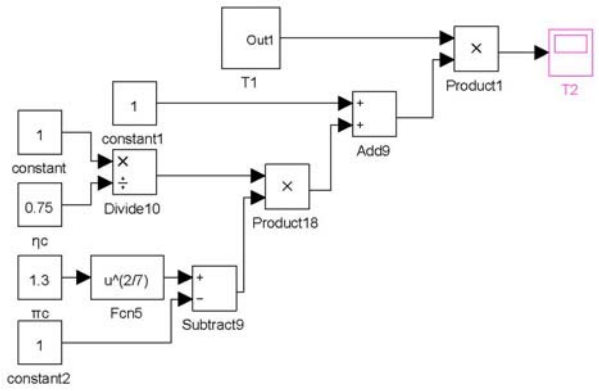

Figure B- 10 Simulation model of compressor

B.4 Model of the Turbine

Finally, based on the analysis shown in Section 6.4, the turbine simulation model is built as follows.

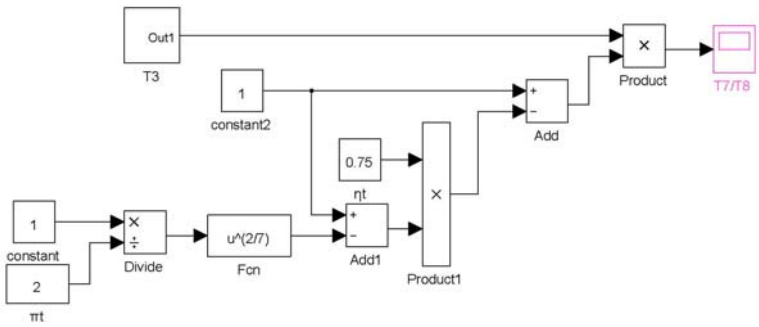

Figure B- 11 Simulation model of turbine

B.5 Model of High Pressure Water Separation System

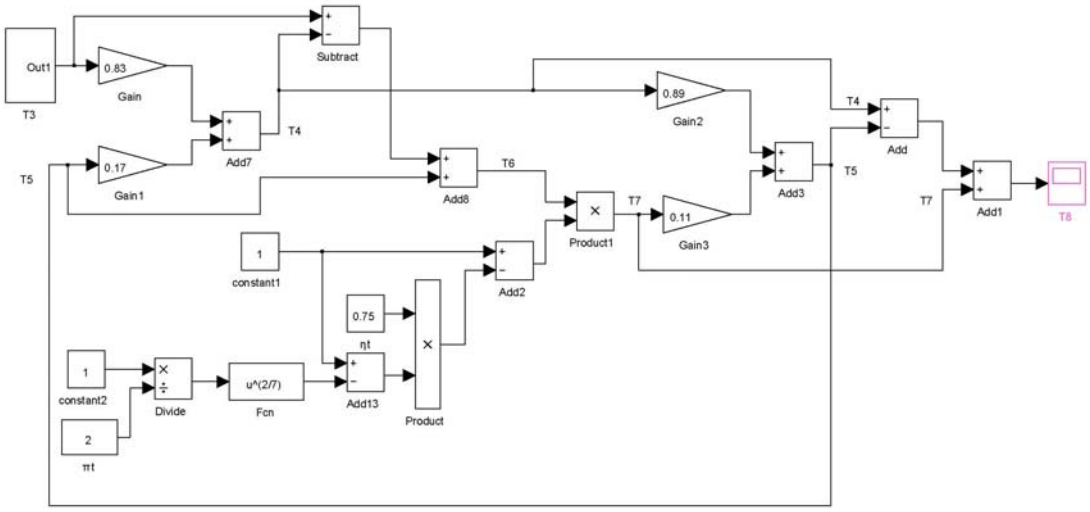

Figure B- 12 Simulation model of HPWS (Reheater, Condenser and Turbine)